THIS REPORT HAS BEEN DELIMITED
AND CLEARED FOR PUBLIC RELEASE
UNDER DOD DIRECTIVE 5200.20 AND
NO RESTRICTIONS ARE IMPOSED UPON
ITS USE AND DISCLOSURE.

DISTRIBUTION STATEMENT A

APPROVED FOR PUBLIC RELEASE;
DISTRIBUTION UNLIMITED.

Armed Services Technical Information Agency

Because of our limited supply, you are requested to return this copy WHEN IT HAS SERVED YOUR PURPOSE so that it may be made available to other requesters. Your cooperation will be appreciated.

AD 40791

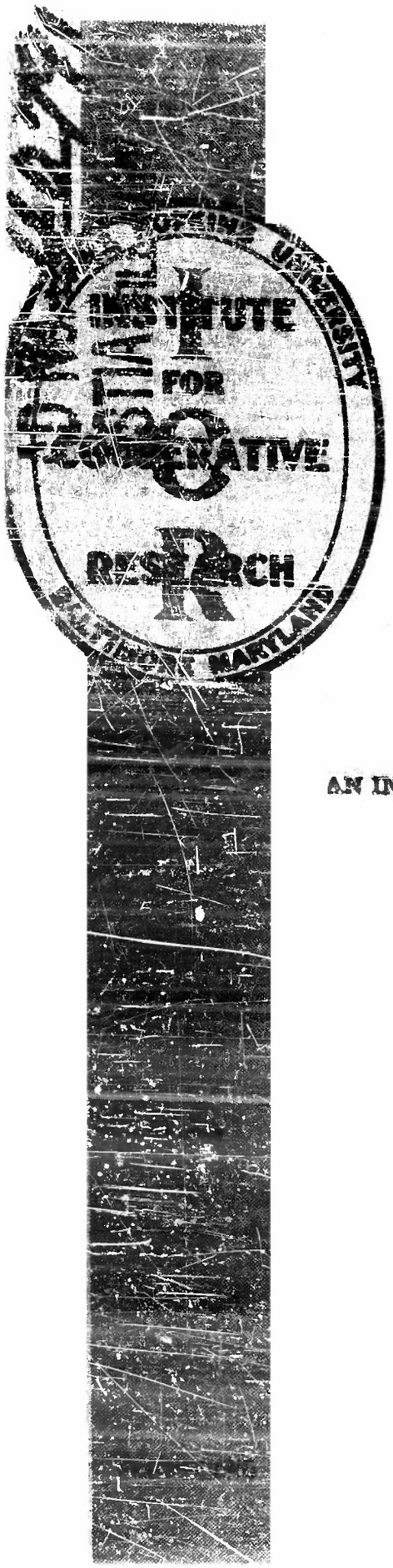
NOTICE: WHEN GOVERNMENT OR OTHER DRAWINGS, SPECIFICATIONS OR OTHER DATA ARE USED FOR ANY PURPOSE OTHER THAN IN CONNECTION WITH A DEFINITELY RELATED GOVERNMENT PROCUREMENT OPERATION, THE U. S. GOVERNMENT THEREBY INCURS NO RESPONSIBILITY, NOR ANY OBLIGATION WHATSOEVER; AND THE FACT THAT THE GOVERNMENT MAY HAVE FORMULATED, FURNISHED, OR IN ANY WAY SUPPLIED THE SAID DRAWINGS, SPECIFICATIONS, OR OTHER DATA IS NOT TO BE REGARDED BY IMPLICATION OR OTHERWISE AS IN ANY MANNER LICENSING THE HOLDER OR ANY OTHER PERSON OR CORPORATION, OR CONVEYING ANY RIGHTS OR PERMISSION TO MANUFACTURE, USE OR SELL ANY PATENTED INVENTION THAT MAY IN ANY WAY BE RELATED THERETO.

Reproduced by

DOCUMENT SERVICE CENTER

KNOTT BUILDING, DAYTON, 2, OHIO

UNCLASSIFIED



The Johns Hopkins University
Mechanical Engineering Department
Internal Flow Research

Report I-20

AN INVESTIGATION OF FULLY DEVELOPED TURBULENT FLOW IN A CURVED CHANNEL

By

Salamon Eskinazi

A Report
to the

Office of Naval Research
Mechanics Branch

Contract Nonr 248(33) - August 12, 1954

The Johns Hopkins University
Mechanical Engineering Department
Internal Flow Research

Report I-20

AN INVESTIGATION OF FULLY DEVELOPED TURBULENT FLOW IN A CURVED CHANNEL

By

Salamon Eskinazi

A Report
to the

Office of Naval Research
Mechanics Branch

Contract Nonr 248(33) - August 12 1954

Approved: George F. Wislicenus
George F. Wislicenus
Research Contract Director

TABLE OF CONTENTS

Page

ACKNOWLEDGMENTS

SUMMARY

LIST OF SYMBOLS - - - - - - - - - i

INTRODUCTION - - - - - - - - - 1

The Wind Tunnel - - - - - - 4

The Hot-Wire Anemometer Equipment 6

ANALYTICAL CONSIDERATIONS - - - - - 9

Analysis for Straight Channel - - 9

Fully Developed Flow in The Straight Channel - - - - - - - - 12

Analysis for the Curved Channel - - 14

Fully Developed Flow in the Curved Channel - - - - - - - - 17

EXPERIMENTAL ANALYSIS - - - - - - 19

The Mean Velocity Measurements - 19

The Static Pressure Drop Along the Length of the Channel - - - - 23

The Intensity of Turbulence - - - 24

Shear Stress in The Straight Parallel Fully Developed Section - - - 28

Page

Shear Stress in the Fully Developed Curved Section - - - - - - - - - 31

Location of the Nul Shear Stress in the Curved Channel- - - - - - - - 33

The Spectrum of the Velocity Fluctuations - - - - - - - - - - - 36

The Microscale of Turbulence - - - 37

The Integral Scale of Turbulence - - 43

Similarity Considerations- - - - - 46

Production of Turbulent Energy - - - 51

The Dissipation of Turbulent Energy - 57

CONCLUSIONS - - - - - - - - - - - - - - - 60

APPENDIX I - - - - - - - - - - - - - - - 63

STATIC AND DYNAMIC HEAT TRANSFER PROPERTIES OF THE HOT-WIRE ANEMOMETER- - - - - - - - - - - - - - - - - 63

Boussinesq's Solution - - - - - - - 64

King's Solution - - - - - - - - - 66

Solution in the Oseen Regime- - - - 67

The Use of Heated Wires for Time Mean Velocity Measurements - - - 68

The Use of Heated Wires for Instantaneous Velocity Measurements - 70

Page

APPENDIX II - - - - - - - - - - 76

THE HOT WIRE ANEMOMETER - - - - - - 76

Foreword - - - - - - - - 76

Description of the Hot-Wire Anemometer - - - - - - - 76

The Power Supply Units - - - - 77

The Bridge Circuit - - - - - 78

The Calibrating Voltage - - - - 80

The Compensating Amplifier - - 81

Symbols in Figure 35 - - - - - 84

REFERENCES - - - - - - - - - - 86

ACKNOWLEDGMENTS

The author would like to express his sincere appreciation to Dr. Hsuan Yeh, Dr. Francis Clauser and to Dr. Stanley Corrsin for their invaluable suggestions and encouragement. The author is also grateful to Dr. George Wislicenus, Chairman of the Mechanical Engineering Department for his interest throughout this work. Many thanks are due to Mr. Henry Macdonald for his help in the design of the hot-wire equipment and to Messrs. John Lumley, John Gitt and Robert Mills, Jr., for their help in the experimental investigations and analysis of the data. Finally an expression of gratitude is directed to Dr. John Weske, to Mr. William Rose and to Mr. Stephen Traugott for their friendly attitude and support of this work and to Mrs. Doris Van-Meter for her excellence in typing this manuscript.

SUMMARY

The problem of investigating the turbulent properties of a flow in curved passages has received very little attention in the past years. The lack of attention is mainly due to the additional complication brought into the problem by the curvature of the flow field. This work attempts to analyze analytically as well as experimentally the turbulent properties of a fully developed two-dimensional flow of air in a curved channel with constant radius of curvature. The results are compared with those of a two-dimensional fully developed flow in a straight parallel channel at the same Reynolds Number. Although the investigation was carried out in a channel with one value of radius of curvature, attempts are made for predictions of flow behaviours in channels with different radii of curvature.

LIST OF SYMBOLS

Straight Parallel Channel, Cartesian Coordinates:

x	Longitudinal coordinate in the direction of flow. The origin is at the entrance of the straight channel.
y	Lateral coordinate in the direction perpendicular to the walls. The origin is the inner wall.
z	Coordinate perpendicular to x-y plane.
u', v', w'	Instantaneous fluctuating velocity components respectively in the x, y, and z directions.
U, V, W	Time mean velocities respectively in the x, y, and z directions.
$\tilde{u}', \tilde{v}', \tilde{w}'$	Root-mean-square of the fluctuating velocity component in the x, y, and z directions.

Curved Parallel Channel, Cylindrical coordinates:

φ	Angular coordinate in the direction of flow. The origin is at the exit of the straight channel or the inlet of the curved channel.
R	Radial coordinate measured from the inner wall.
r	Radial distance measured from the center of the circles described by the two curved walls.
z	Coordinate perpendicular to the r-φ plane.
u', v', w'	Instantaneous fluctuating velocity components respectively in the φ , r and z directions.

U, V, W	The time mean velocity components respectively in the φ , r and z directions.
$\tilde{u}', \tilde{v}', \tilde{w}'$	Root-mean-square of the fluctuating velocity component in the φ , r and z directions.

General Symbols:

p	Local static pressure $P + p'$
ρ	Density of the air
P	Time mean value of static pressure
p'	Instantaneous fluctuating component of static pressure
$\overline{U}$	Space mean velocity at the particular station
P_t	Total pressure
ν	Kinematic viscosity of the air
t	Time coordinate
M	Time constant of the wire
U_m	The maximum mean velocity at a given x or φ.
U_*	Friction velocity $\left(\tau_w/\rho\right)^{\frac{1}{2}}$
Re	Reynolds Number based on maximum mean velocity and half width of channel
d	Width of channel, 3.0 inches
λ	The microscale of turbulence

L	The integral scale of turbulence
n	Component frequency of turbulence
k	Wave number $2\pi n/U$
τ_w	Shear stress at the wall
$F(n)$	Fraction of turbulent energy associated with band width dn
$F(k)$	Turbulent energy associated with band width dk
E	Mean voltage across the wire
e	Fluctuating voltage across the wire
$\mathcal{R}$	Space-Correlation Coefficient

Subscripts:

x	Associated with x-direction
y	" " y "
z	" " z "
φ	" " φ "
r	" " r "
s	" " straight channel
i	" " inner wall
o	" " outer wall

	Associated with		
$\overline{u'^2}$	"	"	Turbulent energy in the direction of mean flow
$\overline{v'^2}$	"	"	Turbulent energy in the lateral or radial direction
η	"	"	The point where the total shear stress is zero

Appendix I has a separate List of Symbols

List of Symbols in Appendix I

D	Diameter of cylinder
c	Specific heat of the air
ρ	density of air
T_o	Temperature of air
t	Time
u	x component of velocity = $U + u'$
v	y component of velocity = $V + v'$
w	z component of velocity = $W + w'$
$\varkappa$	Thermal conductivity of air
$\overline{Nu}$	$\frac{\bar{h}D}{\varkappa}$
$\overline{Pe'}$	$\overline{Re \times Pr} = \frac{\rho c U D}{\varkappa}$
γ	Euler constant, .57721
q'	Heat flow per unit time per unit length
q''	Heat flow per unit time per unit area
T_p	Temperature of plate
T_f	Temperature of fluid
T_h	Temperature of wire when heated

I	Current through wire
R	Resistance of wire
R_o	Resistance of wire at air temperature
R_h	Resistance of wire when heated
ℓ	Length of wire
α	Temperature resistance coefficient
A	$\ell\kappa$ (King's Equation)
B	$\ell\sqrt{2\pi\kappa c\rho UD}$ "
x, y, z, Φ, Ψ	Coordinates
u	$U(x, y, z) + u'(x, y, z, t)$ same treatment applies to other components
Θ	Angle between the wire axis and perpendicular to the mean flow U
$\bar{E}$	Mean voltage of wire (DC)
e'	Fluctuating part of voltage of the wire (AC)
$\tilde{e'}$	rms value of e'
$\tilde{u'}$	rms value of u' (same treatment pertains to other components
$\bar{a}$	Overheat ratio $= \frac{R_h - R_o}{R_o}$
b	$\frac{I^2 - I_o^2}{I^2}$
$\bar{C}$	Per cent degeneracy from constant current case

INTRODUCTION

The problem under consideration is one of turbulent flow in curved channels. This sentence as it stands has a very broad meaning and since today's knowledge of turbulence alone is not sufficient to develop a general theory of turbulence, the author, like all other investigators of turbulent flow problems, must regretfully confine his efforts to a limited phase of the general problem itself.

We know very little about the mechanism of turbulence. We call it today a nasty problem of complex nature. Indeed it is one or at least it seems so because sister sciences like molecular theory of fluids and mathematical theory of statistics do not yet supply the necessary knowledge to help formulate a plausible solution and clear understanding of the mechanism of turbulence. If the general theory of turbulence escapes our comprehension, it is then because of the complexity of the mechanism of turbulence. Furthermore, the general problem of fluid flow brings with it non-linearities in the equations describing the motion of the fluid. Although to a perfectionist this situation might look desperate, it is contrary to the logic of a scientist to sit back

and wait for the missing clues that are to guide us to the general solution of the problem. The purist, who desires to draw conclusions from purely deductive reasoning, will devote his efforts to diminish the lack of knowledge in molecular theory and mathematics which are so badly needed for a clearer understanding of the problem. The artisan or the engineer or in general the laboratory man will contribute his share by investigating the actual flow in simple configurations which demand only a part of the overall knowledge needed to solve the special problem he has chosen. It is hoped that the solution of that comparatively simple problem will show the way to the solution of a broader one. The purist will supply information to the engineer and the engineer to the purist and, hoping that the process is favourably convergent, we will someday arrive at the general solution for the problem of turbulent flow.

In this investigation, the aim of the author is to study the special problem he has chosen. It is one of the study of the mechanism of turbulent motion in a two dimensional curved channel after the incompressible turbulent flow has reached a so-called fully developed

stage. The flow entering the curved section is two-dimensional and fully developed in a straight channel of parallel walls. The initial conditions of the flow before entering the curved channel have already been investigated by Laufer (1) for three different Reynolds Numbers. Wattendorf (2) showed the need of a similar investigation in a curved passage. Wattendorf's studies on a flow around a curved channel contained only investigations of the time mean velocity and pressure. Studies of the effect of curvature on turbulent intensities, shear, turbulence energies and other characteristic turbulent parameters will be presented in this investigation, as well as the mean velocities.

The Wind Tunnel

The wind tunnel was designed for maximum velocities in the neighborhood of 100 ft./sec. Two banks of two blowers in series per bank were necessary to supply the air in the wind tunnel. Each blower has a maximum rating of 4000 c.f.m. and 3 inches of water static head. The fans are driven with 110 volts DC motors at a speed of 1750 r.p.m. The speeds of the motors were controlled with rheostats in series with the armature of the motors. The blowers discharged the air into a plenum chamber 60 inches high and 67 inches wide, (Figure 1). The interior of the plenum chamber is equipped with three screens with different solidity. A fourth screen of low solidity was located at the discharge of the blowers.

A vertical and a lateral contraction followed the plenum chamber to meet the dimensions of the test section. The dimensions of the straight approach section are 3 inches wide, 46 1/2 inches high and 16 feet long. The width and the height of the channel remains constant up to the air exit. An aspect ratio of 15.5 to 1 was chosen in order to insure two-dimensionality in the major middle portion of the channel. Half way downstream of the inlet of the straight parallel

section, 1 by 3 inch slots are purposely located on the channel ceiling and floor in order to evacuate the boundary layer already developed on top and bottom. This bleeding helps to establish two-dimensional flow in the curved section of the channel.

The walls in the straight parallel section are made of 1/2 inch plywood with a plastic surface finish. In order to establish a fully developed flow at the end of the straight parallel section, it was necessary to make the walls 16 ft. long or 64 duct widths.

The curved section has the same heighth and width as the approach section. The walls are made of rolled sheet metal #16 gage. In order to accomodate more than 360° of an arc in the curved section it was necessary to make the radius of curvature of the outer wall in the first quadrant 36 inches and that of the remaining curved portion 30 inches. For the investigation presented here, it was necessary to have only 300° of curved wall because the fully developed stage occurred about the end of the second quadrant. As compared with the original design shown in

Figure 1, this simplified many problems associated with the proper discharge of air. The ratio of the channel width to the outside radius of curvature is $d/r_o = 1/10$ in the equilibrium section of the curved channel.

The maximum time mean velocity at the end of the straight parallel section is 98.36 ft./sec. and the Reynolds Number based on the half width of the channel is 74,200.

The Hot-Wire Anemometer Equipment

It is always a two sided argument to choose between platinum or tungsten wires for measurements of turbulent fluctuating quantities. The proper choice of wire was discussed previously in (6). For the investigations presented here tungsten wires 0.00030 in diameter were used. Two methods of attaching the tungsten wire to the probe needles were employed depending upon the location where the measurements were being taken and the type of measurements. In the region where the length of the wire was not important the wire was welded on to tungsten needles placed approximately 1/8 of an inch apart. For measurements close to the wall and for turbulent scale measurements, the wire was copper plated leaving an uncoated length in

the middle of about 1/16 of an inch. The welding was done in an argon atmosphere and the copper plating in an electrolytic bath of $CuSO_4$ with a current density of about 20 amps/ ft^2 of exposed surface. (Fig. 2).

The hot-wire instrument and its integral parts were designed and built for measurements in this work to handle tungsten wires with time constant up to 2 msec. The hot wire anemometer set contains two separate bridges and two separate compensating amplifiers. This eliminates signal coupling when two wires are used at the same time. The DC heating source was taken from batteries and the DC B+ voltage from a regulated power supply. The description of the electronic equipment is inserted in Appendix II.

An adding and subtracting circuit similar to the one used by Kovasznáy (7) was used.

Time derivatives of the fluctuating quantities were taken with an electronic differentiator built for the purpose. Using an approximately 1 msec. wire in the actual flow conditions, the overall frequency response is flat from 10 to 5000 cycles per second. The frequency response of the compensating amplifier is shown in the Appendix II.

The mean-square values of the turbulent fluctuating quantities were measured through a thermocouple unit. The compensation was adjusted with the square wave input to the wire. This method was compared by feeding a pure white noise to the wire and analyzing the output with the wave analyzer. The results showed that the square wave compensation and the square wave generator gave satisfactory compensation for the thermal lag of the wire.

The frequency analysis of the turbulent fluctuating quantities was made with a Hewlett-Packard wave analyzer. In order to obtain mean-square values of the voltage associated with a band width at a given frequency the output circuit of the wave analyzer was altered. The output was fed into a thermocouple by-passing the rectifier at the output of the wave analyzer.

ANALYTICAL CONSIDERATIONS

The problem to be investigated was discussed in the introduction as a two-dimensional, incompressible, fully developed flow in a curved channel with constant radius of curvature. The initial conditions of the flow before it enters the curved channel were chosen to be fully developed in a straight parallel channel. The reason for this choice is that the initial conditions of the flow are fairly well investigated (1) and especially since the initial character of the flow is fully developed, it will require smaller length of curve channel for the flow to assume a fully developed character again.

Analysis for Straight Channel

The three components of the Reynolds Equation for a general incompressible flow in cartesean coordinates are:

$$\left.\begin{aligned}
&\frac{\partial U}{\partial t}+U\frac{\partial U}{\partial x}+\frac{\partial}{\partial x}(\overline{u'^2})+V\frac{\partial U}{\partial y}+\frac{\partial}{\partial y}(\overline{u'v'})+W\frac{\partial U}{\partial z}+\frac{\partial}{\partial z}(\overline{u'w'})=-\frac{1}{\rho}\frac{\partial P}{\partial x}+\nu\nabla^2 U\\
&\frac{\partial V}{\partial t}+U\frac{\partial V}{\partial x}+\frac{\partial}{\partial x}(\overline{u'v'})+V\frac{\partial V}{\partial y}+\frac{\partial}{\partial y}(\overline{v'^2})+W\frac{\partial V}{\partial z}+\frac{\partial}{\partial z}(\overline{v'w'})=-\frac{1}{\rho}\frac{\partial P}{\partial y}+\nu\nabla^2 V\\
&\frac{\partial W}{\partial t}+U\frac{\partial W}{\partial x}+\frac{\partial}{\partial x}(\overline{u'w'})+V\frac{\partial W}{\partial y}+\frac{\partial}{\partial y}(\overline{v'w'})+W\frac{\partial W}{\partial z}+\frac{\partial}{\partial z}(\overline{w'^2})=-\frac{1}{\rho}\frac{\partial P}{\partial z}+\nu\nabla^2 W
\end{aligned}\right\}\quad(1)$$

and the continuity equations for the mean and turbulent velocities

$$\frac{\partial U}{\partial x} + \frac{\partial V}{\partial y} + \frac{\partial W}{\partial z} = 0 \quad \text{and} \quad \frac{\partial u'}{\partial x} + \frac{\partial v'}{\partial y} + \frac{\partial w'}{\partial z} = 0$$

where U, V, and W are functions of x, y, z in steady state conditions and the turbulent velocity components are functions of x, y, z and also of t.

The three component equations of the turbulent energy can also be derived:

$$\left.\begin{aligned}
a)\ & \frac{1}{2}\frac{\partial \overline{u'^2}}{\partial t} + \frac{1}{2}\left[U\frac{\partial \overline{u'^2}}{\partial x} + V\frac{\partial \overline{u'^2}}{\partial y} + W\frac{\partial \overline{u'^2}}{\partial z}\right] + \left[\overline{u'^2}\frac{\partial U}{\partial x} + \overline{u'v'}\frac{\partial U}{\partial y} + \overline{u'w'}\frac{\partial U}{\partial z}\right] \\
& + \frac{1}{2}\left[\frac{\partial \overline{u'^3}}{\partial x} + \frac{\partial \overline{u'^2v'}}{\partial y} + \frac{\partial \overline{u'^2w'}}{\partial z}\right] = -\frac{1}{\rho}\overline{u'\frac{\partial p'}{\partial x}} + \nu\overline{u'\nabla^2 u'} \\
b)\ & \frac{1}{2}\frac{\partial \overline{v'^2}}{\partial t} + \frac{1}{2}\left[U\frac{\partial \overline{v'^2}}{\partial x} + V\frac{\partial \overline{v'^2}}{\partial y} + W\frac{\partial \overline{v'^2}}{\partial z}\right] + \left[\overline{v'u'}\frac{\partial V}{\partial x} + \overline{v'^2}\frac{\partial V}{\partial y} + \overline{v'w'}\frac{\partial V}{\partial z}\right] \\
& + \frac{1}{2}\left[\frac{\partial \overline{v'^2u'}}{\partial x} + \frac{\partial \overline{v'^3}}{\partial y} + \frac{\partial \overline{v'^2w'}}{\partial z}\right] = -\frac{1}{\rho}\overline{v'\frac{\partial p'}{\partial y}} + \nu\overline{v'\nabla^2 v'} \\
c)\ & \frac{1}{2}\frac{\partial \overline{w'^2}}{\partial t} + \frac{1}{2}\left[U\frac{\partial \overline{w'^2}}{\partial x} + V\frac{\partial \overline{w'^2}}{\partial y} + W\frac{\partial \overline{w'^2}}{\partial z}\right] + \left[\overline{w'u'}\frac{\partial W}{\partial x} + \overline{w'v'}\frac{\partial W}{\partial y} + \overline{w'^2}\frac{\partial W}{\partial z}\right] \\
& + \frac{1}{2}\left[\frac{\partial \overline{u'w'^2}}{\partial x} + \frac{\partial \overline{v'w'^2}}{\partial y} + \frac{\partial \overline{w'^3}}{\partial z}\right] = -\frac{1}{\rho}\overline{w'\frac{\partial p'}{\partial z}} + \nu\overline{w'\nabla^2 w'}
\end{aligned}\right\} \quad (2)$$

where the operator $\nabla^2 = \frac{\partial^2}{\partial x^2} + \frac{\partial^2}{\partial y^2} + \frac{\partial^2}{\partial z^2}$

When all three components of equation 2 are added one obtains the total rate of turbulent energy interchanged in the flow:

$$\left.\begin{aligned} &\frac{1}{2}\frac{\partial \overline{q'^2}}{\partial t} + \frac{1}{2}\left[U\frac{\partial}{\partial x}\overline{q'^2} + V\frac{\partial}{\partial y}\overline{q'^2} + W\frac{\partial}{\partial z}\overline{q'^2}\right] + \frac{1}{2}\left[\frac{\partial}{\partial x}\overline{u'q'^2} + \frac{\partial}{\partial y}\overline{v'q'^2} + \frac{\partial}{\partial z}\overline{w'q'^2}\right] \\ &+ \left[\overline{u'^2}\frac{\partial U}{\partial x} + \overline{u'v'}\frac{\partial V}{\partial x} + \overline{u'w'}\frac{\partial W}{\partial x} + \overline{u'v'}\frac{\partial U}{\partial y} + \overline{v'^2}\frac{\partial V}{\partial y} + \overline{v'w'}\frac{\partial W}{\partial y} + \overline{u'w'}\frac{\partial U}{\partial z}\right. \\ &\left. + \overline{v'w'}\frac{\partial V}{\partial z} + \overline{w'^2}\frac{\partial W}{\partial z}\right] = -\frac{1}{\rho}\left[\frac{\partial}{\partial x}\overline{p'u'} + \frac{\partial}{\partial y}\overline{p'v'} + \frac{\partial}{\partial z}\overline{p'w'}\right] \\ &+ \nu\left[\overline{u'\nabla^2 u'} + \overline{v'\nabla^2 v'} + \overline{w'\nabla^2 w'}\right] \end{aligned}\right\} \quad (3)$$

where $q'^2 = u'^2 + v'^2 + w'^2$

The first term in equation 3 is the rate of change of the mean-square of turbulent kinetic energy in an unsteady flow. The first bracket is the convection of turbulent energy by the mean flow. The second bracket is small scale convection or diffusion of turbulent energy by turbulent motion.

The production of turbulent energy by the mean velocity gradient is expressed in the third bracket. The work due to the fluctuating pressure gradient is represented in the fourth bracket. Finally the last bracket contains the transfer of work by viscous action and the dissipation function. To be more explicit the last term can be rewritten in the form of the two groupings mentioned above

$$\nu \left[\frac{1}{2} \nabla^2 \overline{q'^2} + \overline{\left(\frac{\partial u_i'}{\partial x_j}\right)\left(\frac{\partial u_j'}{\partial x_i}\right)} - \overline{\left(\frac{\partial u_i'}{\partial x_j} + \frac{\partial u_j'}{\partial x_i}\right)\frac{\partial u_i'}{\partial x_j}} \right] \qquad (3a)$$

where the cartesian tensor notation implies summation.

Fully Developed Flow In The Straight Channel:

When the flow is in a steady state this implies that any mean quantity is not a function of time. A two-dimensional channel flow implies that there are no variations of time mean quantities with one coordinate (in this case z) and that there is only one preferred direction for the mean motion (in this case is x). The third restriction is fully developed. This implies that the flow has reached the stage where the time mean quantities no longer change in the direction of the mean motion. Mathematically this means that:

$V = W = 0$ and that for any mean quantity $\bar{g}$; $\frac{\partial \bar{g}}{\partial t} = \frac{\partial \bar{g}}{\partial z} = \frac{\partial \bar{g}}{\partial x} = 0$.

except that P is a function of x. If those conditions are applied to the Reynolds, turbulent energy and the continuity equations we get:

$$\left.\begin{aligned} \frac{\partial}{\partial y}\left(\overline{u'v'}\right) &= -\frac{1}{\rho}\frac{\partial P}{\partial x} + \nu\frac{\partial^2 U}{\partial y^2} \\ \frac{\partial}{\partial y}\left(\overline{v'^2}\right) &= -\frac{1}{\rho}\frac{\partial P}{\partial y} \\ \frac{\partial}{\partial y}\left(\overline{v'w'}\right) &= 0 \end{aligned}\right\} \quad (4)$$

but $\overline{v'w'} = 0$ because the flow cannot sustain shear in the y-z plane (8). The turbulent energy equation becomes:

$$\overline{u'v'}\frac{\partial U}{\partial y} + \frac{1}{2}\frac{\partial}{\partial y}\overline{v'q'^2} = -\frac{1}{\rho}\frac{\partial}{\partial y}\overline{p'v'} + \nu\left[\frac{1}{2}\frac{\partial^2}{\partial y^2}\overline{q'^2} + \left(\overline{\frac{\partial u_i'}{\partial x_j}}\right)\left(\overline{\frac{\partial u_j'}{\partial x_i}}\right) - \left(\overline{\frac{\partial u_i'}{\partial x_j} + \frac{\partial u_j'}{\partial x_i}}\right)\overline{\frac{\partial u_i'}{\partial x_j}}\right] \quad (5)$$

The measurements taken in this work will give us an idea of each term in the energy equation except the diffusion and the work due to the gradient of fluctuating pressure. The dissipation can be estimated from turbulence scale measured. A separate discussion on the computed energy terms will appear later.

Analysis for the Curved Channel:

The three components of the Reynolds Equations for the general incompressible flow in cylindrical coordinates are:

$$\left.\begin{aligned}
&\frac{\partial U}{\partial t} + U\frac{\partial U}{r\partial\phi} + V\frac{\partial U}{\partial r} + W\frac{\partial U}{\partial z} + \frac{UV}{r} = -\frac{1}{\rho}\frac{\partial P}{r\partial\phi} - \frac{\partial}{r\partial\phi}\left(\overline{u'^2}\right) - \frac{\partial}{\partial r}\left(\overline{u'v'}\right) - \frac{\partial}{\partial z}\left(\overline{u'w'}\right) \\
&\qquad + \nu\left[\nabla^2 U - \frac{U}{r^2} + \frac{2}{r^2}\frac{\partial V}{\partial\phi}\right] \\
&\frac{\partial V}{\partial t} + U\frac{\partial V}{r\partial\phi} + V\frac{\partial V}{\partial r} + W\frac{\partial V}{\partial z} - \frac{U^2}{r} = -\frac{1}{\rho}\frac{\partial P}{\partial r} - \frac{\partial}{r\partial\phi}\left(\overline{u'v'}\right) - \frac{\partial}{\partial r}\left(\overline{v'^2}\right) - \frac{\partial}{\partial z}\left(\overline{v'w'}\right) \\
&\qquad + \nu\left[\nabla^2 V - \frac{V}{r^2} + \frac{2}{r^2}\frac{\partial U}{\partial\phi}\right] \\
&\frac{\partial W}{\partial t} + U\frac{\partial W}{r\partial\phi} + V\frac{\partial W}{\partial r} + W\frac{\partial W}{\partial z} = -\frac{1}{\rho}\frac{\partial P}{\partial z} - \frac{\partial}{r\partial\phi}\left(\overline{u'w'}\right) - \frac{\partial}{\partial r}\left(\overline{v'w'}\right) - \frac{\partial}{\partial z}\left(\overline{w'^2}\right) \\
&\qquad + \nu\nabla^2 W
\end{aligned}\right\} \quad (6)$$

The continuity equations for the mean and turbulent velocities are:

$$\frac{\partial U}{r\partial\phi} + \frac{1}{r}\frac{\partial(rV)}{\partial r} + \frac{\partial W}{\partial z} = 0 \quad \text{and} \quad \frac{\partial u'}{r\partial\phi} + \frac{1}{r}\frac{\partial(rv')}{\partial r} + \frac{\partial w'}{\partial z} = 0$$

The three component equations of the turbulent energy in the curved channel can also be expressed in cylindircal coordinates

$$
\begin{aligned}
&\text{a)}\quad \frac{1}{2}\frac{\partial \overline{u'^2}}{\partial t} + \frac{1}{2}\left[U\frac{\partial \overline{u'^2}}{r\partial\phi} + V\frac{\partial \overline{u'^2}}{\partial r} + W\frac{\partial \overline{u'^2}}{\partial z}\right] + \left[\frac{\partial \overline{u'v'}}{r\partial\phi} + \frac{\partial \overline{v'^2}}{\partial r} + \frac{\partial \overline{v'w'}}{\partial z}\right] \\
&\quad + \frac{1}{2}\left[\frac{\partial \overline{u'^3}}{r\partial\phi} + \frac{\partial \overline{u'^2v'}}{\partial r} + \frac{\partial \overline{u'^2w'}}{\partial z} + \frac{1}{r}\overline{u'^2v'} + \frac{2}{r}\overline{u'v'^2}\right] + \left[\frac{1}{r}\overline{u'v'}U + \overline{v'^2}V\right] \\
&\quad = -\frac{1}{\rho}\frac{\partial \overline{p'u'}}{r\partial\phi} + \nu\left[\frac{\partial \overline{u'v'}}{\partial r} + \frac{1}{r}\overline{u'v'} - \overline{u'\nabla^2 u'}\right] \\
&\text{b)}\quad \frac{1}{2}\frac{\partial \overline{v'^2}}{\partial t} + \frac{1}{2}\left[U\frac{\partial \overline{v'^2}}{r\partial\phi} + V\frac{\partial \overline{v'^2}}{\partial r} + W\frac{\partial \overline{v'^2}}{\partial z}\right] + \left[\frac{\partial \overline{u'v'}}{r\partial\phi} + \frac{\partial \overline{v'^2}}{\partial r} + \frac{\partial \overline{v'w'}}{\partial z}\right] \\
&\quad + \frac{1}{2}\left[\frac{\partial \overline{v'^3}}{r\partial\phi} + \frac{\partial \overline{u'v'^2}}{\partial r} + \frac{\partial \overline{v'^2w'}}{\partial z} + \frac{1}{r}\overline{v'^3} - \frac{1}{r}\overline{u'^2v'}\right] - 2U\frac{\overline{u'v'}}{r} \\
&\quad = -\frac{1}{\rho}\frac{\partial \overline{p'v'}}{\partial r} + \nu\left[\frac{\partial \overline{v'u'}}{r\partial\phi} + \frac{1}{r}\overline{v'u'} - \overline{v'\nabla^2 v'}\right] \\
&\text{c)}\quad \frac{1}{2}\frac{\partial \overline{w'^2}}{\partial t} + \frac{1}{2}\left[U\frac{\partial \overline{w'^2}}{r\partial\phi} + V\frac{\partial \overline{w'^2}}{\partial r} + W\frac{\partial \overline{w'^2}}{\partial z}\right] + \left[\frac{\partial \overline{w'u'}}{r\partial\phi} + \frac{\partial \overline{w'v'}}{\partial r} + \frac{\partial \overline{w'^2}}{\partial z}\right] \\
&\quad + \frac{1}{2}\left[\frac{1}{r}\frac{\partial \overline{w'^2u'}}{r\partial\phi} + \frac{\partial \overline{w'^2v'}}{\partial r} + \frac{\partial \overline{w'^3}}{\partial z} + \frac{1}{r}\overline{w'^2v'}\right] \\
&\quad = -\frac{1}{\rho}\frac{\partial \overline{p'w'}}{\partial z} + \nu\overline{w'\nabla^2 w'}
\end{aligned}
\qquad (7)
$$

where the operator $\nabla^2 = \frac{1}{r^2}\frac{\partial^2}{\partial\varphi^2} + \frac{\partial^2}{\partial r^2} + \frac{1}{r}\frac{\partial}{\partial r} + \frac{\partial^2}{\partial z^2}$

Adding the three component equations of the turbulent energy, the rate of turbulent energy interchanged in a flow passing through curved channels is:

$$\left.\begin{aligned}
&\frac{1}{2}\frac{\partial \overline{q'^2}}{\partial t} + \frac{1}{2}\left[U\frac{\partial}{r\partial\varphi}\overline{q'^2} + V\frac{\partial}{\partial r}\overline{q'^2} + W\frac{\partial}{\partial z}\overline{q'^2}\right] + \frac{1}{2}\left[\frac{\partial}{r\partial\varphi}\overline{u'q'^2} + \frac{\partial}{\partial r}\overline{v'q'^2} + \frac{\partial}{\partial z}\overline{w'q'^2} + \frac{\overline{v'q'^2}}{r}\right] \\
&+ \left[\frac{\partial}{r\partial\varphi}\overline{p'u'} + \frac{\partial}{\partial r}\overline{p'v'} + \frac{\partial}{\partial z}\overline{p'w'} + \frac{\overline{p'v'}}{r}\right] + \nu\left[\overline{u'\nabla^2 u'} + \overline{v'\nabla^2 v'} + \overline{w'\nabla^2 w'}\right. \\
&\left. - \frac{\overline{u'^2}}{r^2} - \frac{\overline{v'^2}}{r^2} + \frac{2}{r^2}\overline{u'\frac{\partial v'}{\partial\varphi}} - \frac{2}{r^2}\overline{v'\frac{\partial u'}{\partial\varphi}}\right]
\end{aligned}\right\} \quad (8)$$

where $\overline{q'^2} = \overline{u'^2} + \overline{v'^2} + \overline{w'^2}$

The terms in the energy equation for flow in a curved channel are grouped in the same manner as those in the straight parallel section (equation 3) for easier comparison. The viscous

terms in the energy equation could be separated again into transfer of work by viscous action and the mean dissipation function

$$\nu\left[\frac{1}{2}\nabla^2\overline{q'^2}-\frac{\overline{u'^2}}{r^2}-\frac{\overline{v'^2}}{r^2}+\frac{2}{r^2}\frac{1}{u'^2}\frac{\partial}{\partial\varphi}\overline{v'}+\left(\overline{\frac{\partial u_i'}{\partial x_j}\frac{\partial u_j'}{\partial x_i}}\right)-\left(\overline{\frac{\partial u_i'}{\partial x_j}+\frac{\partial u_j'}{\partial x_i}}\right)\overline{\frac{\partial u_i'}{\partial x_j}}\right] \quad (8a)$$

where x_i, x_j, and x_k are respectively $rd\varphi$, r and z. This notation also implies summation.

Fully Developed Flow in the Curved Channel:

The flow in this section is also steady which eliminates any time derivative of a time averaged quantity. The same definition of two-dimensional fully developed channel flow applies here, therefore:

$$V = W = 0 \quad ; \qquad \frac{\partial\bar{\theta}}{\partial t} = \frac{\partial\bar{\theta}}{\partial z} = \frac{\partial\bar{\theta}}{r\partial\varphi} = 0$$

except that $\bar{P} = f(\varphi)$

Then the Reynolds equations

$$\left.\begin{aligned}
&\frac{\partial}{\partial r}\left(\overline{u'v'}\right)+\frac{2\overline{u'v'}}{r}=-\frac{1}{\rho}\frac{\partial P}{r\partial\varphi}+\nu\left[\frac{\partial^2 U}{\partial r^2}-\frac{U}{r^2}\right]\\
&\frac{\partial}{\partial r}\left(\overline{v'^2}\right)+\frac{\overline{v'^2}}{r}-\frac{1}{r}\left[U^2+\overline{u'^2}\right]=-\frac{1}{\rho}\frac{\partial P}{\partial r}\\
&\frac{\partial}{\partial r}\left(\overline{v'w'}\right)+\frac{\overline{v'w'}}{r}=0
\end{aligned}\right\} \quad (9)$$

The third equation implies that $\overline{v'w'}=Cr$ but the constant must be zero because the fully developed two dimensional flow cannot sustain shear in the $r-z$ plane.

And the turbulent energy equation in the fully developed curved channel flow is:

$$\left.\begin{aligned}\overline{u'v'}\left[\frac{\partial U}{\partial r}-\frac{U}{r}\right]+\frac{1}{2}\cdot\frac{1}{r}\frac{\partial}{\partial r}\left(\overline{rq'^2v'}\right) &= -\frac{1}{\rho}\cdot\frac{1}{r}\frac{\partial}{\partial r}\left(\overline{rp'v'}\right)\\ +\nu\left[\frac{1}{2}\frac{\partial^2\overline{q'^2}}{\partial r^2}+\frac{1}{2r}\frac{\partial\overline{q'^2}}{\partial r}-\frac{1}{r^2}\left(\overline{u'^2}+\overline{v'^2}\right)+\frac{2}{r^2}\overline{\frac{1}{u'^2}\frac{\partial}{\partial\varphi}\frac{v'}{u'}}\right.&\\ \left.+\left(\overline{\frac{\partial u_i'}{\partial x_j}\frac{\partial u_j'}{\partial x_i}}\right)-\overline{\left(\frac{\partial u_i'}{\partial x_j}+\frac{\partial u_j'}{\partial x_i}\right)\frac{\partial u_i'}{\partial x_j}}\right]&\end{aligned}\right\}\quad(10)$$

The measurements in this channel allow us to compute the first term which is the production of turbulent energy in equation 10. The first bracket in the viscous term which is part of the viscous work can also be computed. Finally through the scales of turbulence which have been estimated from measurements approximation of the mean dissipation function can be obtained.

EXPERIMENTAL ANALYSIS

The Mean Velocity Measurements:

The time mean total pressure distributions across the channel were measured with a boundary layer Pitot tube of small aperture. The closest point near the wall that could be measured with this probe was 0.020 in. Wattendorf (2) from simple radial equilibrium of the mean motion has calculated the static pressure distribution across the fully developed section of the curved channel. Neglecting the turbulent terms in the radial Reynolds equations he has compared the calculated values with the measured values at the walls. Wattendorf states that "As a check, the measured value of the outer wall pressure was in good accordance with our calculations." Yeh (5) maintaining the turbulent terms in the radial Reynolds equation 9b, derives an exact radial equilibrium relationship for fully developed two dimensional flow in curved channels including all the fluctuating terms:

$$(P - P_i) = \frac{\rho}{2}\left[\overline{u'^2} + \overline{w'^2} - \overline{v'^2}\right] = \frac{1}{r^2}\int_{r_i}^{r} 2r(P_t - P_i)\,dr - \frac{\rho}{r^2}\int_{r_i}^{r} \overline{w'^2} r\,dr$$

where P is the mean static pressure at a given radius r; P_i is the static pressure at the inner wall and P_t is the total pressure at a given radius r. It is easily seen that if the turbulent terms in the equation above are neglected then simple radial equilibrium $dP/dr = \rho U^2/r$ is satisfied. Measured static pressures at the fully developed section are compared with the calculated values from the total head including and neglecting the turbulence terms (figure 4). The turbulence terms become important only in a region near the wall.

The dimensionless velocity distribution U/U_m at the fully developed curved section is in good accordance with that measured by Wattendorf (2). A comparison of the dimensionless velocity distributions as they proceed around the curve section are plotted in figure 5. The symmetrical profile labeled (initial 0°) corresponds to the fully developed straight section and the profile closest to the top of the sheet represents the velocity distribution at three consecutive stations in the curved channel, namely 172°, 204°, and 236°. The

experimental data show that the flow in the curved channel has reached equilibrium at 172°. The turbulence intensity shows the same evidence and this fact is discussed separately later in this paper. Velocity measurements were made at three vertical stations in order to ascertain the fact that two-dimensionality in the mean velocity existed. The results were very favourable. The center part of the velocity distribution in the fully developed curved section approaches that of a free vortex. The slope of the velocity $\partial U/\partial r$ is steeper near the outer wall than that of the inner wall. This fact together with the fact that the turbulent shear stresses are higher at the outer wall will bring higher turbulent energy production rates near the outer wall. The characteristic velocity U_* at the outer wall is 1.335 times larger than that at the inner wall. The ratio of the shear stresses at the walls will be the square of the ratio of the characteristic velocities. For further evidence of two-dimensionality, the space mean velocity at the mid-height of the straight fully developed section and at 172° and 236° were found to be respectively 89.75 f.p.s., 89.32 f.p.s. and 89.20 f.p.s. which

is in good agreement. The velocity and turbulence level distributions at the two fully developed sections are shown in figures 6 and 7.

Looking at the distributions presented in figure 6 and 7, the location of the nul point of the vorticity no longer coincides with the nul point of the laminar nor turbulent shear stresses. In the curved fully developed region, the nul value of the vorticity, laminar shear and turbulent shear assume separate locations. In the straight channel, all three nul points are in the same location and this determines the edge of the boundary-layer or free-stream. However in the curved channel it becomes difficult to locate the so-called point of free-stream or the point where the two boundary-layers meet. In other words the location of the point where the influence of the boundary layer at one wall ends and the influence of the other wall begins is not easily seen as in the case of the straight channel. These difficulties will be discussed again in the mean velocity similarity considerations.

The Static Pressure Drop Along the Length of the Channel:

The distribution of the wall static pressure drop in the direction of the mean flow is represented in Figure 3. The level of the static pressure is arbitrarily considered to be zero at the beginning of the straight "approach" section and the drop is expressed as a ratio of dynamic head based on the space mean velocity at the fully developed straight section. In the part of the paper describing the wind tunnel it was pointed out that the boundary layers growing on the ceiling and floor of the straight channel were evacuated through bleeding slots in order to prevent secondary motion in the curved channel. The effect of this bleeding can be seen in the static pressure drop a little after the mid-length of the straight channel. The entrance to the curved channel begins at $x/d = 60$. At this point, due to centrifugal forces in the curved section the static pressure drop divides into two separate curves. The upper one belongs to the outer wall and the lower one to the inner wall. The abscissa in the curved region represents actual arc lengths $rd\varphi$ of each wall. The pressure drop with angle $\partial p/\partial \varphi$ is the same on both walls. This fact was already established by

Wattendorf (2). The static pressure drop in the first quadrant of the curved channel is not smooth. The measured points deviate at about $\pm$ 0.05 of the dynamic head. When the metal walls were rolled, a seam had to be made 45° after the entrance to the curved channel and in addition as it was explained in the description of the wind tunnel that the first quadrant was of a different curvature than the rest of the curved section. As shown in Durand (3) if the surface of the wall is wavy with an approximate contour of a sine wave and if the maximum amplitude of the wave is in the order of 1/16 inch and the wave length about 18 inches then the variation of the static pressure as a ratio of the dynamic head is calculated and found to be $\pm$ 0.05. The waves on the walls of the first quadrant are certainly within the figures quoted above.

The Intensity of Turbulence:

The local root-mean square of the intensities of turbulence in the straight and curved portions of the channel were measured with hot-wires 0.0003 in. in diameter. The needles holding the wire and the wire itself were made of tungsten. A new technique of spot welding the wire in an argon atmosphere was developed and

discussed in (4). In an inert atmosphere the wire can be brought to an incandescent bright glow without burning the wire. This turned out to be also a satisfactory method of melting the impurities on the wire after a run. The welding was done with just a 1.5 volt dry-cell battery.

The calibration constants of the wire were determined in a calibration duct of low turbulence designed for the purpose. It was found from experience that a tungsten wire maintains a more constant calibration over a period of runs than a platinum wire of the same dimensions.

In order to insure the existence of two-dimensionality in the channel, measurements of intensity of turbulence were taken at three vertical stations in the fully developed straight section and the fully developed curved section. The results showed an absence of secondary flow in those regions. In order to establish that the flow was fully developed as far as intensity of turbulence was concerned in the curved channel, measurements were taken at three peripheral stations 172°, 204°, and 236°. The results were compared and variations were not more than the experimental accuracy. Evidence of

this work shows that the flow settles down to a fully developed pattern in an arc of 172°. This was also certified by Wattendorf (2) basing his reasoning on mean velocity profiles.

Wattendorf's second channel of smaller radius of curvature $d/r_o = 1/5$ which is half the value of the present channel still showed the same arc length necessary for the flow to become fully developed. For straight channel flow of a given width it takes the flow a certain number of widths (generally for favourable pressure gradient about 60 widths) until it reaches equilibrium. This reasoning leads us to believe that the equilibrium region in a curved channel cannot be a function of the angle alone because for very small radii of curvature the flow has to undergo a tremendous change in a small distance and this is not believed to be possible. From this discussion one can see the need of further investigations in channels with smaller radii of curvature.

The local turbulence intensity levels were measured in the fully developed regions and in addition in the curved transition region. The comparison of the distributions in Figure 8 show that the local level of turbulence u'/U enters the curved section with a symmetric pattern and undergoes a considerable change in

the first 26°. The local intensity level is increased on the outer wall by a considerable production and the intensity near the inner wall is suppressed. As the flow proceeds in the transition region of the curved channel, an attempt to restore the original distribution can be noticed. At the fully developed curved section, the values of the local turbulent intensities in the major half of the inner wall side remain smaller than those in the straight section and the values in the vicinity of the outer wall are higher than those in the straight section.

The analysis of the flow in the curved transition region is beyond the scope of this investigation although very interesting effects are taking place there.

The local turbulent intensity level in the lateral direction for the straight section and the radial direction for the curved fully developed section v'/U were measured with an X-meter with tungsten wires 0.0003 inch in diameter. The wires were approximately perpendicular and they were placed 45° to the direction of the mean flow. Figure 9 shows that curvature has a similar effect on v'/U as that on u'/U mentioned in the previous paragraph.

The maximum correlation coefficient $\frac{\overline{u'v'}}{\tilde{u}'\tilde{v}'}$ is plotted in Figure 10. A comparison is made with the values obtained by Laufer in a pipe flow at Re=50,000.

Measurements of w' were not carried out in this investigation; Since the root-mean square value of w' is very close to that of v'. In the analysis of this work they will be assumed to be the same.

Shear Stresses in the Straight Parallel Fully Developed Section:

Denoting in the conventional way the turbulent shear stress $\tau_t = -\rho\overline{u'v'}$ and the laminar shear stress $\tau_l = \mu\frac{\partial U}{\partial y}$, taking the first Reynolds equation in equation 4 and integrating with respect to y across the channel an expression for the total shear stress as a function of y can be obtained. Remembering that the pressure drop in x-direction is not a function of y.

$$\tau = \tau_t + \tau_l = \rho U_*^2 \left[1 - \frac{2y}{d} \right] \qquad (11)$$

which is a straight line with negative slope passing through zero in the middle of the channel. The term ρU_*^2 is the

shear stress at the wall. In the fully developed straight section, the shear stress at both walls has the same absolute value. The shear stress at the wall calculated from the pressure drop is:

$$\tau_w = -\frac{d}{2}\frac{\partial p}{\partial x}$$

The total shear stress distribution is plotted in Figure 11 together with the measured turbulent shear stress across the channel. The laminar shear stress is very small in the major portion of the channel. It becomes of importance only in a region very close to the wall. To be exact its value drops to 20% of the total shear at a friction distance parameter of $yU_w/\nu = 20$. This corresponds to a distance from the wall of approximately twice the thickness of the sublayer. Turbulent shear stress measurements in this section were only taken up to a value of $y/d = 0.05$. The experimental points depart somewhat from the values of shear stresses predicted by the pressure drop. The author believes that the values of shear stresses derived from the pressure drop are accurate and that the discrepancy lies in the measured values. It might be important

to note that by the same coincidence Laufer (1) in his shear stress measurements in the channel flow obtained excellent correlation between his measured quantities and the ones calculated from the pressure drop at the two lower Reynolds Numbers. For its highest Reynolds Number of 61,600 the measured shear stresses were at most 30% lower than the calculated values from the pressure drop. At the present moment the author does not know of any explanation except of a Reynolds Number effect based on the wire diameter.

The turbulent shear stresses were measured with an X-meter and independently with a wire allowed to rotate in the air stream. The wires made of tungsten were 0.0003 inch in diameter and copper plated leaving a bare length approximately 1/8 inch.

The measured shear stress was obtained by taking the difference of the mean square of the a-c components of the voltages of the two wires.

$$\overline{e_1^2} = \overline{\left(-\frac{\partial E_1}{\partial U}u' - \frac{\partial E_1}{U\partial\theta}v'\right)^2} \text{ and } \overline{e_2^2} = \overline{\left(-\frac{\partial E_2}{\partial U}u' + \frac{\partial E_2}{U\partial\theta}v'\right)^2}$$

The shear stress coefficient at the wall is $\frac{\tau_w}{\rho U_m^2} = .001735.$

Shear Stresses in the Fully Developed Curved Section:

The tangential component of the Reynolds equation (9) can also be written in the form:

$$\frac{1}{\rho} r \frac{\partial P}{\partial \varphi} + \frac{\partial}{\partial r}(r^2 \overline{u'v'}) = \nu \frac{\partial}{\partial r}\left[r^3 \frac{\partial}{\partial r}\left(\frac{U}{r}\right)\right]$$

Keeping again in mind that the pressure drop $\partial P / \partial \varphi$ is not a function of r, the equation above can be integrated with respect to r:

$$\frac{1}{2} \frac{\partial P}{\partial \varphi} = -\rho \overline{u'v'} + \mu r \frac{\partial}{\partial r}\left(\frac{U}{r}\right) + \frac{C}{r^2} \qquad (12)$$

The integration brings a constant C to be determined by the vanishing value of the shear stress in the channel. The total shear stress is made out of two parts. The turbulent shear stress $\tau_t = -\rho \overline{u'v'}$ and the laminar shear stress $\tau_\ell = \mu r \frac{\partial}{\partial r}\left(\frac{U}{r}\right)$

If r_n is denoted to be the radial distance where the shear stress vanishes inside the channel, the integration constant is determined and the total shear stress as a function of the radius and the pressure drop is found to be:

$$\tau = -\frac{1}{2} \frac{\partial P}{\partial \varphi}\left[\left(\frac{r_n}{r}\right)^2 - 1\right] \qquad (13)$$

The value of r_n is determined from the experimental measurements and the total shear stress distribution plotted as a function of R/d in Figure 12. The shear stress at the inner wall is smaller than that at the outer wall. The values of the shear stress coefficients are:

at the inner wall $\frac{\tau_i}{\rho U_m^2} = 0.00139$; at the outer wall $\frac{\tau_o}{\rho U_m^2} = 0.00248$

These values were used for the universal velocity distribution U/U_* versus $R\bar{U}_*/\nu$ and they are seen to be satisfactory when compared with those of the straight channel. This comparison is made in Figure 25. The experimental turbulent shear stress measurements show the same consistent tendency that their absolute value is less than the calculated shear stress. This discrepancy has already been discussed for the straight parallel section. Wattendorf (2) attempted through the mixing length theory to predict the vanishing point of the total shear stress in the curved channel. He found that neither of the assumptions:

$$\tau = \rho\varepsilon\left(\frac{\partial U}{\partial r} - \frac{U}{r}\right) \quad \text{nor} \quad \tau = \pm\rho l^2\left(\frac{\partial U}{\partial r} + \frac{U}{r}\right)^2$$

gave satisfactory answers.

Here ε is the apparent coefficient of kinematic viscosity and ℓ the mixing length. The total shear stress does not vanish where the laminar shear is zero nor where the vorticity vanishes(as in a straight channel flow.)Evidence from Wattendorf's work also shows the independence of the total shear stress, the laminar shear and the vorticity. The location of the nul shear stress point will be discussed in more detail in the next section.

Location of the Nul Shear Stress in Curved Channels:

In the discussion of the total shear stress in the fully developed section of the curved channel, equation 13 was derived for the distribution of the shear stress as a function of the peripheral pressure drop, the radius where the shear stress assumes a nul value and the radius where the shear stress is to be computed.

$$\tau = -\frac{1}{2}\frac{\partial P}{\partial \varphi}\left[\left(\frac{r_n}{r}\right)^2 - 1\right]$$

At the walls of the curved channel the values of the shear stress are

$$\tau_o = -\frac{1}{2}\frac{\partial P}{\partial \varphi}\left[\left(\frac{r_n}{r_o}\right)^2 - 1\right] \qquad \text{outer wall}$$

$$\tau_i = -\frac{1}{2}\frac{\partial P}{\partial \varphi}\left[\left(\frac{r_n}{r_i}\right)^2 - 1\right] \qquad \text{inner wall}$$

Using the definition for U_* and dividing the absolute value of the two wall shear stresses, an expression can be found for the location of the nul shear stress in the channel as a function of the ratio of the U_* values at both walls and the ratio of the width of the channel to the inner radius of curvature:

$$\left(1 + \frac{R_n}{r_i}\right)^2 = 1 + \frac{2\left(\frac{d}{r_i}\right) + \left(\frac{d}{r_i}\right)^2}{\left(\frac{U_{*o}}{U_{*i}}\right)^2\left(1 + \frac{d}{r_i}\right)^2 + 1} \qquad (14)$$

Here R_n is the distance of the nul value of the shear stress from the inner wall, d is the width of the channel and r_i is the inner radius of curvature. A family of curves for various ratios of U_{*_o}/U_{*_i} which is a function of

Reynolds number and roughness of walls is plotted in Figure 13. The ratio of U_{*_o}/U_{*_i} in this work is 1.33 and the ratio of the channel width to the inner radius is 0.111 . The two values given above correspond to a ratio $R_n/r_i = 0.035$ or to an actual distance from the inner wall of 0.945 inch and a ratio $R/d = 0.135$ which is the exact location on the shear stress distribution in Figure 12. Wattendorf (2) in his second channel had a U_* ratio of 1.195 and a value of $d/r_i = 0.25$. This corresponds to $R_n/r_i = 0.08$ and since his inner wall had a radius of curvature of 20 cm., the nul shear stress occurs at 1.6 cm. from the inner wall. The limit of equation 14 as r_i approaches infinity reduces to $U_{*_o}/U_{*_i} = 1.0$ which is the value for the fully developed straight channel.

Refering to Figure 13, in the region below the dotted line, the nul point is nearer the inner wall and in the upper region the nul point is nearer the outer wall.

The Spectrum of the Velocity Fluctuations:

The energy spectra of the turbulent velocity components u' and v' have been measured and are shown in figures 14, 15, 16, and 17. The figures are plotted in such a way that the integrated curves represent the kinetic energy associated with the velocity component analyzed. A Hewlett-Packard wave analyzer was used for the purpose. A filter half band width of 30 cycles per second was used for all the measurements. The output of the analyzer which is proportional to the ordinates of the curves is the portion of the total signal intercepted within the band width of the analyzer at the particular tuning frequency. The wave number k is used for abcissa in preference of the frequency because it is associated with the size of the eddy. It must be made clear that these curves represent a so-called "one dimensional spectrum" and that the concept of kinetic energy of a fluid particle associated with its size cannot be drawn from them. Figures 14 and 16 represent the spectra associated with u' in the straight and curved channel. The influence of curvature is slightly noticed in the low values of wave number

or low frequencies. The next two figures 15 and 17 which are the spectra of the v' component show a marked effect of curvature. The larger motions of the fluid elements are more affected by the curvature than the smaller ones. With smaller radii of curvature the influence should be felt in eddies of smaller sizes. Curves of the second moment of the spectra are also shown in Figures 18, 19, 20 and 21. Actually, the area under the second moment of the three-dimensional power spectrum is a measure of the turbulent energy dissipation and they are inversely proportional to the square of the microscale of turbulence.

The Microscale of Turbulence:

The microscale of turbulence is a length associated with the turbulent dissipation and originated from the statistical treatment of trubulence. Since it has been shown that at large enough Reynolds numbers the smaller size eddies contribute to the main dissipation of turbulent energy into heat, roughly speaking, the microscale of turbulence, λ , is an average linear dimension

of the smaller size eddies contributing to the dissipation. A discussion on the average size of the eddies will be a different topic of discussion. In his work on the statistical theory of turbulence, G. I. Taylor has shown that the microscale can be related to the Eulerian space correlation. It can be shown that

$$\left.\frac{\partial^2 R_x^{u'}}{\partial x^2}\right|_{x=0} = -\frac{1}{\lambda_x^2}$$

$$\left.\frac{\partial^2 R_y^{v'}}{\partial y^2}\right|_{y=0} = -\frac{2}{\lambda_y^2}$$

where R stands for the space correlation coefficient of the turbulent velocities. G. I. Taylor has also shown the relationship between the space correlation coefficient and the one dimensional trubulent energy spectrum. It followed from Taylor's work that the space correlation coefficient is the cosine transform of the one dimensional energy spectrum function (9)

$$R_x^{u'} = \int_0^\infty F_{\overline{u'^2}}(n)\ \frac{2\pi n x}{U}\, dn$$

$$F_{\overline{u'^2}}(n) = \frac{4}{U}\int_0^\infty R_x^{u'} \cos\ \frac{2\pi n x}{U}\, dx$$

Using the relations stated above one gets the microscale in terms of the energy spectrum. One dimensional energy spectra for the u' and v' velocity components were measured with a Hewlett-Packard wave analyzer. Space correlations were not included in this work, and therefore all microscale calculations will be based on the spectrum functions.

$$\frac{1}{\lambda_x^2} = \frac{4\pi^2}{U^2}\int_0^\infty n^2 F_{\overline{u'^2}}(n)\,dn$$

$$\frac{2}{\lambda_y^2} = \frac{4\pi^2}{U^2}\int_0^\infty n^2 F_{\overline{v'^2}}(n)\,dn$$

Where $F_{\overline{u'^2}}(n)$ is the fraction of the turbulent energy $\overline{u'^2}$ associated with a band width dn at a frequency n. Since w' measurements have not been taken, λ_z will be assumed to have the same magnitude as λ_y or λ_x. Furthermore for small turbulence levels, Taylor has made the hypothesis that in the direction of the mean flow the time relationships could be interchanged with space relationships through the velocity at the point. Experimental evidence has shown that the time and space correlation

coefficient in the direction of the mean flow are essentially the same if the mean velocity is constant. The rate of turbulence energy dissipation can be expressed in the form

$$\left(\overline{\frac{\partial u'}{\partial x}}\right)^2 = \frac{\overline{u'^2}}{\lambda_x^2} \qquad \text{and} \qquad \frac{1}{2}\left(\overline{\frac{\partial u'}{\partial y}}\right)^2 = \frac{\overline{u'^2}}{\lambda_y^2}$$

and since the space derivative dx in the direction of the mean flow can be interchanged with Udt then a second method of measuring λ_x or λ_y can be obtained

$$\frac{1}{U^2}\left(\overline{\frac{\partial u'}{\partial t}}\right)^2 = \frac{\overline{u'^2}}{\lambda_x^2}$$

The time derivative of u' was measured with an electronic differentiator. Distributions of the second moment of the power spectra $n^2\overline{F}(n)$ are shown in figures 18, 19, 20, and 21.

In isotropic turbulence it is necessary that the three components of the microscale* be equal. In fully developed channel flow or shear flow this condition is no longer satisfied. At a point in the channel flow

* As defined in the first equation of this page.

variations of the three component microscales will take place as well as variations of each component across the channel. Figures 22 and 23 show distribution of the calculated microscales in the fully developed straight and curved sections. The two independent methods of obtaining λ_x and λ_φ show good correspondence. The essential importance that can be drawn from the distribution of the microscales is that of the influence of the curvature. It is apparent from the distributions shown in Figures 22 and 23 that the microscale in the direction of flow decreases in the portion of the inner wall of the fully developed curved section and increases in the outer portion. The radial component microscale in the curved section is larger than λ_y in the straight section for the major portion of the channel width except near the inner wall where they are equal. This does not necessarily imply that the energy dissipated near the outer wall is smaller than that at the inner wall because although the microscales are larger the turbulent kinetic energies are larger too. As compared with Laufer's channel flow

at the highest Reynold's number, the levels of the microscale are higher in this channel although the mean velocity is larger than that of Laufer. As mentioned at the beginning of this paragraph two independent checks of the microscale measurements were made and the measurements are consistent with each other. The values of λ/d are approximately three times larger than those of Laufer at a Reynolds number of 61,600. The average ratio of L/d is exactly the same as that found by Laufer. As a result of the high values of the microscale the Reynolds number of the turbulence $\tilde{q}'\lambda/3\nu$ are also high. It is customary in isotropic turbulence behind grids to give the proportionality factor between the ratio of the scales and the reciprocal of the Reynolds number of turbulence. The proportionality factor was found to be fairly constant across the channel in the straight and curved channel. The values of the proportionality factor ranged from 15 to 20. for this channel.

$$\frac{\lambda}{L} = \frac{A}{\sqrt{Re_L}}$$

The Integral Scale of Turbulence:

In the definition of the microscale it was stated that the integral scale denoted by L can be considered as the average size of the eddies in turbulence. This length is mathematically related to the space integration of the Eulerian space correlation coefficient:

$$L_x = \int_0^\infty R_x \, dx$$

$$L_y = \int_0^\infty R_y \, dy$$

$$L_z = \int_0^\infty R_z \, dz$$

In order to obtain L_x, L_y and L_z two independent hot wires must by used where one is generally maintained fixed and the other moved in the direction of x, y or z. The average of the product of the wire signals divided by the product of the individual root-mean square values of the signals determines the correlation coefficient. Since the correlations of velocities were not measured in this work, an alternate and simpler approximate

method depending on the compensated and uncompensated values of the hot-wire signal was used.(1). This method can only be valid for the determination of L in the direction of flow. In order to have a general idea of the variations of L_r across the channel, the same method was used. Although the results of radial integral scale are not exact, they give a good idea of the trend across the channel. Figures 22 and 23 show the distribution of the integral scales across the channel and the effect of curvature on the eddy size. This effect is exactly the same as that experienced by the microscale. A second independent method of estimating the integral scale was accomplished by finding the extrapolated values of the power spectrum at zero frequency. The values obtained in this manner are not represented here but their magnitude and trend are consistent with those shown in Figures 22 and 23. The magnitude of the integral scale as a ratio of the width of the channel compares very well with those of other experimenters.

From the stability criterion for laminar boundary layer flow in curved channels first explained by Rayleigh (23) and then by Prandtl (24), it can be deduced that any perturbation near the outer wall will be unstable. The same perturbation near the inner wall will show to be stable. If a particle near the outer wall is moved towards the outer wall it will find itself in a surrounding with less pressure gradient and therefore will continue to move in the same direction. If the particle is moved away from the outer wall it will find itself in a surrounding with larger radial pressure gradient and therefore will continue moving away from the outer wall. This implies instability because the disturbance grows in the direction it originated. The opposite takes place near the inner wall, any perturbation brings a restoring force which brings the particle back to where it started. Near the inner wall, $\overline{u'v'}$ is negative which means if the perturbation is such that ΔU or u' is positive then v' must be negative or visa versa. This consideration shows the same stabilizing effect near the inner wall and unstabilizing effect near the outer wall. As a conclusion the outer wall can be called an "agitated region" and the inner wall a "damped region".

Similarity Considerations:

The question of finding similarity in all properties of fully developed flows in general is still an open one. There is enough evidence that in a fully developed straight parallel channel the mean velocity as a ratio of U_* is a function only of yU_*/ν near the wall regardless of the Reynolds number. The turbulent properties of the flow in geometrically similar fully developed flows show a larger variations from a so-called universal law. This departure is even larger in geometrically non-similar flows. The turbulence measurements of a fully developed flow in a diffuser or in a curved channel (Figure 24) show this departure very well. There is enough evidence that the mean velocity in the vicinity of the wall even for geometrically non similar flows shows a definite dependency on the dimensionless parameter yU_*/ν . The velocity measurements in the two walls of the curved channel together with those of the straight channel are shown in Figure 25. In the largest portion of the boundary layer it is generally assumed that the dependence of

the mean velocity is on y/d rather than yU_*/ν . This dependence has been shown to be fairly true for straight channels with favorable pressure gradients. The symbol d stands generally for the half width of the channel where the shear stress and the vorticity are nul at that point. The similarity of the mean velocity in the major center portion of the channel is expressed in the form

$$\frac{U_m - U}{U_*} = f\left(\frac{Y}{d}\right)$$

where U_m is the maximum velocity or the free-stream velocity which also occurs at the center of the channel for fully developed straight channel or pipe flow. In a curved channel, the point of nul vorticity is where the product Ur assumes a maximum or in other words where $d(U\mathcal{T})/dr$ is zero. On the other hand the point where the laminar shear stress is zero does not correspond to the same nul point of the vorticity. The nul value of the laminar shear occurs where $d(U/r)/dr$ is zero. The major difficulty that arises from this is that of determining where one boundary layer

ends and the other begins. Wattendorf (2) assumed that the free-stream point occurred where the free-vortex velocity distribution was tangent to the actual distribution or in other words where the vorticity was nul. Taking the difference between the potential velocity of the free vortex and the actual measured velocity at each r and dividing by the corresponding U_* at each wall he plotted his points as a function of R/b. The width b was the so-called thickness of the layer which is the distance from the wall to the location of the nul vorticity. Distributions $(U_p - U)/U_*$ versus R/b were not satisfactory. The inner wall values, the outer wall values and the values of the straight channel lined-up on three entirely different curves. The results of the present work show exactly the same behavior. Finally by rearrangement of the variables Wattendorf succeeded in collapsing the dimensionless mean velocity distributions at the inner and outer wall to a single curve but this treatment did not agree with the distribution in the straight parallel channel. Another consideration that was brought in was that in a straight

channel the free stream corresponds to U_m = const and for the curved channel Ur = const. It was decided then to try

$$\frac{(Ur)_{max} - (Ur)}{(U_* r)_{o \text{ or } i}} = f\left(\frac{R}{b}\right)$$

This consideration did not show any better results than the others. The author for lack of better ideas leaves this particular phase of the problem where Wattendorf left it.

In Figure 25, the velocities in the boundary layers near the walls are plotted together with Wattendorf's measurements in channel II which corresponds to $\frac{d}{r_o} = \frac{1}{5}$ or twice the value as compared to that investigated by this author. It is apparent that in the region near the walls, the straight wall and the two curved walls show good similarity in the mean velocity up to a distance from the wall where they branch out. The branching points for both channels do show that they are not essentially a function of $\frac{yU_*}{\nu}$. The author followed Clauser's suggestion,

that the points in the neighborhood of the inner wall should be more sensitive to R/r or $\frac{d-R}{r}$ for the outer wall, when the boundary layers at both curved walls in Wattendorf's channel and the present one were plotted as a function of R/r or $\frac{d-R}{r}$ the branching points fall at approximately the same value of the abcissa, but unfortunately the values of the ordinates $\frac{U}{U_*}$ did not correspond. This implies very clearly that the distance from the wall divided by the radius of curvature at that distance is an essential parameter in curved flows. A similar influence of the radius of curvature can also be attributed to the turbulence and one can see clearly from the spectral distributions in the curved channel that not all sizes of eddies are influenced the same amount by the curvature. A similar parameter $\frac{1}{kr}$ can be said to be an essential one in the turbulent motion in curved channels.

Prcduction of Turbulent Energy:

From the turbulent energy equation 5, the turbulent energy produced per unit time and per unit volume in a two dimensional fully developed flow in a parallel straight channel is $\overline{u'v'}\,\partial U/\partial y$. For a two-dimensional fully developed flow in a curved channel the production term in cylindrical coordinates in equation 10 is $\overline{u'v'}\left[\frac{\partial U}{\partial R} - \frac{U}{R}\right]$ In the limit, when the radius of curvature r approaches infinity, the two expressions above become identical. It has been established that most of the turbulent energy is produced in a region very close to the walls. The maximum rates occur at the edge of the laminar sub-layer which corresponds generally to a friction distance parameter $\frac{yU_*}{\nu} = 10$. The rate of energy production drops by a factor of ten when the friction distance parameter is 100. (corresponding approximately to 0.050 inch from the wall in this channel). In the distance where $25 < \frac{yU_*}{\nu} < 100$ the variations of the turbulent shear stress $\rho\overline{u'v'}$ are negligable and the dimensionless shear stress $\frac{\overline{u'v'}}{U_*^2}$ is nearly constant and equal to 1.0. The space derivative of

the mean velocity changes considerably in this region and it is necessary to have accurate values of these derivatives to abtain reliable values of the turbulent energy production. In the sub-layer, the opposite situation occurs namely that the mean velocity space derivative is constant and the turbulent shear stress varies from its maximum to a value of zero at the wall. For the determination of the mean velocity space derivative graphical differentiation is not generally very adequate.

Let us attempt at this point to formulate similarity conditions for the production of turbulent energy. In a fully developed flow in a region close to the wall including the laminar sublayer (where the production is significant), it has been shown that:

$$\frac{U}{U_*} = f\left(\frac{yU_*}{\nu}\right) \qquad \text{and that} \qquad \frac{\overline{u'v'}}{U_*^2} = g\left(\frac{yU_*}{\nu}\right)$$

From these two expressions a dimensionless production term can be obtained by differentiating the first expression and multiplying by the second.

$$\frac{\nu}{U_*^4}\overline{u'v'}\frac{\partial U}{\partial y} = f'\left(\frac{yU_*}{\nu}\right) g\left(\frac{yU_*}{\nu}\right) = h\left(\frac{yU_*}{\nu}\right)$$

This implies that the dimensionless rate of production of turbulence energy is universal near the wall, i.e., it is only dependent on $\frac{yU_*}{\nu}$ the friction distance parameter. Away from the wall it is found that the dependency of the mean velocity and the turbulent shear stress is of a different nature.

$$\frac{U}{U_*} = \ell\left(\frac{y}{d}\right) \quad \text{and} \quad \frac{\overline{u'v'}}{U_*^2} = m\left(\frac{y}{d}\right)$$

There the dimensionless rate of production is

$$\frac{d}{U_*^3}\,\overline{u'v'}\,\frac{dU}{dy} = \ell'\left(\frac{y}{d}\right) m\left(\frac{y}{d}\right) = n\left(\frac{y}{d}\right)$$

Away from the wall in the center portion of the channel the dimensionless production rate of turbulent energy is only a function of y/d. To verify the validity of the analysis shown above, the author will compare the experimental values obtained in this channel and those measured by Laufer (10) in the pipe flow.

It is well established that the dimensionless mean velocity distribution near the wall outside the laminar sublayer of a fully developed flow obeys the universal

logarighmic law:

$$\frac{U}{U_*} = A + B \log_{10} \frac{yU_*}{\nu}$$

where A and B are constants. This law holds well in the straight fully developed approach section for values $25 < \frac{yU_*}{\nu} < 2000$ and for the fully developed curved section of this wind tunnel $25 < \frac{yU_*}{\nu} < 200$ (Figure 25). In the laminar sublayer region $\frac{U}{U_*} = \frac{yU_*}{\nu}$. By differentiating the logarithmic equation the derivative of the mean velocity can be found to be: $\frac{\nu}{U_*^2} \frac{dU}{dy} = \frac{.4343 B \nu}{y U_*}$ Since B and U_* are constants the derivative $\frac{dU}{dy}$ in the region where the law applies is given as a function of y. In the laminar sublayer the space derivative of the velocity is U_*^2/ν. The turbulent shear stress distribution in a fully developed straight channel from equation 11 is:

$$\frac{\overline{u'v'}}{U_*^2} = 1 - \frac{2y}{d}$$

This expression is valid from anywhere in the channel up to the buffer zone. In the region near the wall the term $1/y >> 2/d$.

The turbulent energy production in a dimensionless form can be expressed as previously

$$P_{r_*} = \frac{\nu \overline{u'v'}}{U_*^4} \frac{dU}{dy}$$

and this quantity outside the buffer region becomes:

$$P_{r_*} = \frac{.4343 B \nu}{U_*} \left[\frac{1}{y} - \frac{2}{d} \right] \qquad (15)$$

and in the laminar sublayer:

$$P_{r_*} = \frac{\overline{u'v'}}{U_*^2}$$

If one plots these two equations as a function of yU_*/ν, they agree extremely well with Laufer's (10) measured data and the data obtained in this investigation for the straight channel and also for the boundary layers in the inner and outer walls of the curved fully developed section. (Figure 26) The full line represents the analytic values calculated from Laufer's value of B and U_*. The equations depart from the experimental points only in

the immediate vicinity of the edge of the sub-layer. This could be overcome if $\frac{U}{U_*} = f\left(\frac{yU_*}{\nu}\right)$ is more accurately approximated at the edge of the sub-layers.

The mere fact that the dimensionless production curves of the inner and outer walls of the curved channel and of the straight section and also of the values measured by Laufer (10) coincide so well, suggests that the turbulent production is only dependent on yU_*/ν near the wall. Then it becomes apparent that the absolute value of the turbulent energy production is simply proportional to U_*^4 or to the square of the shearing stress at the wall. The values of U_* for this investigation are as follows: $U_* = 4.08$ ft/sec. for the straight channel, $U_* = 3.57$ ft/sec. for the inner wall and $U_* = 4.77$ ft/sec. for the outer wall. The relative comparison of the rates of energy production near the walls of this channel are plotted in Figure 27. In this figure the maximum production value for the straight channel has been made aribtrarily equal to 1.0. These results substantiate very well the fact that the turbulent intensity on the side of the outer wall is higher than that measured near the inner wall.

The Dissipation of Turbulent energy:

In the analytical considerations the dissipation function was fully represented in tensor notation in equations 3a and 8a as $\overline{\Phi} = \mu \overline{\left[\frac{\partial u_i'}{\partial x_j} + \frac{\partial u_j'}{\partial x_i}\right]\frac{\partial u_i'}{\partial x_j}}$. This expression when expanded contains twelve mean derivative terms and their sum specifies the mean rate of turbulent energy dissipation at a given point in the flow:

$$\overline{\Phi} = \mu\left[2\overline{\left(\frac{\partial u'}{\partial x}\right)^2} + 2\overline{\left(\frac{\partial v'}{\partial y}\right)^2} + 2\overline{\left(\frac{\partial w'}{\partial z}\right)^2} + \overline{\left(\frac{\partial v'}{\partial x} + \frac{\partial u'}{\partial y}\right)^2} + \overline{\left(\frac{\partial w'}{\partial y} + \frac{\partial v'}{\partial z}\right)^2} + \overline{\left(\frac{\partial u'}{\partial z} + \frac{\partial w'}{\partial x}\right)^2}\right] \qquad (16)$$

The author does not know of any direct way of measuring the space derivative terms in the expression shown above. Generally an alternate approximate method is used to estimate each term in the dissipation function. Through Taylor's hypothesis for small intensities of turbulence, the space derivatives in the direction of the mean flow $\left(\frac{\partial}{\partial x}\right)$ is always related to the time derivative and the mean velocity $\frac{\partial}{U\partial t}$. With an electronic differentiator the voltage fluctuations of the hot-wire can be differentiated. The other space derivatives can also be estimated through Taylor's (13)

expansion of the space correlation coefficient into the space derivatives of the turbulent velocities

$$R_y = 1 - \frac{1}{2!}\frac{y^2}{\overline{u'^2}}\overline{\left(\frac{\partial u'}{\partial y}\right)^2} + \frac{1}{4!}\frac{y^4}{\overline{u'^2}}\overline{\left(\frac{\partial^2 u'}{\partial y^2}\right)^2} - \cdots\cdots$$

From the above expression it follows that the curvature of the correlation coefficient R_y curve at the origin is a measure of $\overline{\left(\frac{\partial u'}{\partial y}\right)^2}$

$$\overline{\left(\frac{\partial u'}{\partial y}\right)^2} = 2\overline{u'^2}\lim_{y\to 0}\left(\frac{1-R_y}{y^2}\right) = \frac{2\overline{u'^2}}{\lambda_y^2} \qquad (17)$$

A similar analysis can be done for the remaining space derivatives except of course that the product of derivatives in equation 16 bring special difficulties.

If the turbulence is statistically isotropic the mean rate of turbulent energy dissipated reduces to

$$\overline{\Phi} = 15\mu\frac{\overline{u'^2}}{\lambda^2} \qquad (18)$$

Laufer in his channel flow measurements has found that for his work the use of λ_y in the isotropic relation shown in equation 18 gave him a closer estimate of the dissipation

than any other microscale. In the present work, it was mentioned that the values of the microscale measured were suprisingly high compared with other experimenters. It can be seen from the isotropic relation given above that the absolute values of the dissipation across the channel will turn out to be smaller as compared with the values of other experimenters. It is for this reason that the calculated values of the dissipation in this channel are made relative to the value of the dissipation at the center of the curved channel. Figure 28 shows the relative magnitude of the mean rate of dissipation at the three walls. The value of the dissipation at the center of the curved channel was arbitrarily chosen to be 1.0. The curves in Figure 28 show near the wall the same trend as the production of turbulent energy shown in Figure 27.

CONCLUSIONS

Until the time of the writing of this paper, the only experimental investigations on flow in curved channels available and known to the author were based only on mean velocity and mean pressure measurements. The purpose of this paper is to bring additional information on the effect of curvature and especially on some important turbulent statistical quantities. The transition problem from straight channel flow to curved fully developed flow is beyond the scope of this paper. A comparison is made here on the effect of curvature on an initial straight fully developed flow and the final character of the flow as it reaches equilibrium in the curved channel.

1. The work performed in this curved channel is with walls of comparatively large radius of curvature, it appears evident that the flow reaches equilibrium in the curved section at approximately 170° of constant curvature. It must be kept in mind that the initial conditions of the flow at the entrance of the curved channel are also fully developed.
2. The effect of curvature on the mean velocity distribution is such that the center portion of the flow approaches the velocity distribution of a free vortex.

3. The use of simple radial equilibrium neglecting the turbulent terms in the radial Reynolds equation shows only a maximum of 1/2% discrepancy when referred to the dynamic pressure at the point.

4. The level of turbulence intensity is reduced in the portion of the inner wall and increased towards the outer wall. This fact agrees well with Rayleigh's stability criterion.

5. Depending on the Reynolds number of the mean flow and on the roughness of the curved walls, an expression is given for the determination of the location of the nul shear stress in the curved channel.

6. The effect of curvature on the scales of turbulence is to increase them near the outer wall and decrease them near the inner wall. In different words one may say that the average size of the eddies magnified near the outer wall and damped near the inner wall as compared with their initial size in the straight channel. From the one-dimensional power spectra it becomes evident that the energy associated with the large particles are reduced near the inner wall and augmented near the outer wall.

7. As compared with the straight channel, the turbulent energy produced and dissipated is larger at the vicinity outer wall and smaller at the inner wall.

8. The logarithmic similarity law for the mean velocity in the vicinity of the walls applies well for the straight and curved walls. The turbulent quantities show a marked distinction when compared with the conventional straight wall similarity conditions.

APPENDIX I

STATIC AND DYNAMIC HEAT TRANSFER PROPERTIES OF THE HOT-WIRE ANEMOMETER

Heat Convection Theory of Hot-Wires

The differential equation governing the transfer of heat by forced convection from a cylinder into an incompressible homogeneous fluid passing over the heated cylinder is represented in Cartesian coordinates by:

$$\rho c \frac{DT}{Dt} = \rho c \left[\frac{\partial T}{\partial t} + u \frac{\partial T}{\partial x} + v \frac{\partial T}{\partial y} + w \frac{\partial T}{\partial z} \right] = \lambda \nabla^2 T \qquad \text{I-I}$$

The velocity components u, v, and w functions of x, y, z and t must be separately determined from the Navier-Stokes equations for the particular case of fluid flow around a cylinder. When the fluid flow field is determined then by substituting the three velocity components u, v, and w in equation I-1, the temperature field may be determined.

Boussinesq first and then King were interested in obtaining a solution for the temperature distribution of an air stream passing over a heated cylinder.

By assuming steady state in a two-dimensional frictionless fluid, Boussinesq (19) succeeded in transforming the simplified equation I-1 from flow passing over a cylinder to

flow over a flat plate. Then in the new coordinate system equation I-1 becomes:

$$\rho c U \frac{\partial T}{\partial \Phi} = \alpha \left[\frac{\partial^2 T}{\partial \Phi^2} + \frac{\partial^2 T}{\partial \Psi^2} \right] \qquad \text{I-2}$$

where U in this case is a constant, Φ is the coordinate along the plate in Figure (29) and Ψ is the coordinate perpendicular to the plate.

Boussinesq Solution

In 1903 Boussinesq made the following assumptions:

(a) for the problem of Fig. (29) mass only flows in the Φ direction,

(b) α is a constant, c and ρU are also constants,

(c) the thermal conductivity in the Φ direction is zero or $\frac{\partial^2 T}{\partial \Phi^2} \ll \frac{\partial^2 T}{\partial \Psi^2}$

(d) the initial temperature of the fluid is a constant, T_o,

(e) the temperature T_f of the plate is $f(\Phi) + T_o$, where the function $f(\Phi)$ should be such that when $\Phi < 0$, $f(\Phi) = 0$,

(f) the temperature of the plate should be the same as that of the fluid in contact with the plate; or when $\Psi = 0$, then $T = T_f$

On account of the conditions imposed above, the differential equation I-2 reduced to:

$$\frac{\partial T}{\partial \Phi} = \frac{\varkappa}{\rho U c} \frac{\partial^2 T}{\partial \Psi^2} \qquad \text{I-3}$$

and the solution becomes:

$$T - T_o = \frac{2}{\sqrt{\pi}} \int_{\mu}^{\infty} f\left(\Phi - \frac{\Psi^2}{4m\mu^2}\right) e^{-\mu^2} d\mu \qquad \text{I-4}$$

where $\mu = \frac{\Psi}{2\sqrt{m\Phi}}$ and $m = \frac{\varkappa}{\rho U c}$

The total heat flow per unit length can be found then; taking $T_o = 0$

$$q' = \int_0^{2D} q''(\Phi)\, d\Phi = -\int_0^{2D} \varkappa \left(\frac{\partial T}{\partial \Psi}\right)_{\Psi=0} d\Phi = \frac{4\sqrt{2}}{\sqrt{\pi}} T_p \sqrt{Pe} \qquad \text{I-5}$$

and the average Nusselt's number is:

$$\overline{Nu} = \frac{4\sqrt{2}}{\pi^{3/2}} \sqrt{Pe} \qquad \text{I-6}$$

This solution gives a linear relationship between the Nusselt's number and the square-root of the Péclet number.

King's Solution

In 1914, L. V. King (20) presented a solution to equation I-2. This means that contrary to Boussinesq the thermal conductivity in the Φ direction is non-zero.

Also in this case, on account of the transformation from fluid flow around a cylinder to fluid flow along a flat plate, there exists no flow of fluid in the Ψ direction. The thermal conductivity $\varkappa$ is constant in all directions, and the same assumption applies to the specific heat and the density. The fluid is assumed to be non-viscous and potential. The boundary conditions set by King are as follows:

(a) the rate of heat flow per unit area q" over the plate is constant and uniform,

(b) the initial fluid temperature T_o is a constant,

(c) the temperature of the fluid T_f is equal to the temperature of the plate T_p only at the downstream edge. To say that $T_p = T_f$ everywhere on the plate will be inconsistent with condition (a).

The solution of the temperature field obtained by King is the following:

$$T(x,y) - T_o = \frac{1}{2\pi\varkappa}\int_0^{2D} \Theta(\xi)\, e^{\frac{1}{2m}(\Phi-\xi)}\, K_o\left|n\sqrt{\Psi^2+(\Phi-\xi)^2}\right| d\xi \qquad \text{I-7}$$

Where $q'' = \int_0^{2D} \Theta(\xi)\, d\xi$ is the heat flow per unit area of the plate assume as a constant.

The solution given in equation I-7 was further simplified by King by expanding it into two assymptotic series, one for low values of $\overline{Pe'}$ and the other for larger values.

The appropriate solution for low $\overline{Pe'} < .067$ or $\overline{Nu} < .53$ is:

$$q' = \frac{2\pi\kappa (T_p - T_o)}{(1-\gamma) - \ln \frac{1}{2}\overline{Pe'}} \quad \text{and} \quad \overline{Nu} = \frac{2}{(1-\gamma) - \ln \frac{1}{2}\overline{Pe'}} \qquad \text{I-8}$$

and that for high values of $\overline{Pe'} > .067$ or $\overline{Nu} > .53$

$$q' = \left[\kappa + \sqrt{2\pi\kappa\rho c D U}\right]\left[T_p - T_o\right] \text{ and } \overline{Nu} = \frac{\sqrt{2\pi\overline{Pe'}} + 1}{\pi} \qquad \text{I-9}$$

Cole and Roshko (22) have recently derived a solution of heat transfer from heated cylinders for Reynolds numbers in the Oseen regime. In this regime, diffusions is the dominating process through which heat is transferred near the cylinder.

The boundary conditions set for this solution are

(a) The initial fluid temperature for upstream of the cylinder is constant

(b) The temperature at the surface of the wire is uniform and constant.

The solution of the heat equation for an infinite cylinder in the Oseen flow regime is

$$\overline{Nu} = \frac{2}{(\ln 8 - \gamma) - \ln \overline{Pe}}$$

A comparison of Boussinesq's, King's and Cole and Roshko's solutions is made in Figure 30. A comparison between King's equation, and actual experimental values obtained in the laboratory are presented in Fig. 31.

The Use of Heated Wires for Time Mean Velocity Measurements

Referring to equation I-9 one can see that if the properties of the air surrounding the wire remain constant and if the heated resistance of the wire is kept constant then a linear relationship should exist between the heat input into the wire and the square-root of the velocity. Experimental evidence shows that Nu is a linear function of $\sqrt{Pe}$ for large enough Péclet numbers. Although King showed the linear relationship, the constants in his solution do not agree with those determined in the laboratory Figure 31. If the heat input is supplied by an electric current, then one can rewrite equation I-9 in the following manner:

$$I^2 R_h = \left[A + B\sqrt{U}\right]\left[T_h - T_o\right] \qquad \text{I-10}$$

since $T_h - T_o = \frac{R_h - R_o}{\alpha_o R_o}$, it is sometimes convenient to write equation I-10 in the following way:

$$I^2 = \left[A + B\sqrt{U}\right] \frac{R_h - R_o}{\alpha_o R_h R_o} \qquad \text{I-11}$$

The value of R_o is determined by the temperature of the surrounding fluid. If one adopts beforehand a value of $(R_h - R_o)/ R_o$, called the overheat ratio, then the value of R_h is indirectly fixed and for each value of the overheat ratio one obtains linear relationship between I^2 and $\sqrt{U}$ at constant angle between axis of wire and U. Fig. 32 shows a family of curves for various values of overheat ratios. Those curves are called the calibration curves of the wire for static or mean velocity response. If the axis of the wire makes an angle Θ with the direction of the mean velocity U then the apparent heat convecting velocity with respect to the wire is $U \cdot \cos \Theta$. Equation I-11 is still valid and $U \cos \Theta$ should be used instead of U

The Use of Heated Wires for Instantaneous Velocity Measurements

In a turbulent flow field, the velocity vector at every point of the field is a function of time. In most turbulent fluid flow applications, the conception of time dependency is not a transient one. The time average of the velocity vector remains constant at the point but the magnitude and direction of the velocity vector fluctuates as a function of time around the mean. This means that we can represent the velocity vector by an average constant quantity and a fluctuating time dependent part, $v(x, y, z, t) = V(x, y, z) + v'(x, y, z, t)$. In the previous section we have already discussed measurements of the time mean of the velocity vector, $V(x, y, z)$. The analysis becomes somewhat more involved for measurements of the time dependent part of the velocity. The complex wave form of the time dependent part of the velocity in a turbulent flow field reveals appreciable effects produced by minute eddies travelling with frequencies up to 15,000 or 20,000 cycles per second. This fact introduces the problem of having a heated wire capable of reproducing faithfully without amplitude or phase distortion signals at high frequencies.

However small a wire can be manufactured, it still has a mass and thermal properties which by themselves will never be able to communicate undistorted information at higher frequencies. This problem is usually remedied by artificial electronic compensation to make up for the loss of information at high frequencies. The following analysis will take for granted that the wire is faithful or made to be so electronically. Furthermore, the dynamic response analysis that will follow will only be valid for small disturbances compared to the magnitude of the average quantity.

Let us consider a two-dimensional channel flow as shown in Fig. 34 with U the magnitude of the time mean velocity and u', v' and w' the fluctuating components in the x, y, and z directions. When the axis of the heated wire is placed perpendicular to U, the wire will be sensitive to u' fluctuations Since $\Theta = 0$ any change of direction of the velocity vector created by $\Delta\Theta_1 = \tan^{-1}\frac{v'}{U+u'}$ and $\Delta\Theta_2 = \tan^{-1}\frac{w'}{U+u'}$ from the point M Fig 33 will certainly be negligible. However, if the wire would be placed originally at say $\Theta = 45°$ then any disturbance created by v' in the form of $(45° + \Delta\Theta_1)$ and $(45° - \Delta\Theta_1)$ will be in the same

order of magnitude as those created by u'. In order to intercept w' fluctuations the axis of the wire must be in the x - z plane and making an appreciable angle with U.

Consulting Figure 34 let us place two wires 1 and 2 with their middle in the same point in space both making equal angles Θ with the main direction of flow U. Adopting a positive direction of u' and v' as shown in Figure 34 one obtains the velocity components V_1 and V_2 effective to each wire.

$$V_1 = \sqrt{(U+u')^2 + v'^2}\ \cos(\theta - \Delta\theta)$$

$$V_2 = \sqrt{(U+u')^2 + v'^2}\ \cos(\theta + \Delta\theta) \qquad \text{I-12}$$

where: $\Delta\theta = \tan^{-1}\dfrac{v'}{U+u'}$

If one expands the coefficients above into a binomial expansion and neglecting second order terms, one obtains:

$$V_1 = U\cos\theta + u'\cos\theta + v'\sin\theta \qquad \text{I-13}$$

$$V_2 = U\cos\theta + u'\cos\theta - v'\sin\theta$$

The term U cos Θ is constant with time only the remaining terms are functions of time. Those time dependent terms will create voltage fluctuations or ac voltage in the wire above the dc level maintained to keep the wire heated at a velocity U cos Θ. Let $E = IR_h$ be the magnitude of the dc voltage and $e'(t)$ be the fluctuating voltage created by the fluctuating velocity components. Since the dc component of the voltage in the wire does not go through the compensating amplifier, then we will consider the time dependent part for the moment.

Since $e'(t)$ is caused by a fluctuating velocity then one can write that:

$$e_1'(t) = F_1\left[u'(t)\cos\theta + v'(t)\sin\theta\right]$$

$$e_2'(t) = F_2\left[u'(t)\cos\theta - v'(t)\sin\theta\right] \qquad \text{I-14}$$

where F can be found from circuit analysis (21) to be $F = -\frac{\bar{a}\,E\,\mathcal{E}\,b}{2U\cos\theta}$

Where $\bar{a}$ is the time average overheat ratio, E is the mean dc voltage of the wire, $b = \frac{I^2 - I_o^2}{I^2}$ where I is the mean value of the current in the wire and I_o^2 is the fictitious point representing the square of the current at zero velocity in the static

calibration curve. The term $\mathcal{E}$ represents a correction factor for the degeneracy from a constant current condition. This quantity depends on the heating circuit of the hot-wire anemometer set and should be computed for the particular set.

Since the rms values of the turbulent fluctuations represent the energy contained in turbulence, it becomes necessary to take the rms value of equation I-14.

$$\sqrt{\overline{e_1'^2(t)}} = \tilde{e}_1' = F_1\left[\tilde{u}'\cos\theta + \tilde{v}'\sin\theta\right]$$

$$\sqrt{\overline{e_2'^2(t)}} = \tilde{e}_2' = F_2\left[\tilde{u}'\cos\theta - \tilde{v}'\sin\theta\right] \qquad \text{I-15}$$

From these equations one can see that if θ becomes zero then both wires are perpendicular to the mean direction of flow and both equations reduce to:

$$\tilde{e}' = F\tilde{u}' = -\frac{\bar{o}\,E\,\mathcal{E}b}{2}\,\frac{\tilde{u}'}{U} \qquad \text{I-16}$$

Equation I-16 must be used to determine the value of u'. In order to obtain the energy involved in other turbulent terms such as $\tilde{v}'$, $\overline{u'v'}$, $\tilde{w}'$ and $\overline{u'w'}$ one must square first, add and subtract equations (15):

$$\overline{e_1'^2} - \overline{e_2'^2} = \frac{\bar{a}^2 E^2 \bar{\epsilon}^2 b^2}{U^2}\left[\overline{u'v'}\tan\theta\right]$$

$$\overline{e_1'^2} + \overline{e_2'^2} = \frac{\bar{a}^2 E^2 \bar{\epsilon}^2 b^2}{U^2}\left[\overline{u'^2} + \overline{v'^2}\tan^2\theta\right] \qquad \text{I-17}$$

These equations hold true for wire having the same calibration characteristics at both positions. $F_1 = F_2$. If the voltage response of both wires is not the same, in order to solve Equation I-15 in the form of I-17 it becomes then necessary to match F_1 and F_2 with a voltage divider or a potentiometer. If a subtracting and adding circuit is available, the operation in Equation I-17 can be done electrically.

APPENDIX II

THE HOT WIRE ANEMOMETER

Foreword

This type of a hot-wire anemometer was designed mainly for the purpose of compensating tungsten wires with a relatively large time constants (0.52 to 2 msec.). The set is built with two separate bridges and two differential compensating amplifiers. The presence of separate bridges and amplifiers enables to perform direct space correlations measurements and furthermore avoids interference of one bridge on the other when two wires are used concurrently. The design and wiring was done at the Mechanical Engineering Department of The Johns Hopkins University under ONR sponsorship. This instrument was used for measurements of turbulence intensity, shear, and turbulent energy spectrum in subsonic turbulent air flow in curved channels.

Description of the Hot Wire Anemometer

This description will contain only components which are essential to reproduce correctly the static and dynamic information from the turbulent flow. Recording instruments such

as ammeters, voltmeters; voltage adding, subtracting, multiplying circuits; filters, oscilloscope etc. will not be included in this description. The compact unit shown in Figure 35 contains the following components:

1. The Power Supply Units:

A. The Lambda Regulated Power Supply: This unit is manufactured by the Lambda Electronic Corporation of Corona N. Y. It is the model 28 with input voltage of 105-125 volts at 50-60 cps. The DC output voltage is regulated and may be adjusted from 200-325 volts at 0. 10 amperes. The B^+ voltage in this set is adjusted to 300 volts and supplies the plate voltage to the amplifiers and the square wave generator. No ground connections are made in the power supply; the B^- is grounded in the individual chassis of the instrument in order to prevent circulating ground currents. The AC voltage is unregulated and rates 6. 3 volts at 3 amperes. This AC voltage is fed to the square wave generator tube filaments and also used for calibrating voltage. The amplifier filaments are heated with battery DC voltage in order to reduce hum. Figure 35 shows the Lambda Power Supply at A.

B. DC Power from Batteries: Three 6 volts automotive batteries are used to supply the heating current to the hot-wires in the bridges and also to supply the filament current to the amplifier tubes. Figure 37 shows the lay-out of the batteries where 18 volts are used for supplying the hot-wire bridge currents and 6 volts for the amplifier tube filaments. In Figure 35 switch B connects the batteries to the circuit and a pilot light C will go on when switch B is turned on. The DC voltmeter D will indicate the voltage of the batteries. The output leads of the Lambda supply and the batteries are brought to a terminal box behind the bridge panel. Power to the bridges, amplifiers, square-wave generator is then distributed by means of plug-in cables. This arrangement was chosen to facilitate easy removal of a defective unit.

2. Bridge Circuit - Heat Control and Bridge Terminals:

The twin bridges are identical, as are the two heat control panels E_1 and E_2. The bridge itself is not an integral part of the set shown in Figure 35. The set was especially designed in this fashion so as to give the experimenter the privilege of choosing an accurate and non-inductive bridge. The described

set-up uses a Leeds and Northrup No. 4725 Wheatstone bridge because of its accuracy and practically negligible inductance. Figure 39 shows the bridge connections to the four terminals in the main chassis. The four bridge terminals are lettered S, T, Q and P where P is grounded. Eight alternate binding posts are provided in the heat control panel for the following reasons. Across the first set of two posts S and T the bridge has a leg of 100 ohms resistance. The current in the hot-wire is measured between these two terminals. The second pair of posts T and P provide the connections to superimpose the square wave signal on the DC battery voltage in order to compensate for time lag of the wire with the RC network in the compensating amplifier. The third pair S and P is across the variable resistance leg of the bridge. The voltage between these terminals is used as a differential input to the amplifier for accurate compensation. The fourth pair of terminals Q and P are directly connected across the hot-wire and are used to supply the fluctuating hot-wire voltage to the amplifier.

The heat control circuit which supplies heating current to the bridge can be seen in the layout Figure 38 or in the photograph Figure 35. When switch B is on, the bridge will be supplied with enough current to measure the cold resistance of the hot-wire on account of the higher resistor of 3.3K in the line. When switch F is turned on, the 3.3K resistor is by-passed and higher current flows into the bridge. The variable resistors G=250Ω and H=25Ω control the heating current supplied to the bridge. A 50Ω resistor in series with the variable resistors is introduced to protect partially the bridge for possible mistakes. A DC milliammeter I (0 - 500ma) is located next in series to indicate the current on top of the bridge. A galvanometer K connected across the bridge between S and Q and a sensitivity switch J shunting a 51K resistor is used for balancing the bridge accurately.

3. The Calibrating Voltage:

A standard voltage is necessary to calibrate and check instruments. Its use is especially necessary to determine the gain of the amplifier during actual test runs. The

voltage supply for the calibration of voltage network comes from the AC power of the Lambda supply. A switch L closes the circuit and the current flowing through the line is controlled by the variable 10K resistor M. A milliammeter N (0 - 1ma) indicates the current flowing and a voltage divider R will give the desired voltage at the output terminals 0. Top circuit of Figure 38.

4. The Compensating Amplifier:

The purpose of the amplifier in this instrument is to compensate electronically for the decrement of information transmitted by the hot-wire due to the thermal lag. Furthermore, it serves the purpose of magnifying the small AC voltage fluctuations of the wire created by turbulence. This amplifier uses feed-back around one stage, Figure 40. The compensation level from ceiling to floor is 28 db. Figure 42 shows the frequency response of the uncompensated amplifier as well as the response of the amplifier with compensation for 0.5 and 2 msec. wire. A cathode follower is added in the circuit in order to lower the output impedence. In this present system, two values of capacitance $C_6 = 0.005 \mu f$ and $C_5 = 0.02 \mu f$. together with the 100K

variable resistor R_4 will compensate wires between 0.5 and 2msec. The design of this circuit was preferably adopted for possibilities of tracking a second stage of compensation to the first, if needed.

The specifications of the amplifier are as follows:

Maximum gain (Low frequency)..... 80 db

Compensation level (ceiling to floor)..... 28 "

Common-mode rejection ratio..... 165

Output volts (.707 of peak) input shorted when amplifier is set to compensate a 1 msec. wire (hum and noise)..... 2.8 mv.

Compensation range..... Figure 42

Output impedence..... less than 500 ohms.

When power supply and batteries are on, the amplifiers and the square wave generators are in operation. Consulting Figure 35 again, Switch A1 has two positions. The down position is the usual position for one signal going through the amplifier. The up position is used for subtracting two signals going through the amplifier at the same time. The subtraction is done by a simple phase shift of the second input.

Jack V is for the single input and jack W is used for the differential input. The amplifier output is taken across the binding posts U. Dial C1 is the gain control of the amplifier. Dial Z and switch B1 represent the compensation network. The switch B1 has three positions as follows: The middle position is the uncompensated signal of the hot-wire, the upper position introduces a 0.02 μf. capacitance in the compensating circuit and the lower position a capacitance of 0.005 μf. The variable resistance Z is used together with the capacitors to match the time constant of the wire. A duplicate amplifier is now located on the other side of the square wave generator. The amplifier and square wave generator panel is plastic, this separates the ground of this panel from the main chassis. The amplifiers and the square wave generator are built in separate miniboxes in order to reduce hum, noise and circulating ground currents.

SYMBOLS IN FIGURE 35

A	Power supply on-off switch
B	Battery power on-off "
C	Pilot light to indicate batteries on
D	DC voltmeter - Battery voltage (0-20 volts)
E	Heat control panel
F	Heat switch
G	Coarse heat control pot. (250 ohms)
H	Fine " " " (25 ")
I	Bridge current milliammeter (0-500 ma.)
J	Sensitivity switch of galvanometer
K	Galvanometer
L	Calibration voltage on-off switch
M	Current control in calibration voltage (10 K)
N	AC milliammeter in calibration voltage (0-1 ma.)
O	Calibration voltage output terminals

P, Q, S, T four terminals of Wheatstone bridge

R	Calibration voltage divider (5Ω, 10Ω, 50Ω)
U	Output terminals of amplifier
V	Input jack of amplifier
W	Second input jack of amplifier
X	Output terminals of square wave generator
Y	Output terminals of second amplifier
Z	Resistance control of compensation (100 K)
A1	Single or differential input switch of amplifier
B1	Capacitance control of compensation (0.005μf. and 0.02μf.)
C1	Gain control of amplifier (1 Meg.)
D1	Frequency control of square wave generator (0.25 Meg.)
E1	On-off switch of square wave generator
F1	Amplitude control of square wave generator (100 K)

REFERENCES

1. Laufer, John: Investigation of a Turbulent Flow in a Two-Dimensional Channel. NACA TN 2123, July 1950.

2. Wattendorf, F. L. : A Study of the Effect of Curvature on Fully Developed Turbulent Flow. Proc. Roy. Soc. , Vol. 148, 1935.

3. Durand, W. F: Aerodynamic Theory, Vol. IV. p. 25-27 January 1943.

4. Eskinazi, S. , Gitt, J. S. , Lumley, J. L. : The Spot Welding of Hot-Wire Probes. Nonr. Prog. Report I-11, JHU August 1953.

5. Wislicenus, G. F, Yeh, H. : A Program of Research in the Field of Turbulent Flow in Ducts, in a Space of Revolution, and in Turbomachinery, Nonr Report I- 8 JHU. December 1952.

6. Eskinazi, S: Fully Developed Flow in Curved Parallel Channel. Nonr Prog. Report I-10, April 1953.

7. Kovasznáy, L. S. G: Development of Turbulence Measuring Equipment. NACA TN 2839, January 1953.

8. Rotta, J: On the Theory of Turbulent Boundary Layer. NACA TM 1344, February 1953.

9. Taylor, G. I: The Spectrum of Turbulence. Proc. Roy. Soc., A 164, 1938.

10. Laufer, John: The Structure of Turbulence in Fully Developed Pipe Flow. NACA TN 2954, June 1953.

11. von Kármán, T: Turbulence and Skin Friction Jour. of Aero. Sciences, January 1934.

12. Clauser, F. H: Turbulent Boundary Layers in Adverse Pressure Gradients, Journal of Aero. Sciences, February 1954.

13. Taylor, G. I: Statistical Theory of Turbulence. Proc. Roy. Soc. Part I-IV, 1935.

14. von Wilcken, H: Turbulente Grenzschichten an gewolbten Flachen. Ing. Archiv, 1930.

15. Kampé de Fèriet: Introduction to the Statistical Theory of Turbulence. Notes on Lecture Series No. 8 Univ. of Maryland, 1950-51.

16. Goldstein, S: Statistical Theory of Turbulence. Notes on Lectures Series No. 6, Univ. of Maryland, 1950.

17. Goldstein, S: Modern Developments in Fluid Dynamics. Vol. I and II, Oxford Univ. Press, 1938.

18. Schubauer, G. B., Klebanoff, P. S: Theory and Application of Hot-Wire Instruments in the Investigation of Turbulent Boundary Layers. NACA ACR No. 5K27.

19. Boussinesq, J: Comptes Rendus, Vol. 133 p, 257 Journal des Mathematiques. Vol. 1 pp. 285-332, 1905.

20. King, L. V: On the Convection of Heat from Small Cylinders in a Stream of Fluid. Phil. Trans. of Roy. Soc. A., Vol. 214, 1914.

21. Kovasznáy L. S. G: Calibration and Measurement in Turbulence Research by The Hot-Wire Method. NACA TM 1130, June 1947.

22. Cole, J. and Roshko A: Heat Transfer from Wires at Reynolds Numbers in the Oseen Range. Heat Transfer and Fluid Mechanics Institute Uni- of California, June 30, 1954.

23. Rayleigh, Lord: On the Dynamics of a Revolving Fluid Sci. Paper, Vol. 6, 1916,

24. Prandtl, L: Effect of Stabilizing Forces on Turbulence NACA TM 625, 1931.

25. Liepman, H. W: Investigations on Laminar Boundary-Layer Stability and Transitions on Curved Boundaries NACA W-107, August 1943.

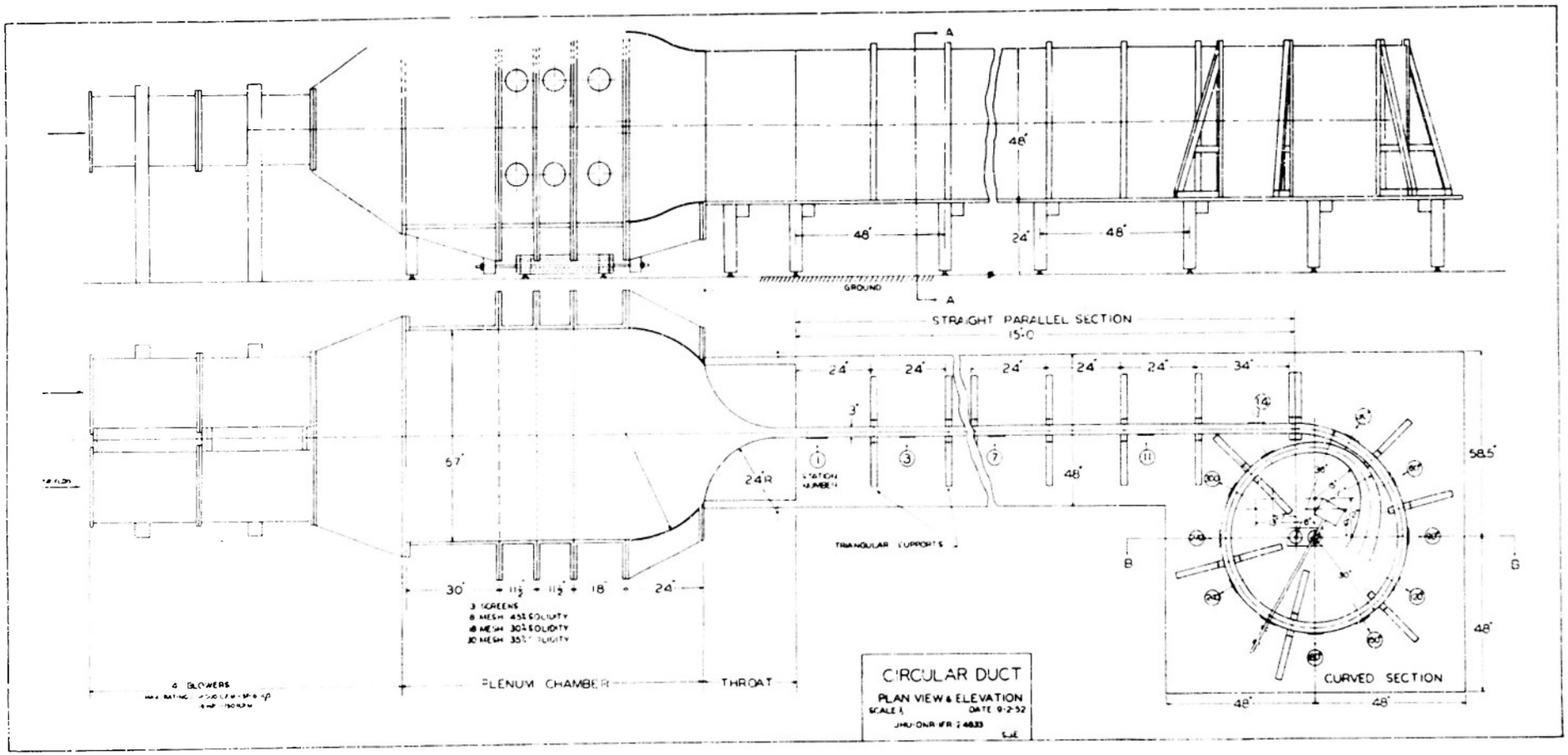


Figure 1. The assembly of the wind-tunnel for investigations of flow in curved passages.

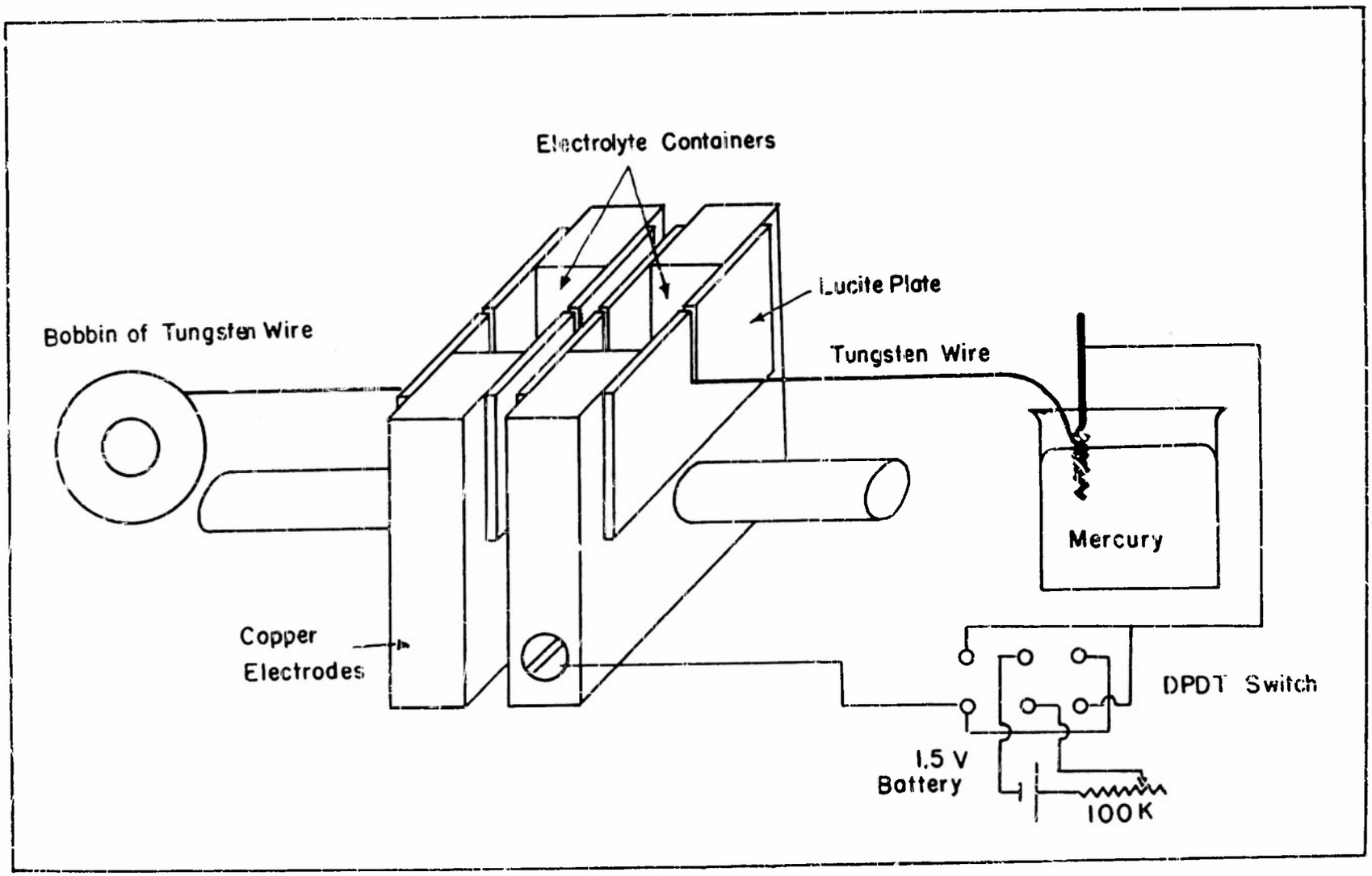
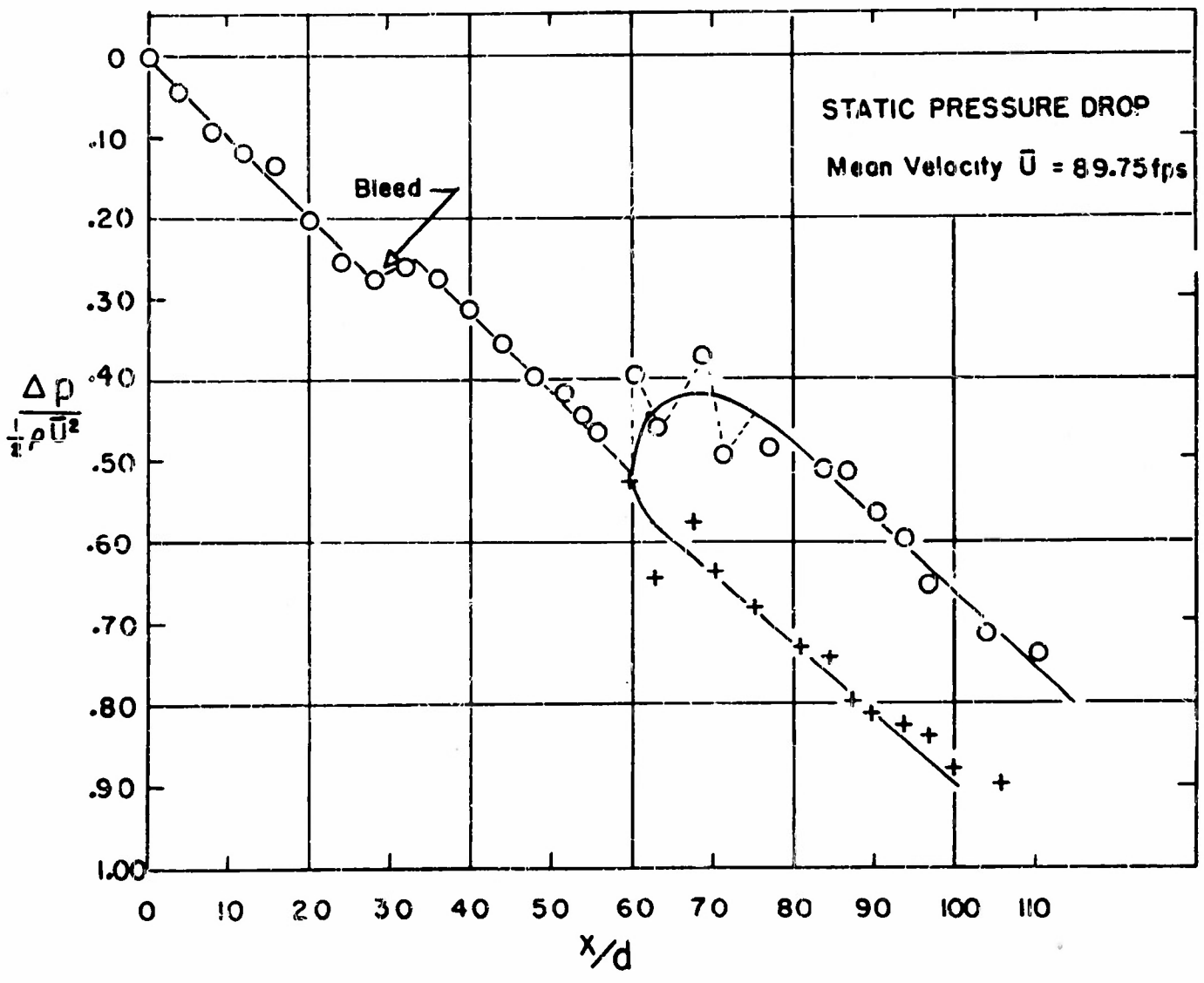


Figure 2. Assembly for copper plating tungsten wires.



CHANNEL LENGTH AS RATIO OF THE WIDTH

Figure 3. Static pressure drop along the length of the channel.

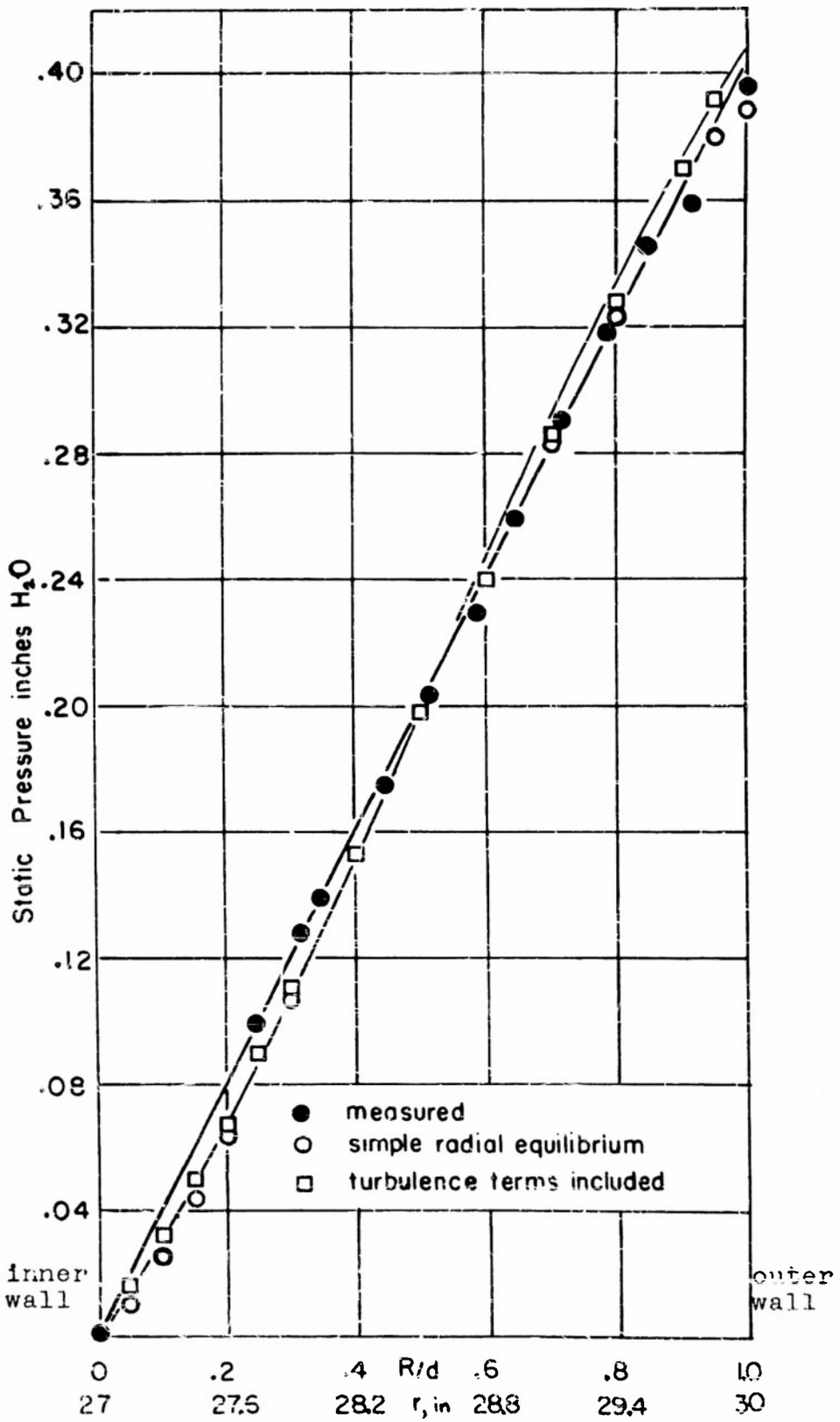


Figure 4. Radial static pressure distribution at the fully developed curved section.

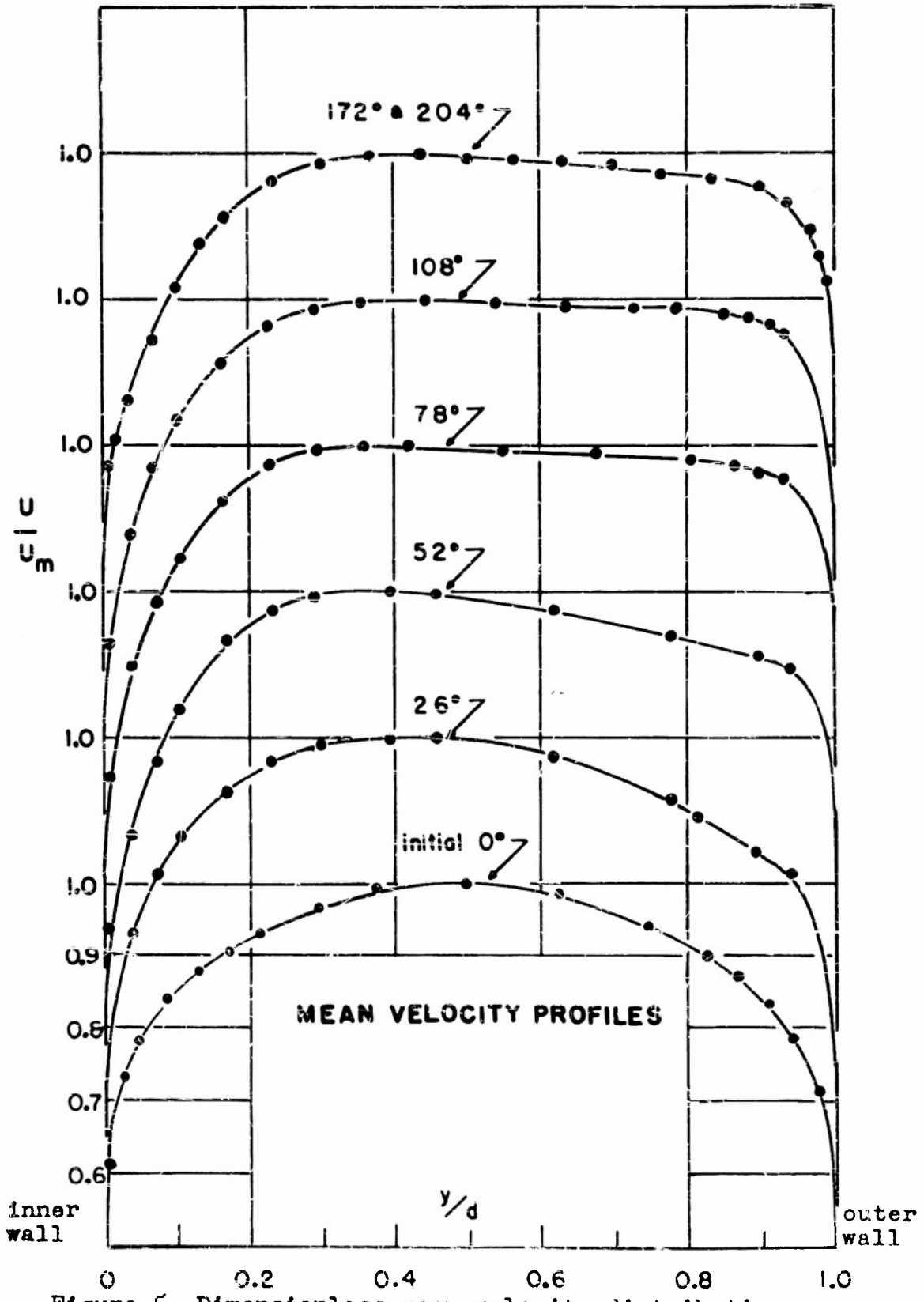


Figure 5. Dimensionless mean velocity distributions in the straight and curved sections.

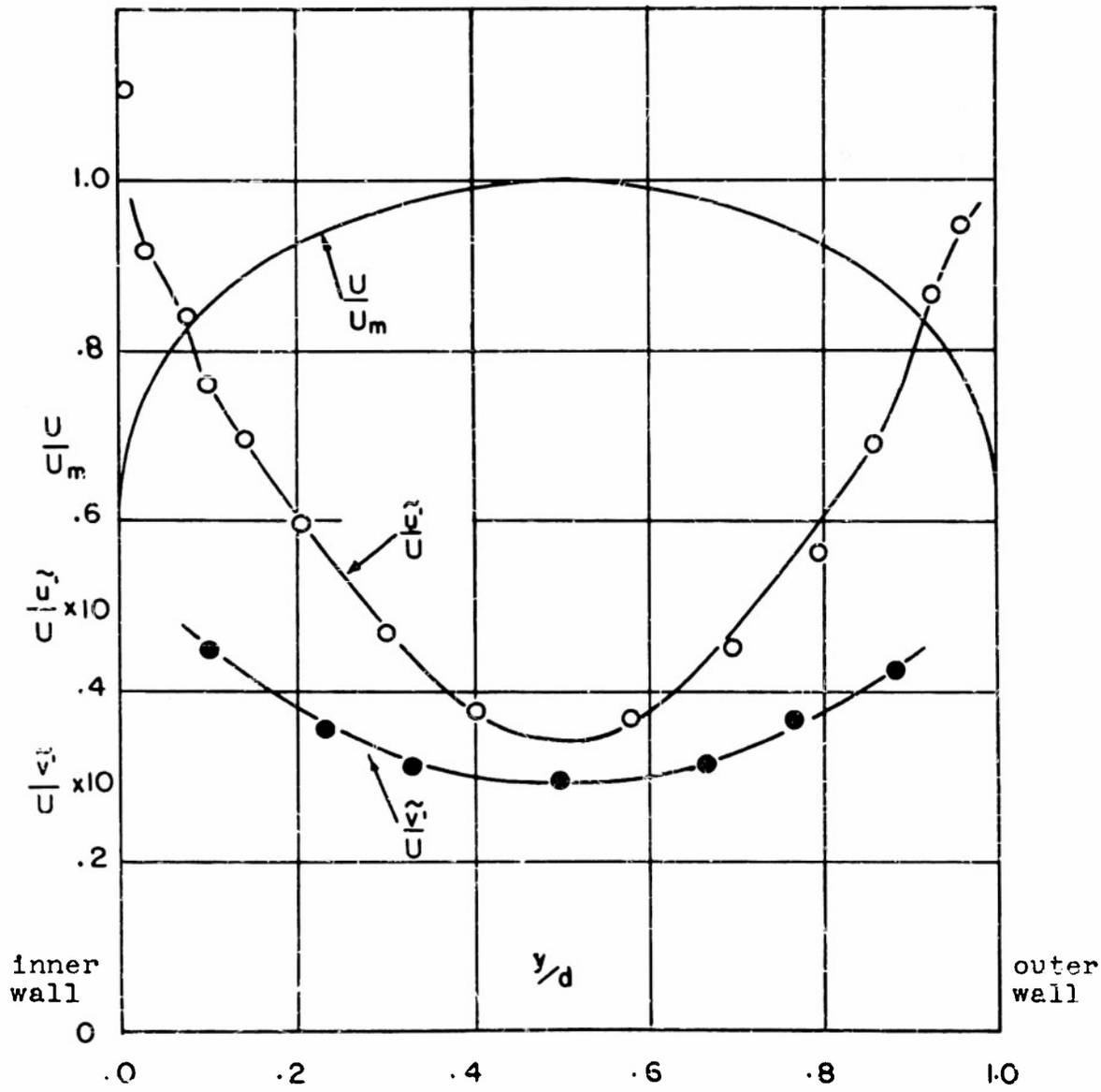


Figure 6. Mean velocity and turbulence level distributions across the fully developed straight section.

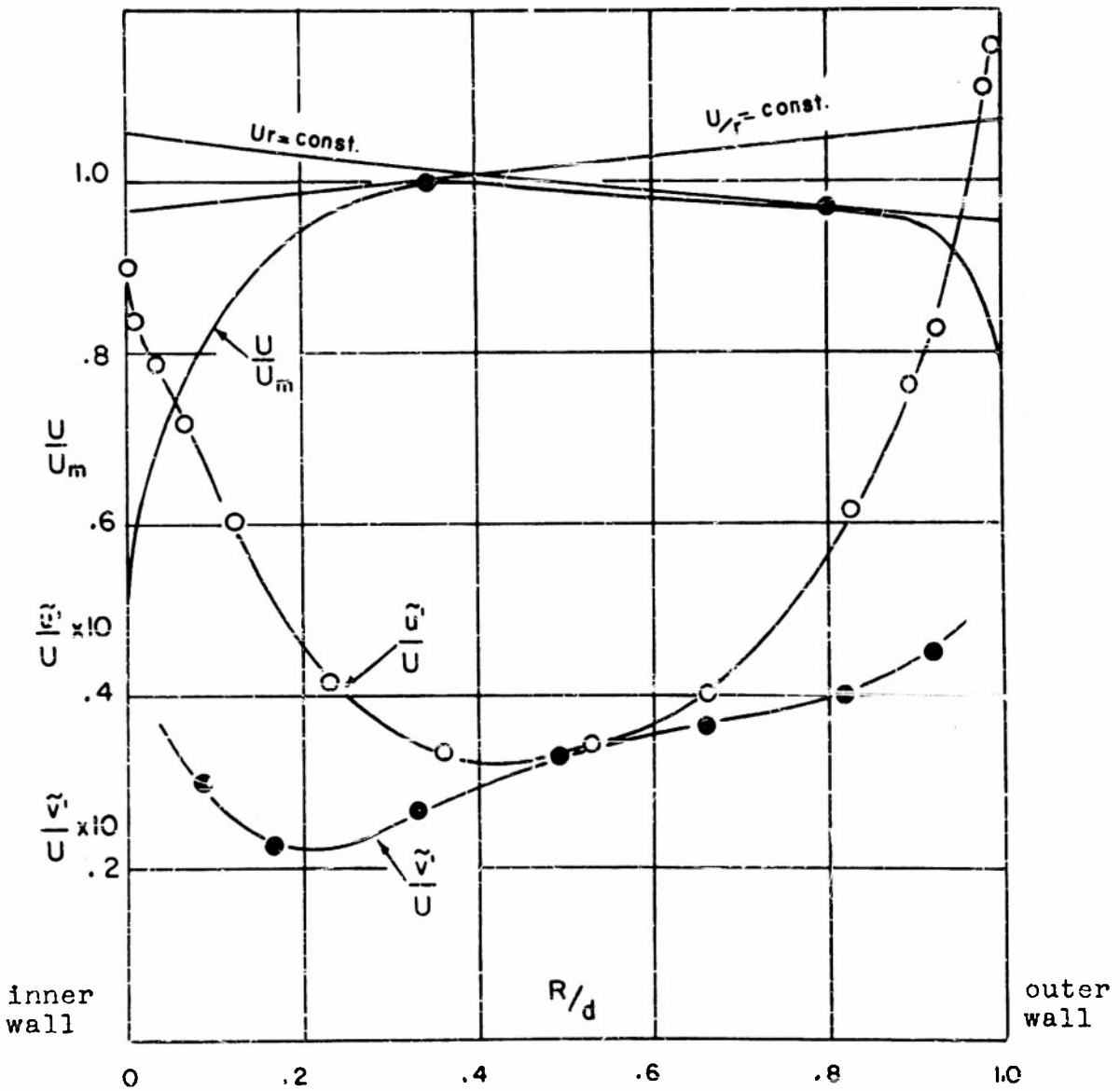


Figure 7. Mean velocity and turbulence level distributions across the fully developed curved section.

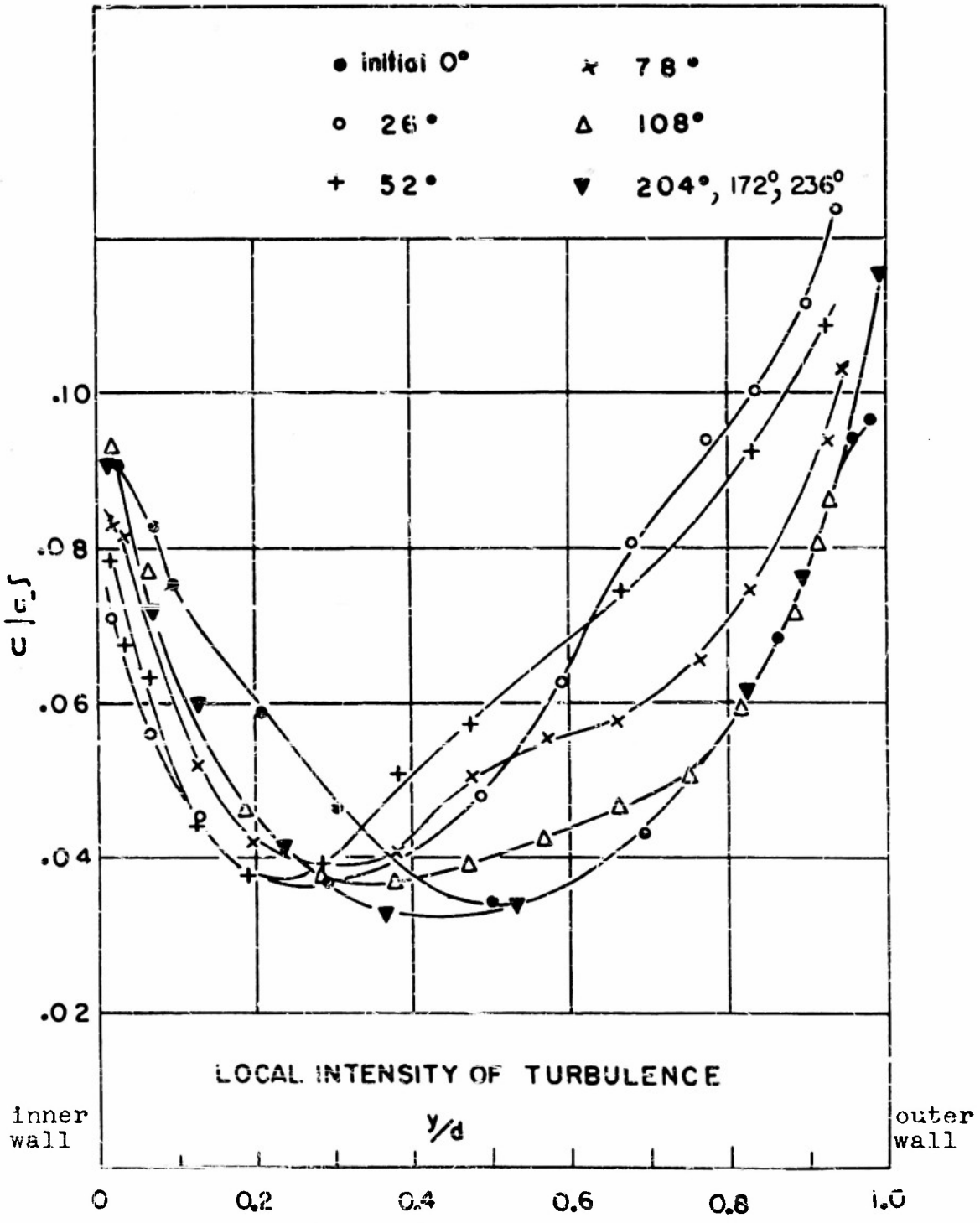


Figure 8. Distribution of local intensities of turbulence in the direction of flow.

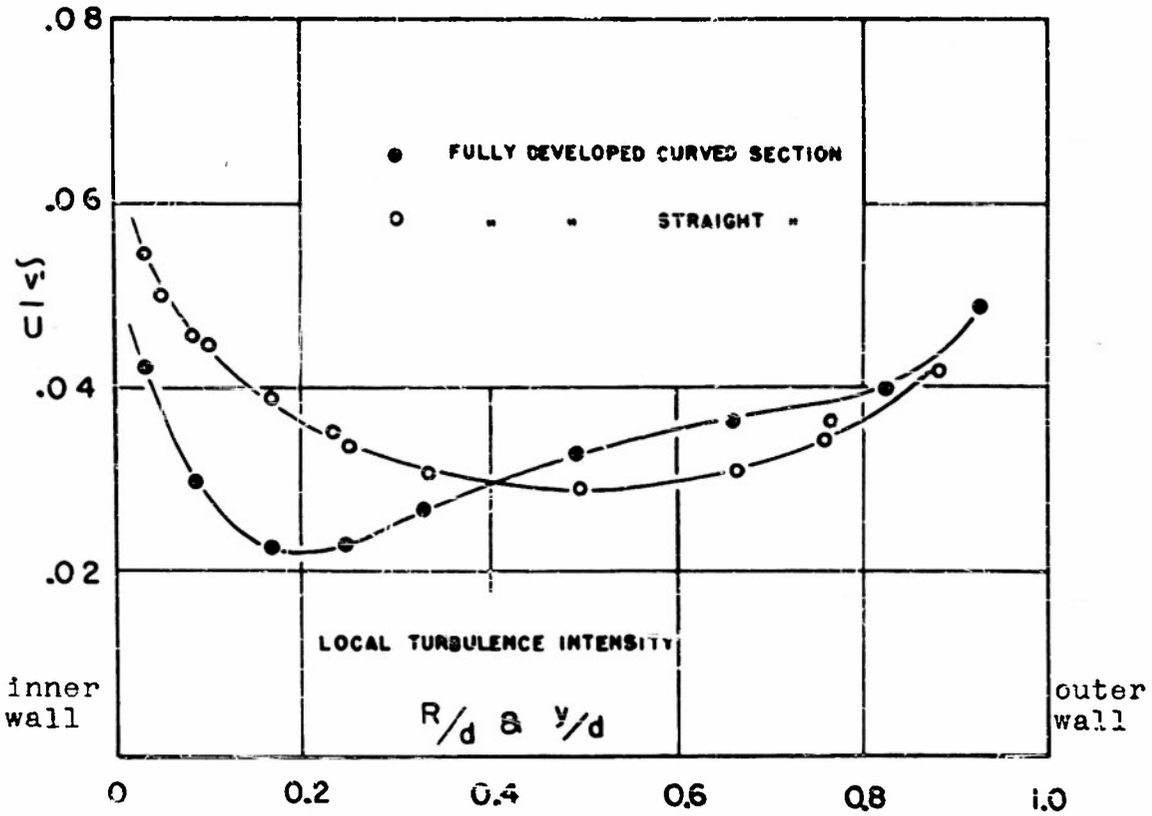


Figure 9. Distribution of the root-mean square of v' in the straight and curved fully developed regions.

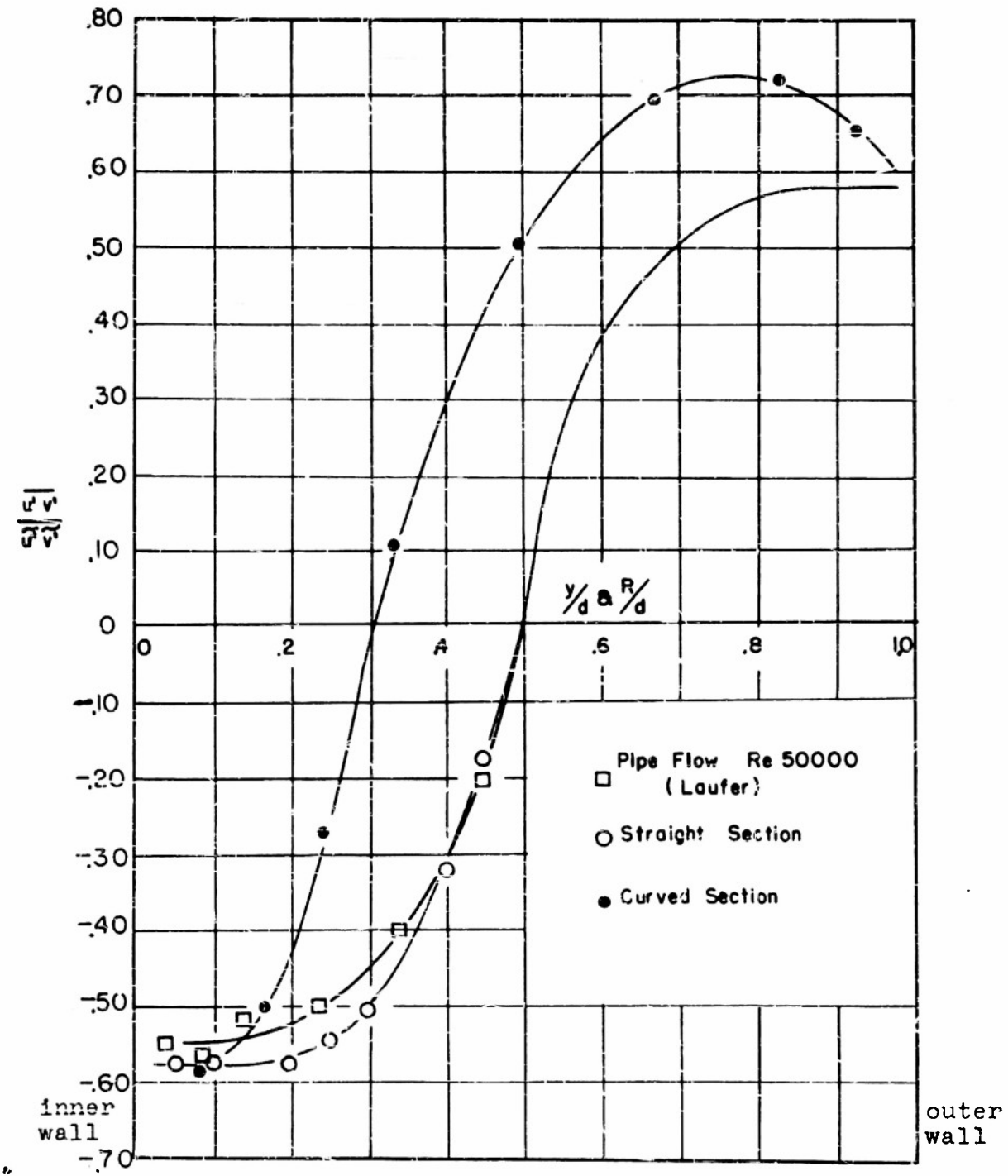


Figure 10. Variations of maximum correlation coefficients across the straight and curved fully developed sections.

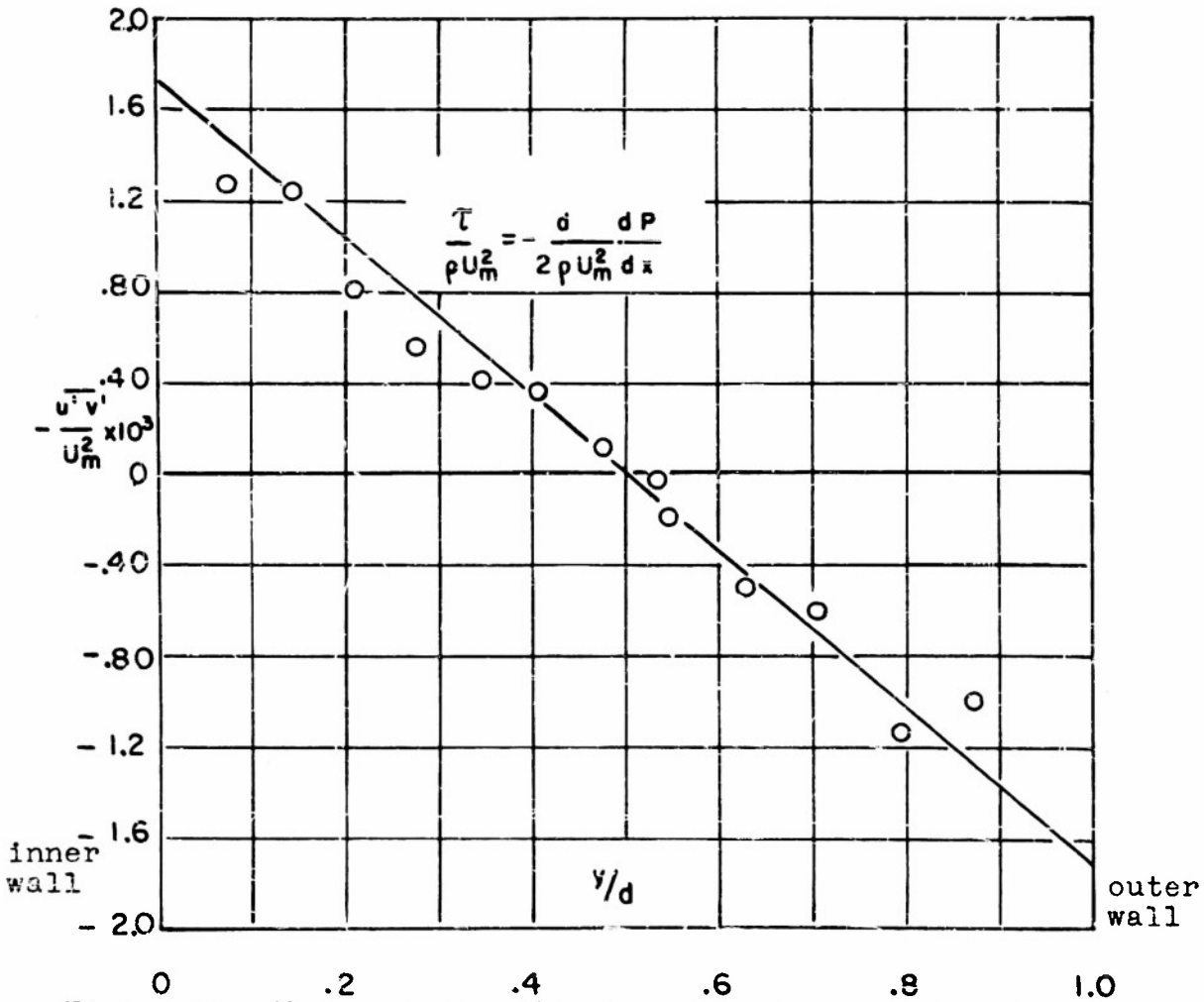


Figure 11. Shear stress distribution across the fully developed straight section.

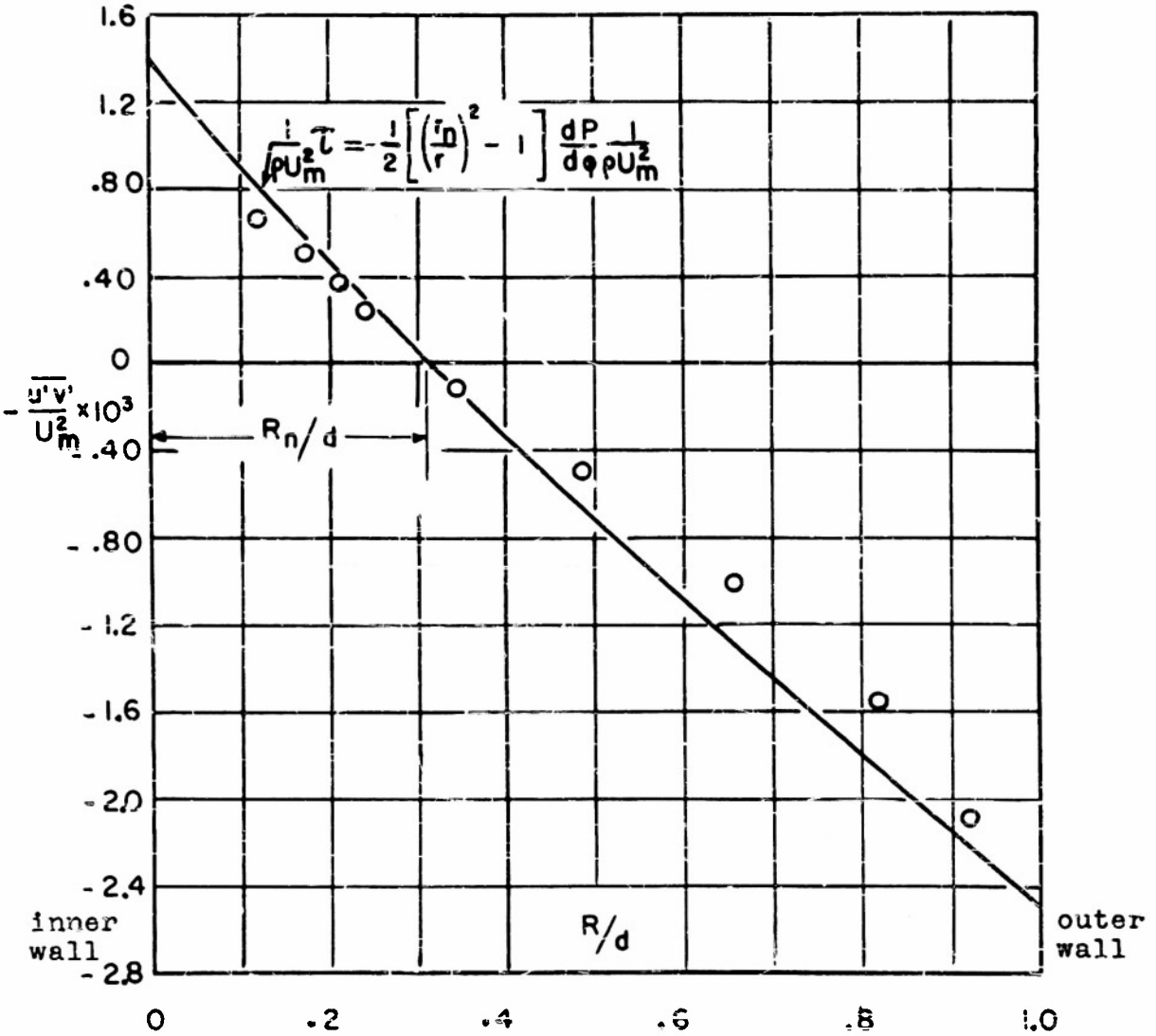


Figure 12. Shear stress distribution across the fully developed curved section.

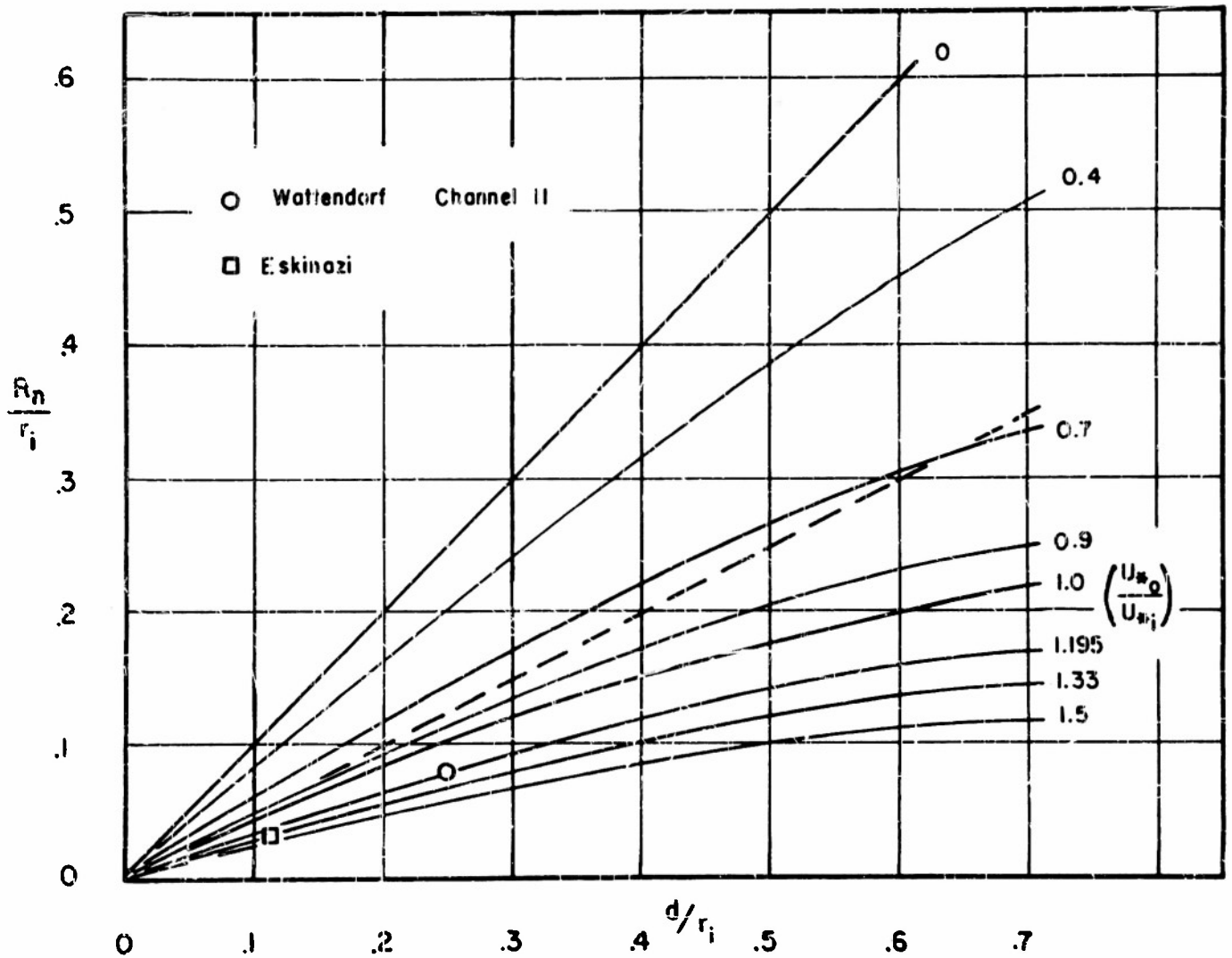


Figure 13. Location of the nul value of shear stress in the fully developed curved section.

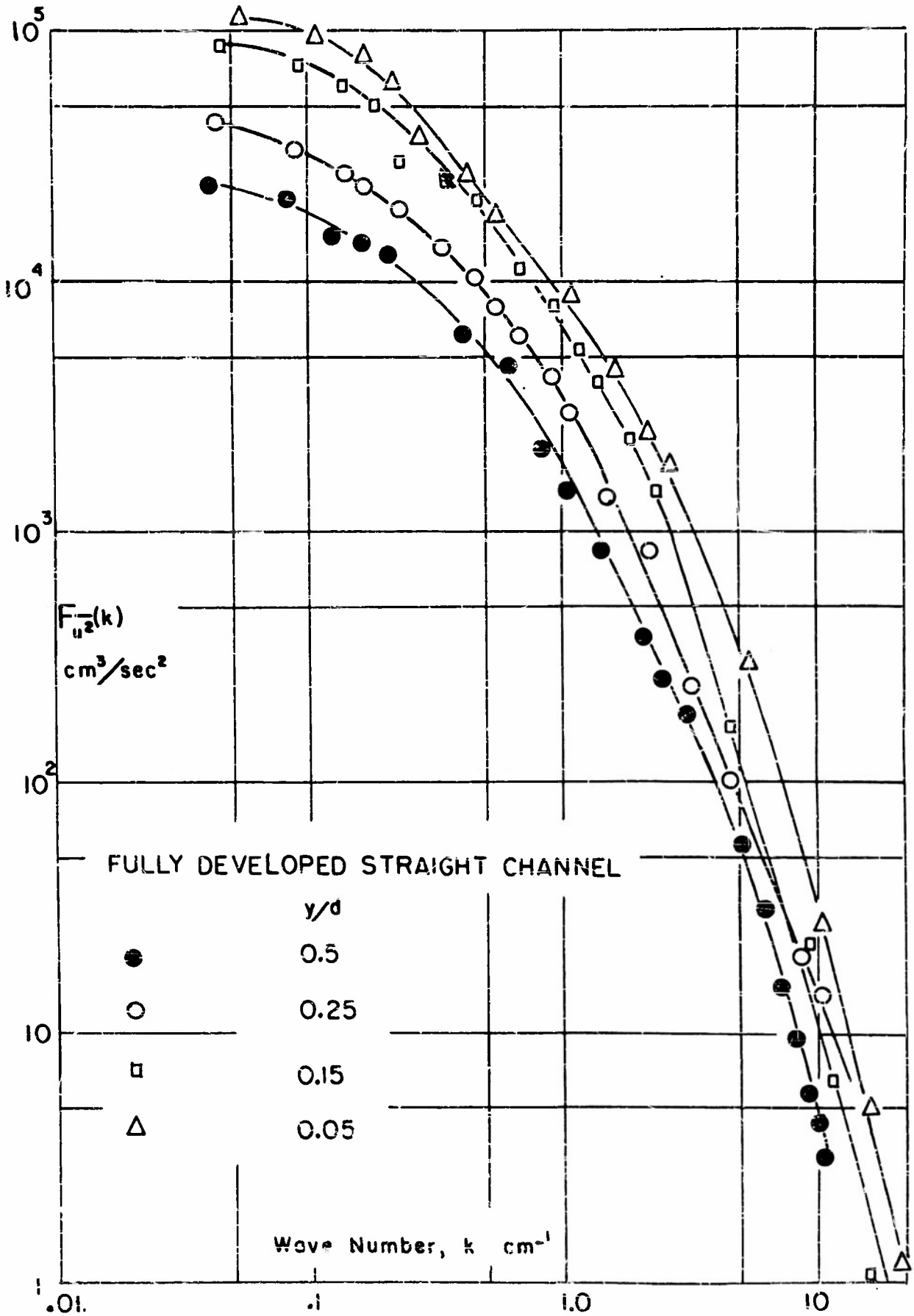


Figure 14. Spectrum of u' in the straight fully developed section.

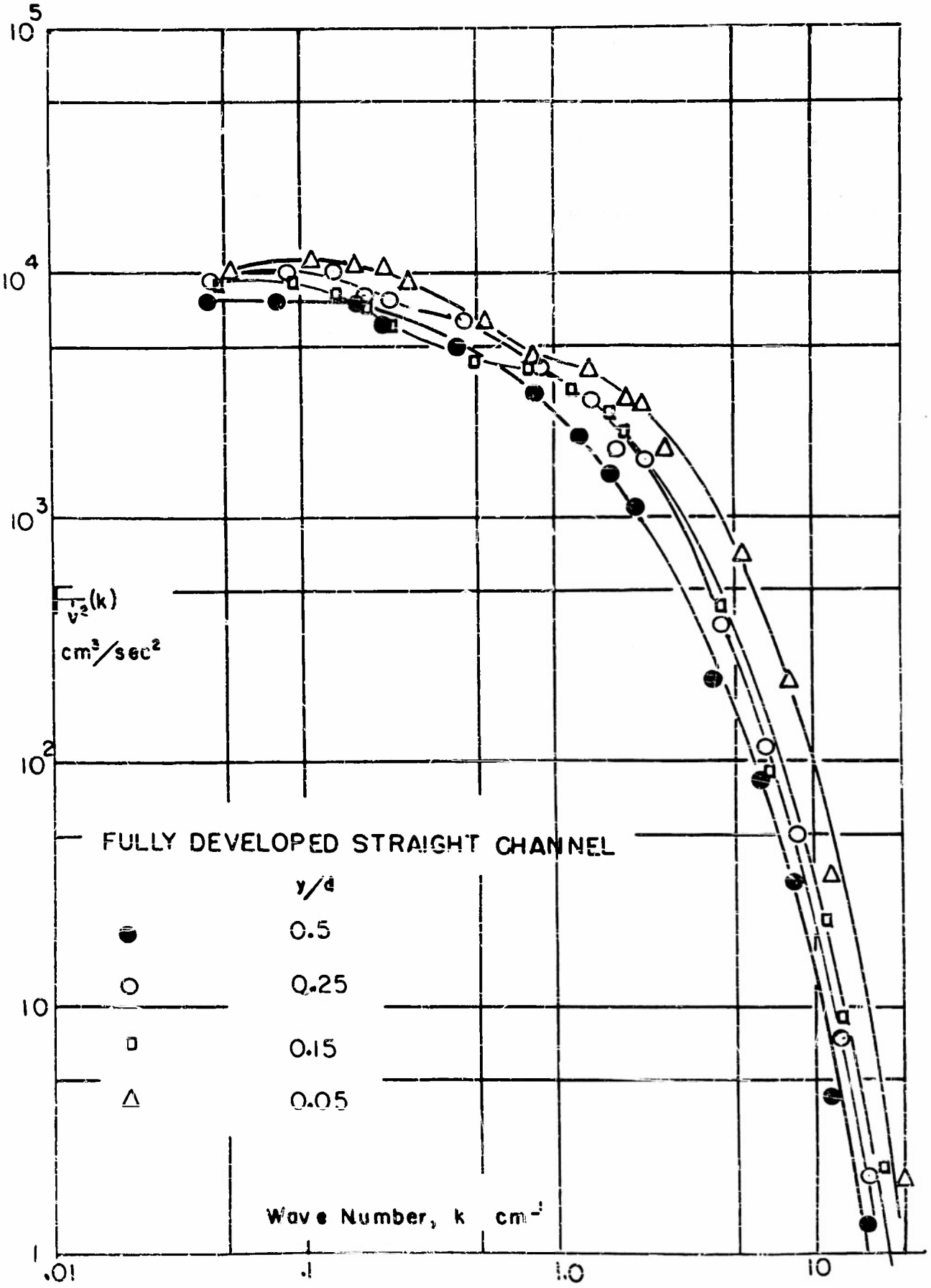


Figure 15. Spectrum of v' in the fully developed straight section.

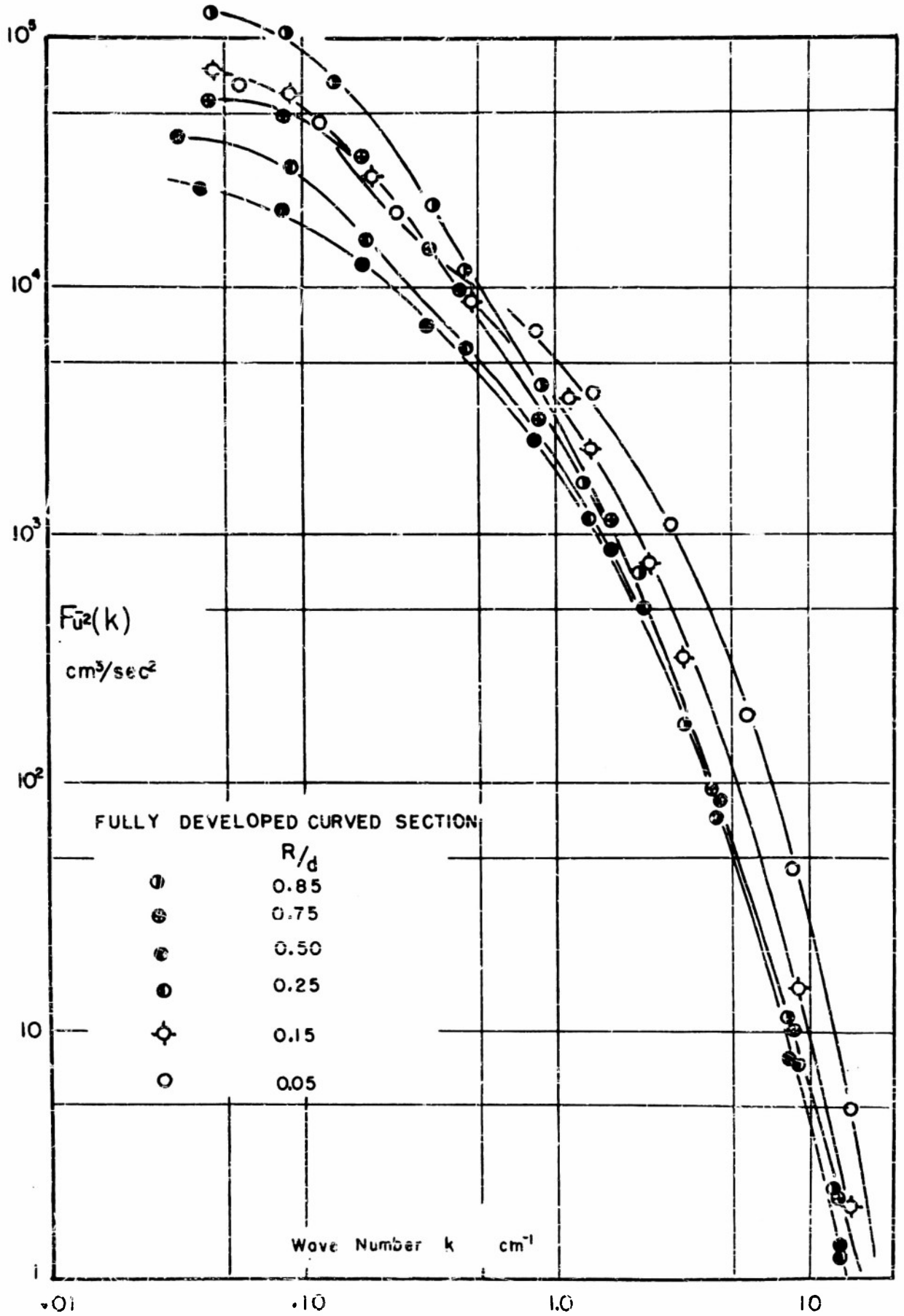


Figure 16. Spectrum of u' in the fully developed curved section.

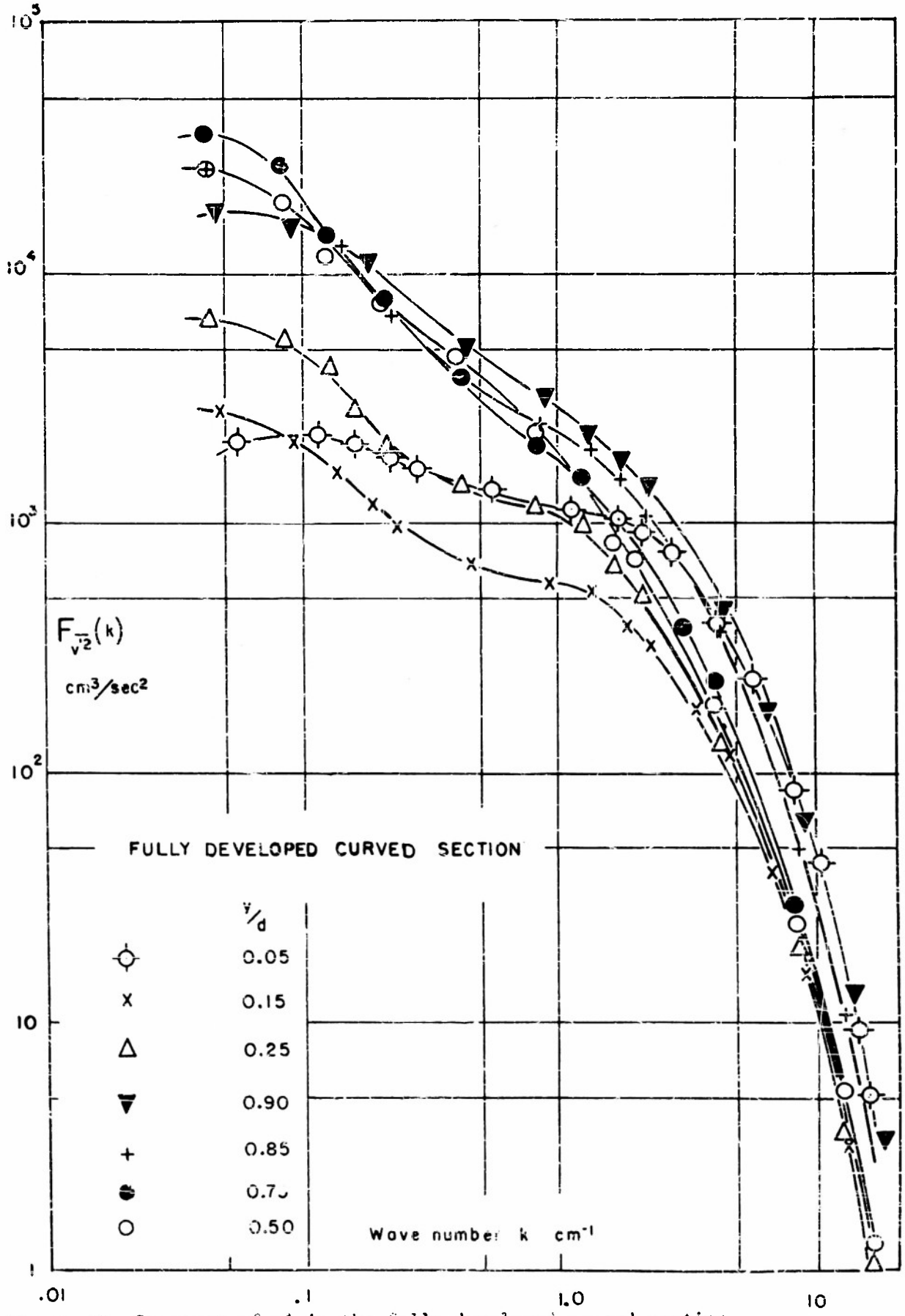


Figure 17. Spectrum of v' in the fully developed curved section.

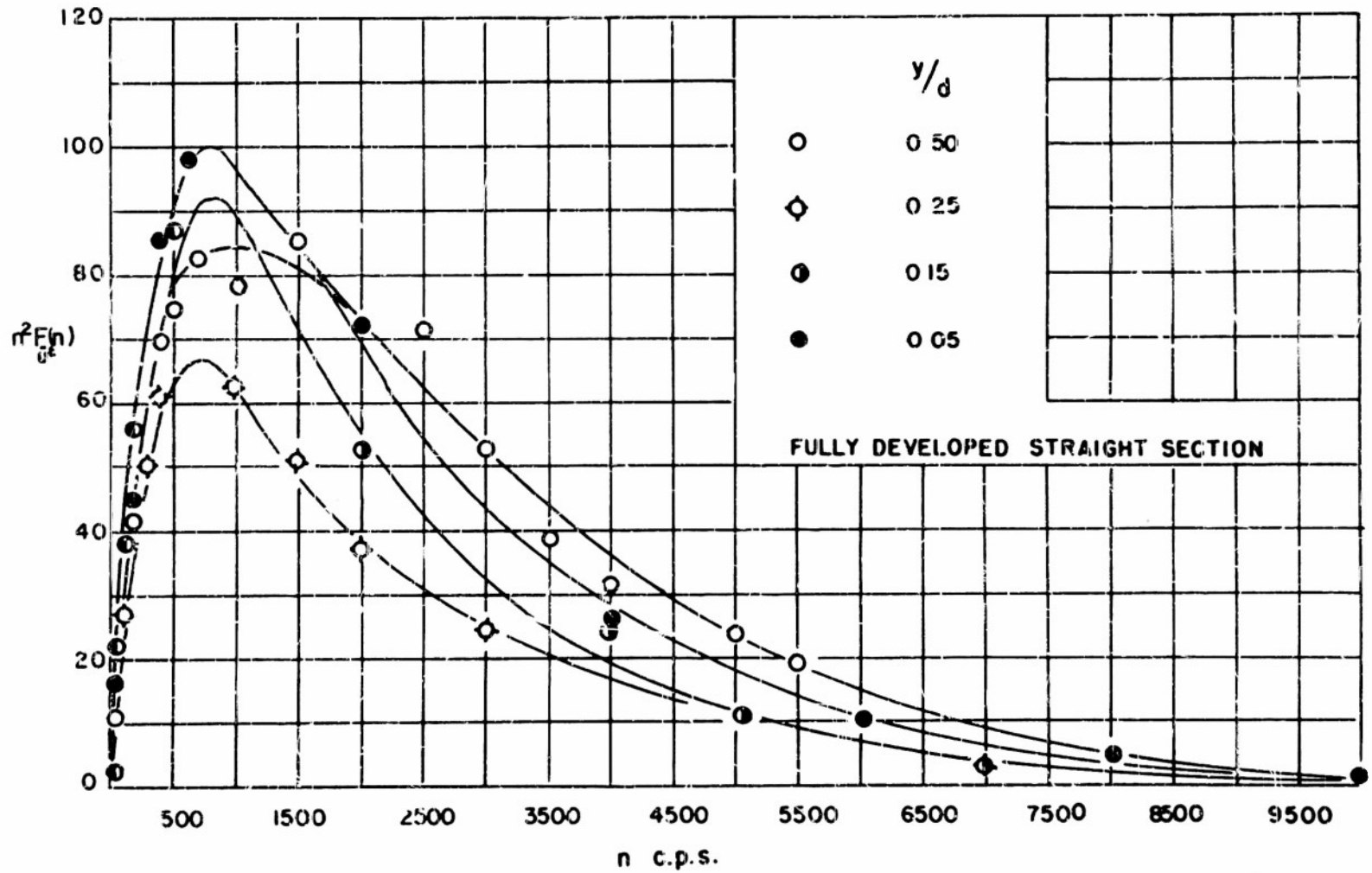


Figure 18. Second moment of u' spectrum in the fully developed straight section.

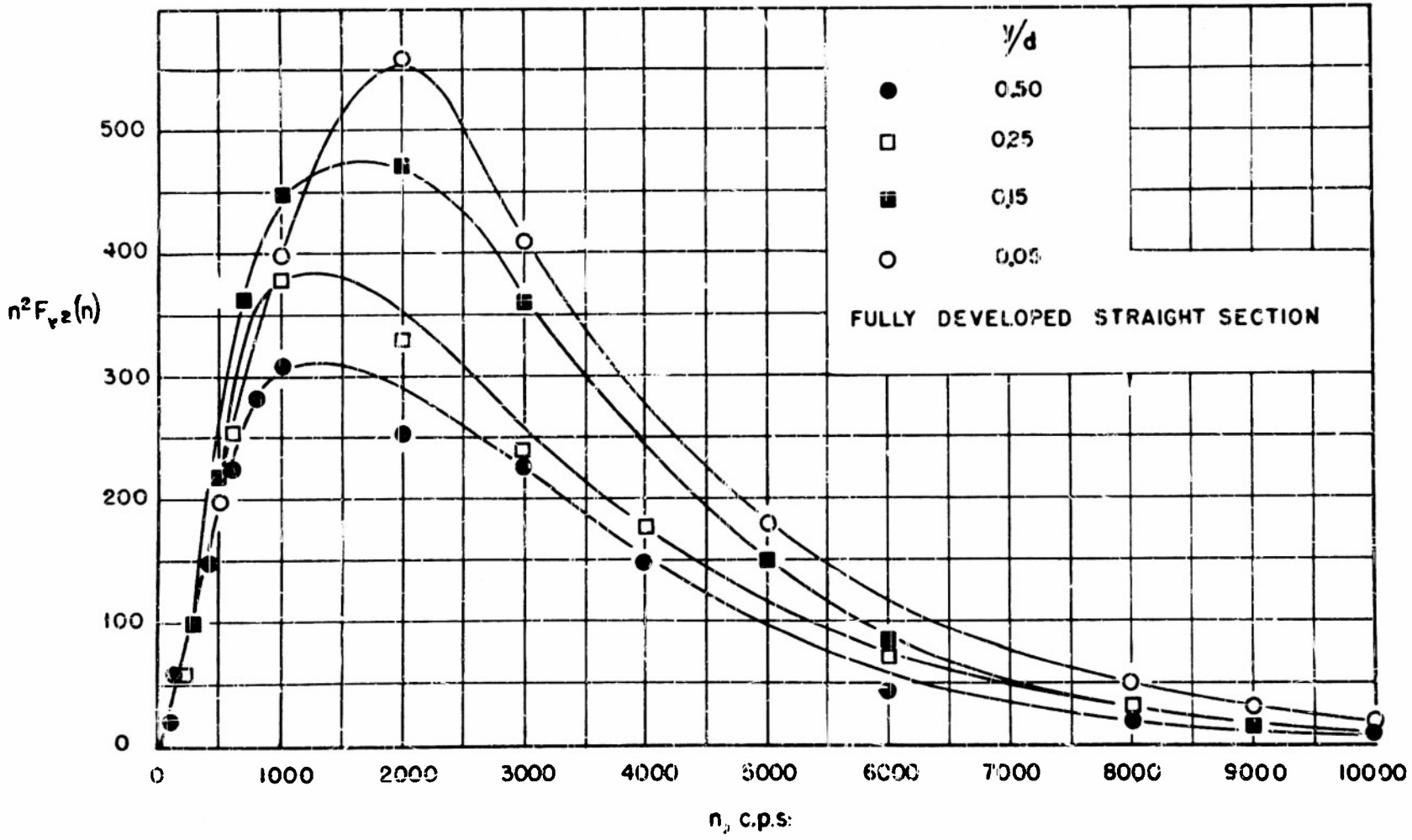


Figure 19. Second moment of v' spectrum in the fully developed straight section.

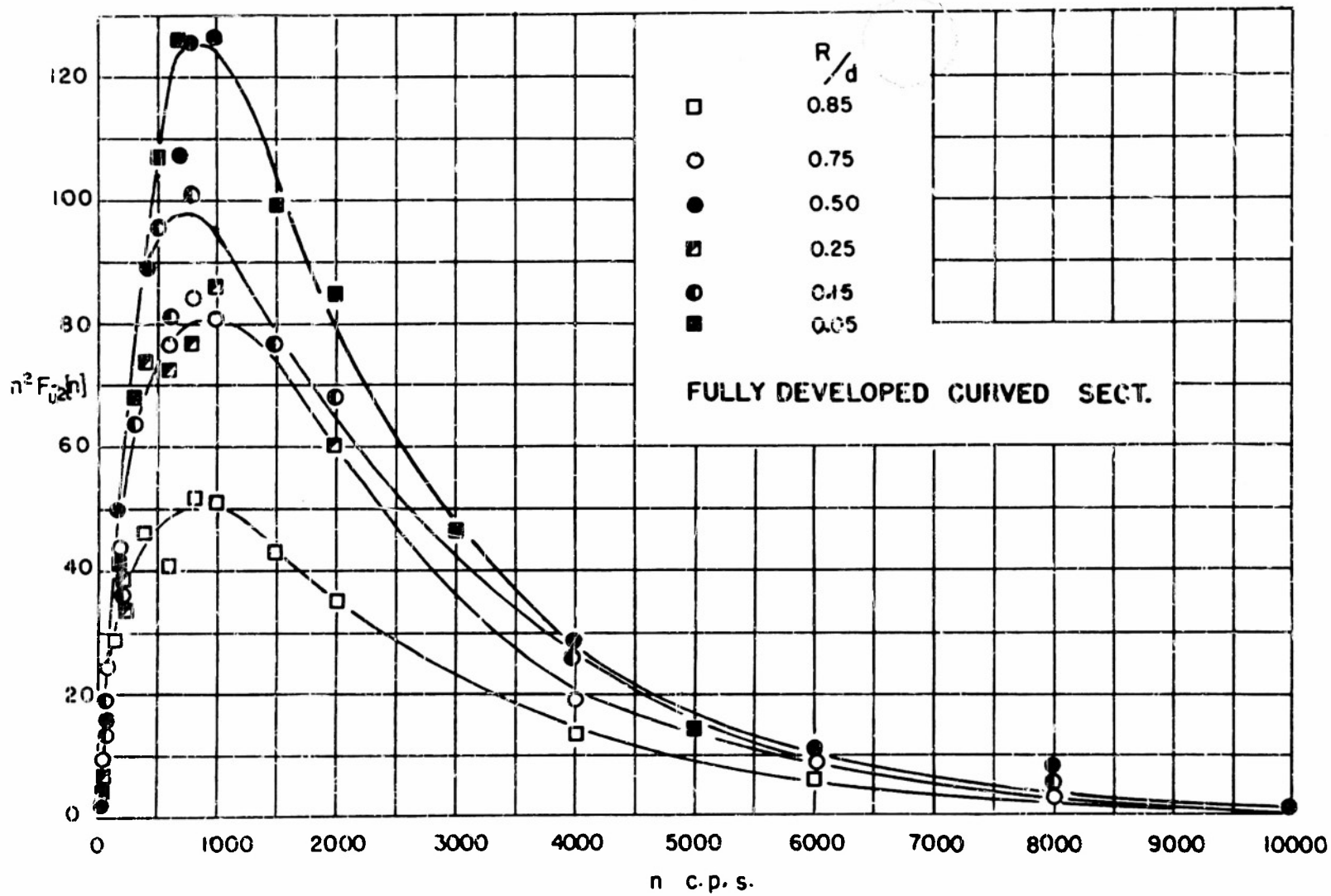


Figure 20. Second moment of u' spectrum in the fully developed curved section.

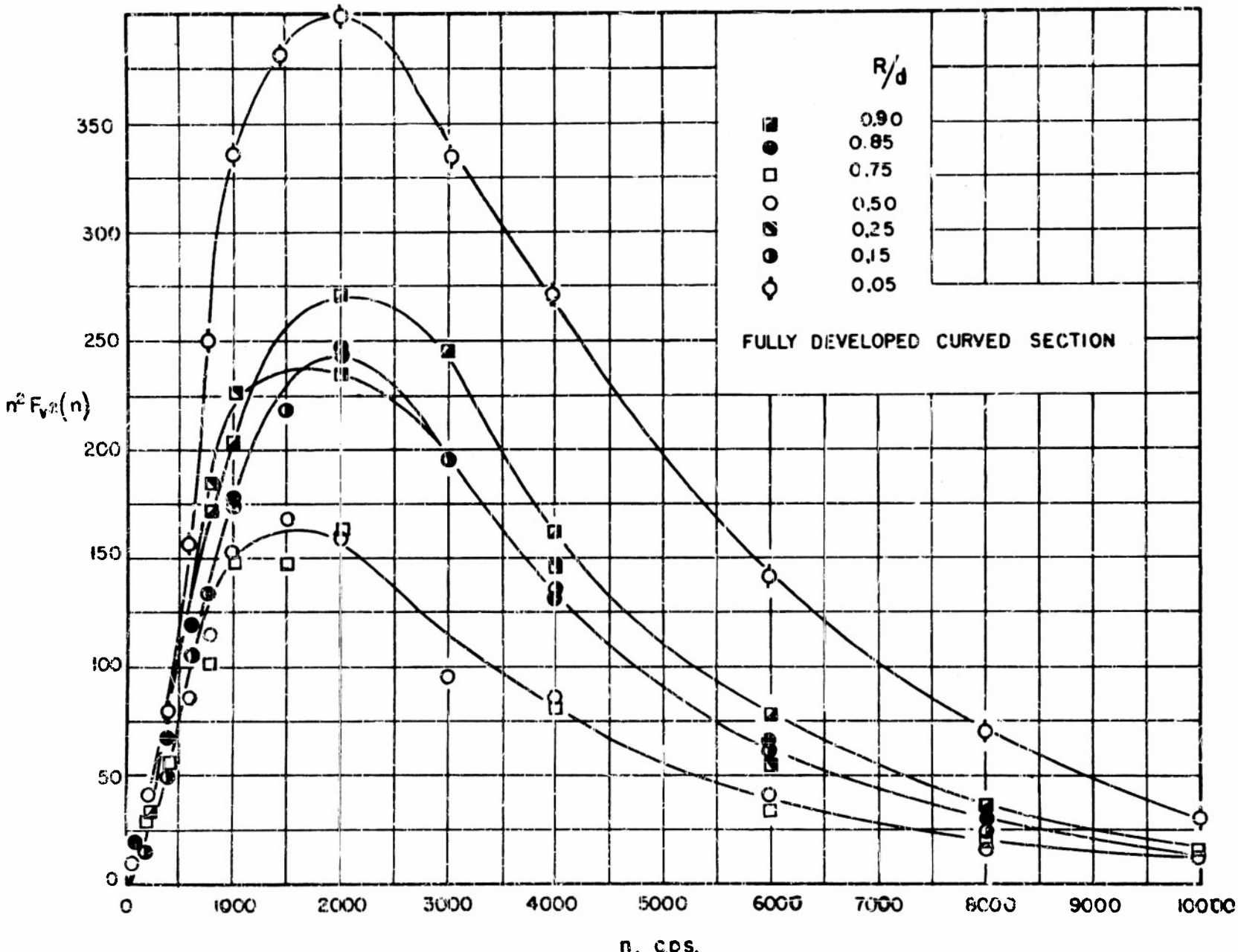


Figure 21. Second moment of v' spectrum in the fully developed curved section.

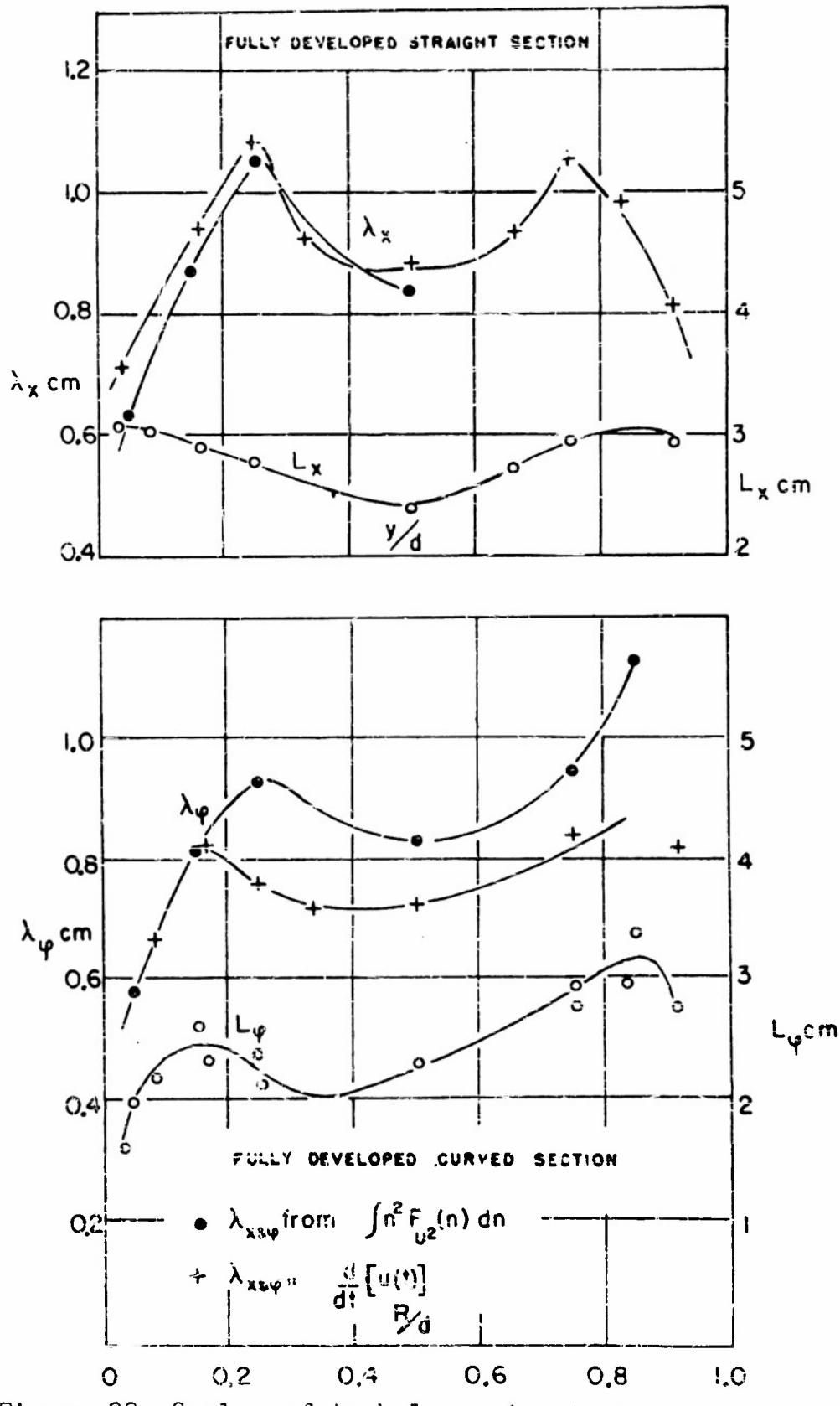


Figure 22. Scales of turbulence in straight and curved sections

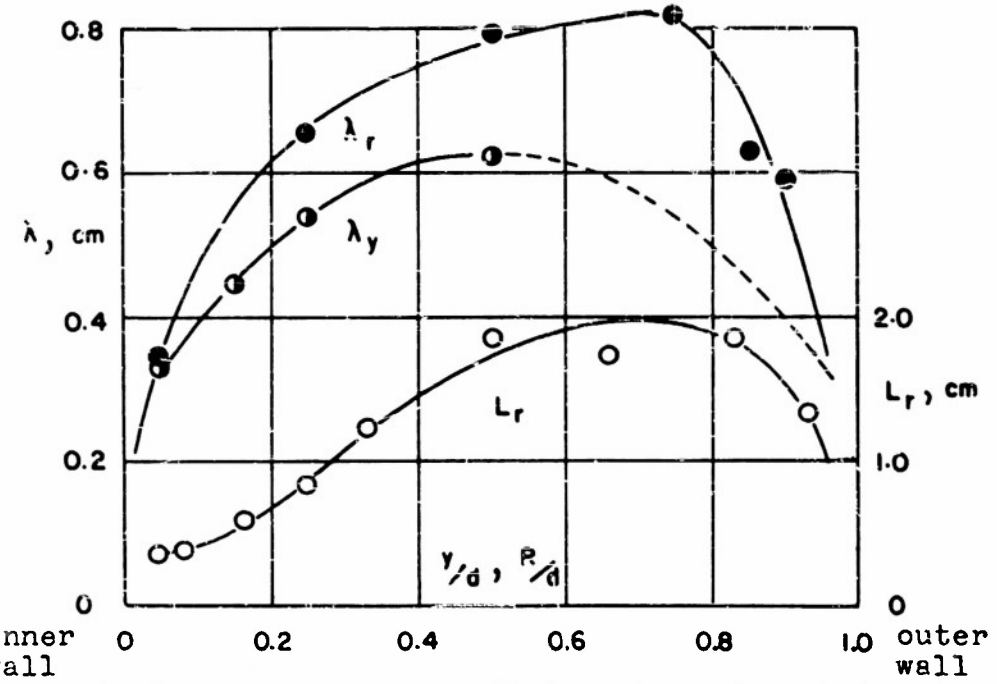


Figure 23. Transversal and radial scales of turbulence.

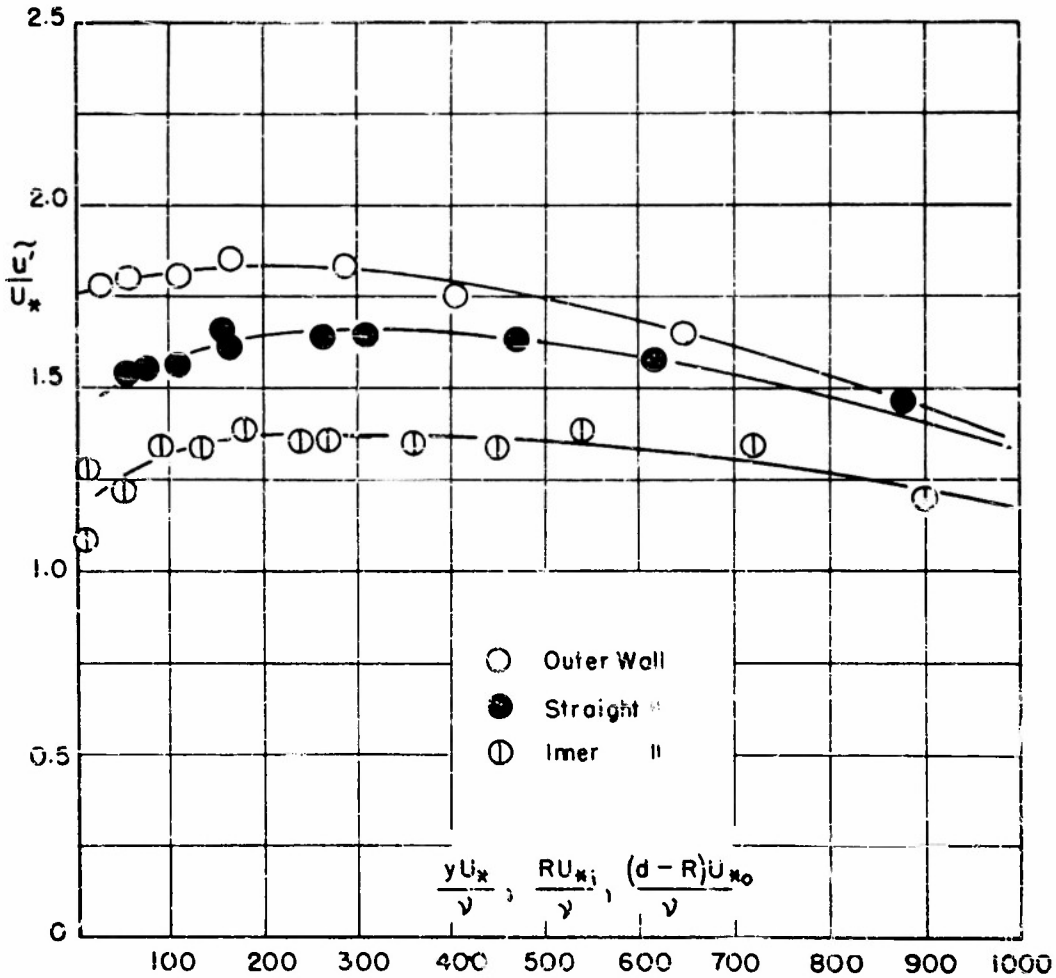


Figure 24. Similarity in the turbulence intensity.

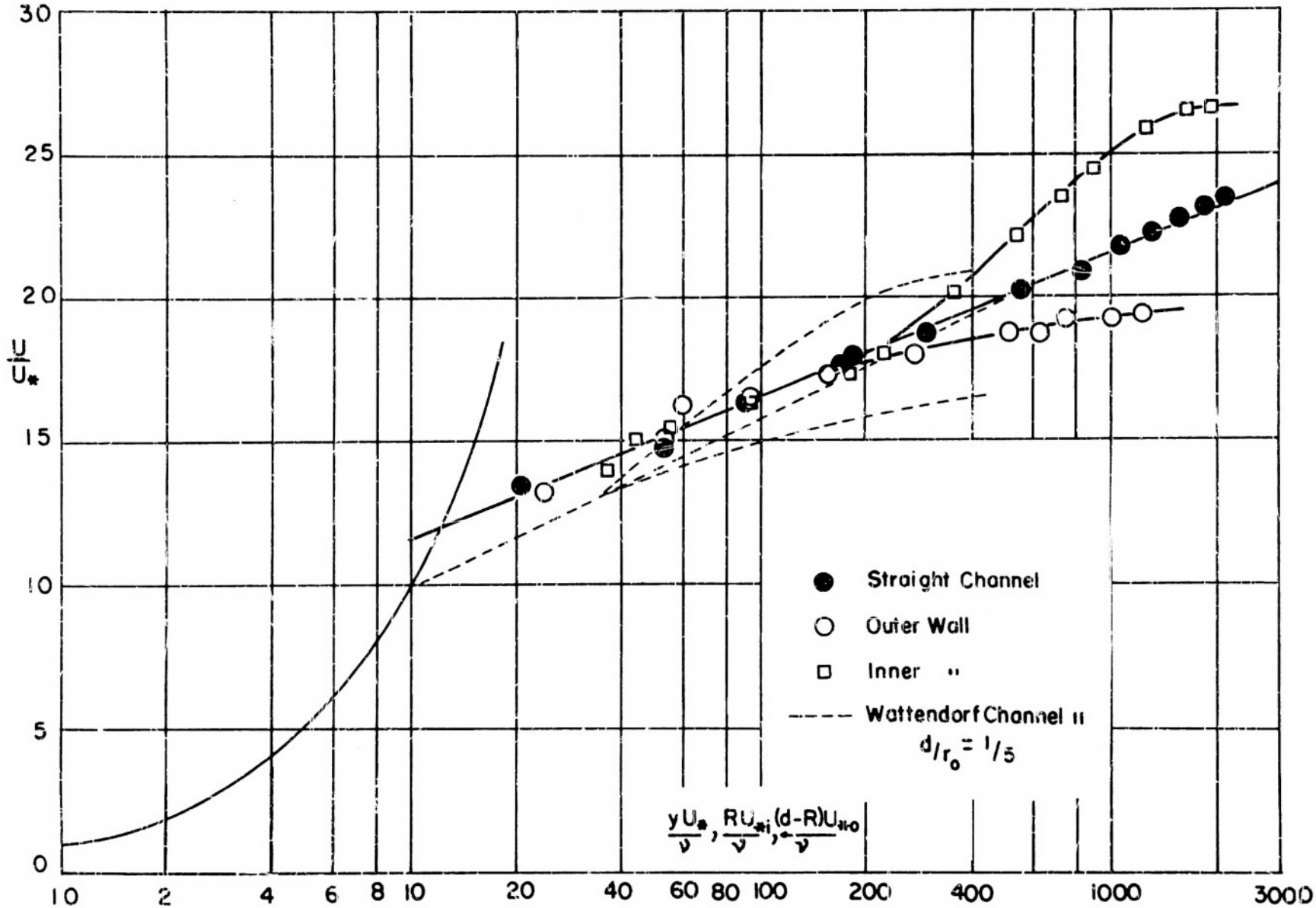


Figure 25. Similarity in the mean velocity distribution.

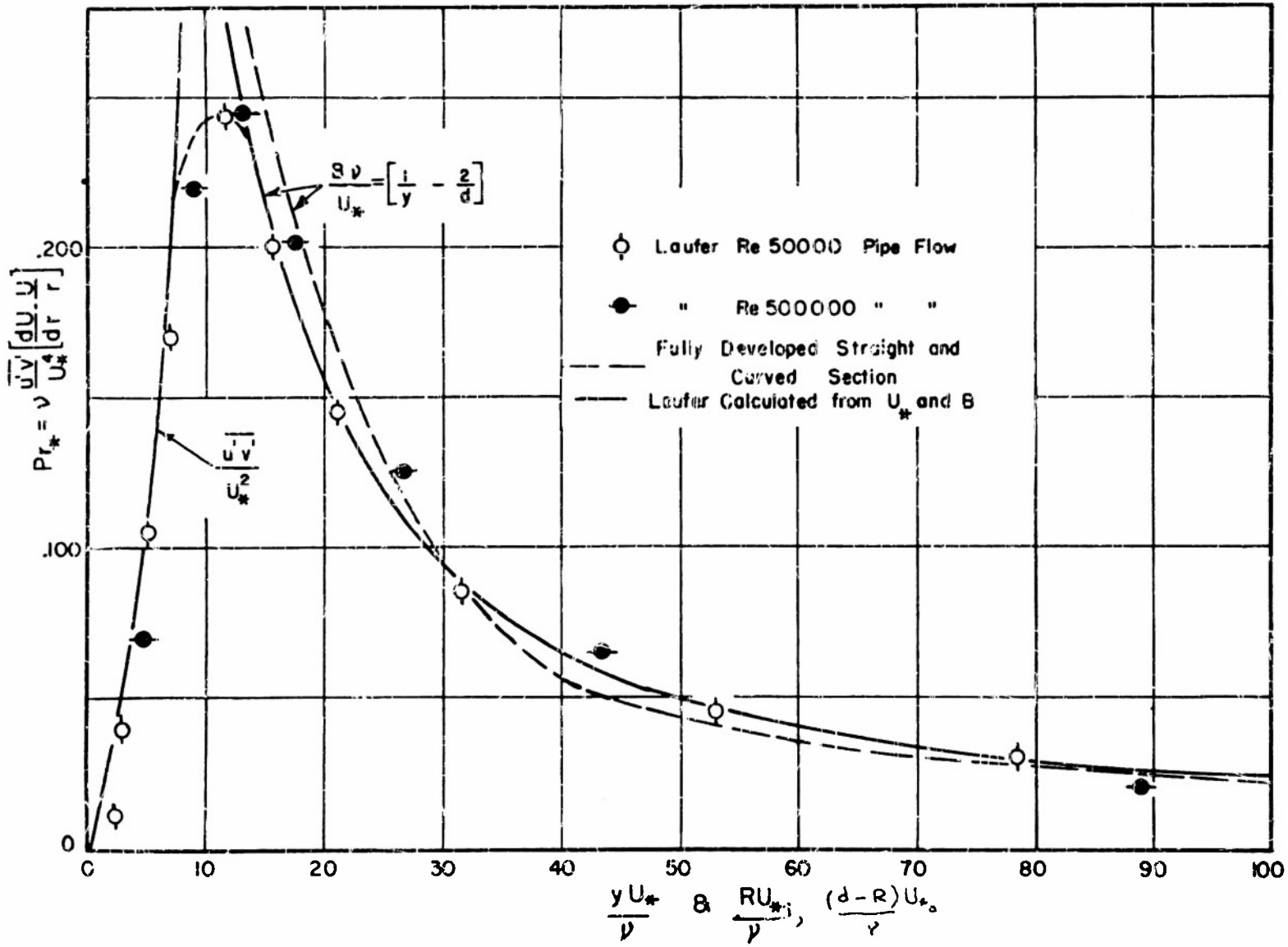


Figure 26. Dimensionless turbulent energy production near the wall.

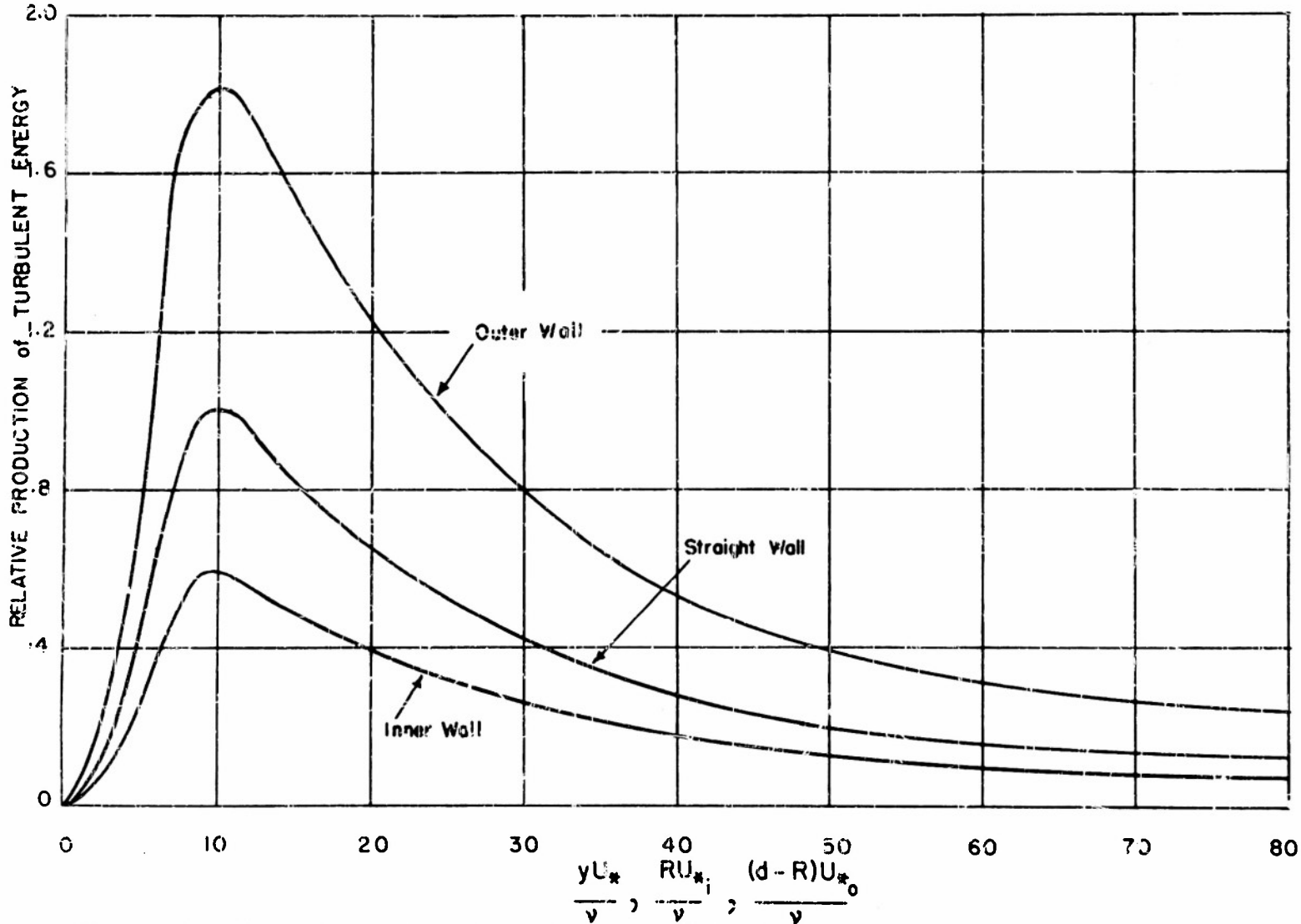


Figure 27. Relative rate of production of turbulent energy at different walls.

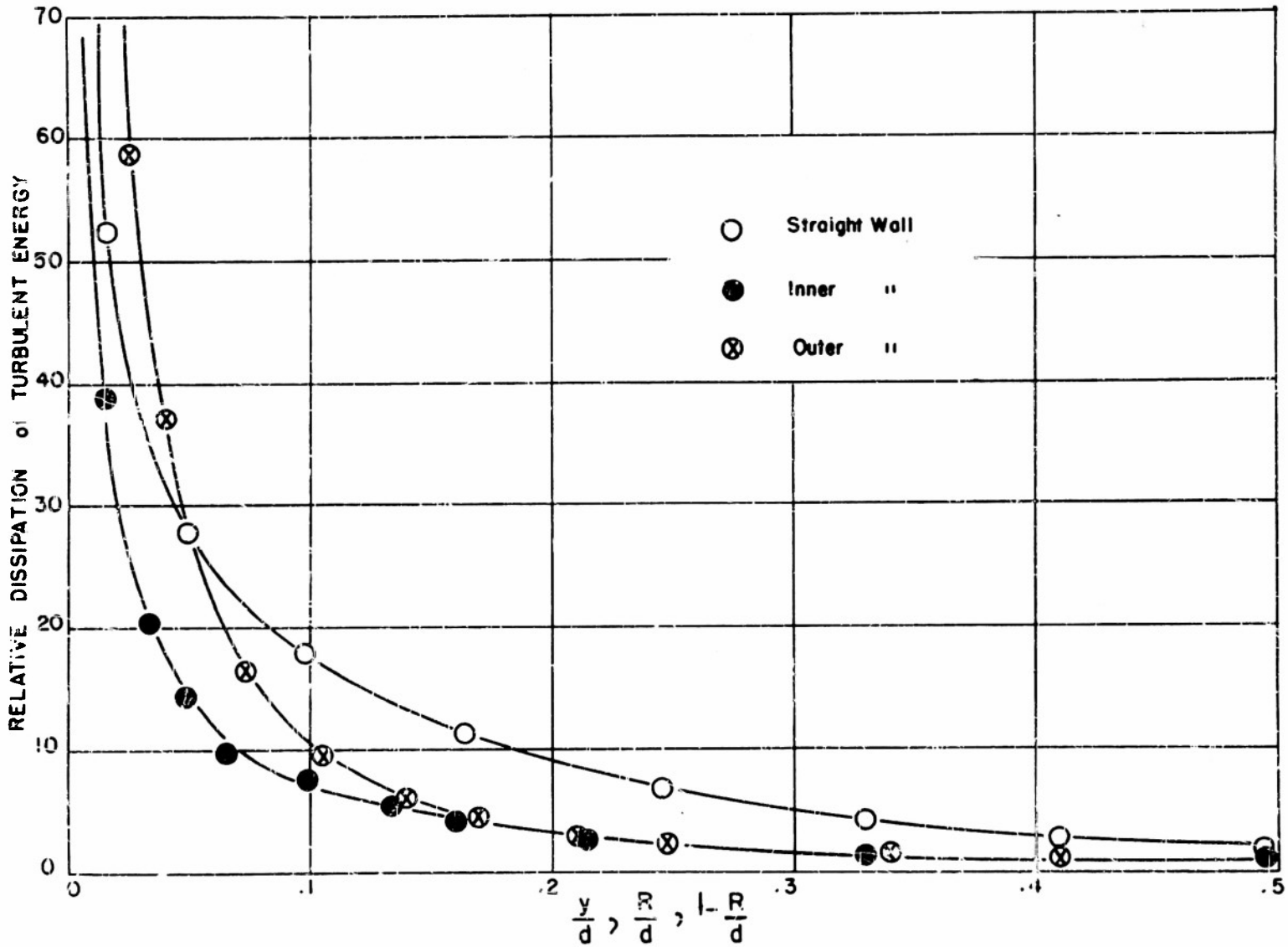


Figure 28. Relative rate of dissipation of turbulent energy at different walls.

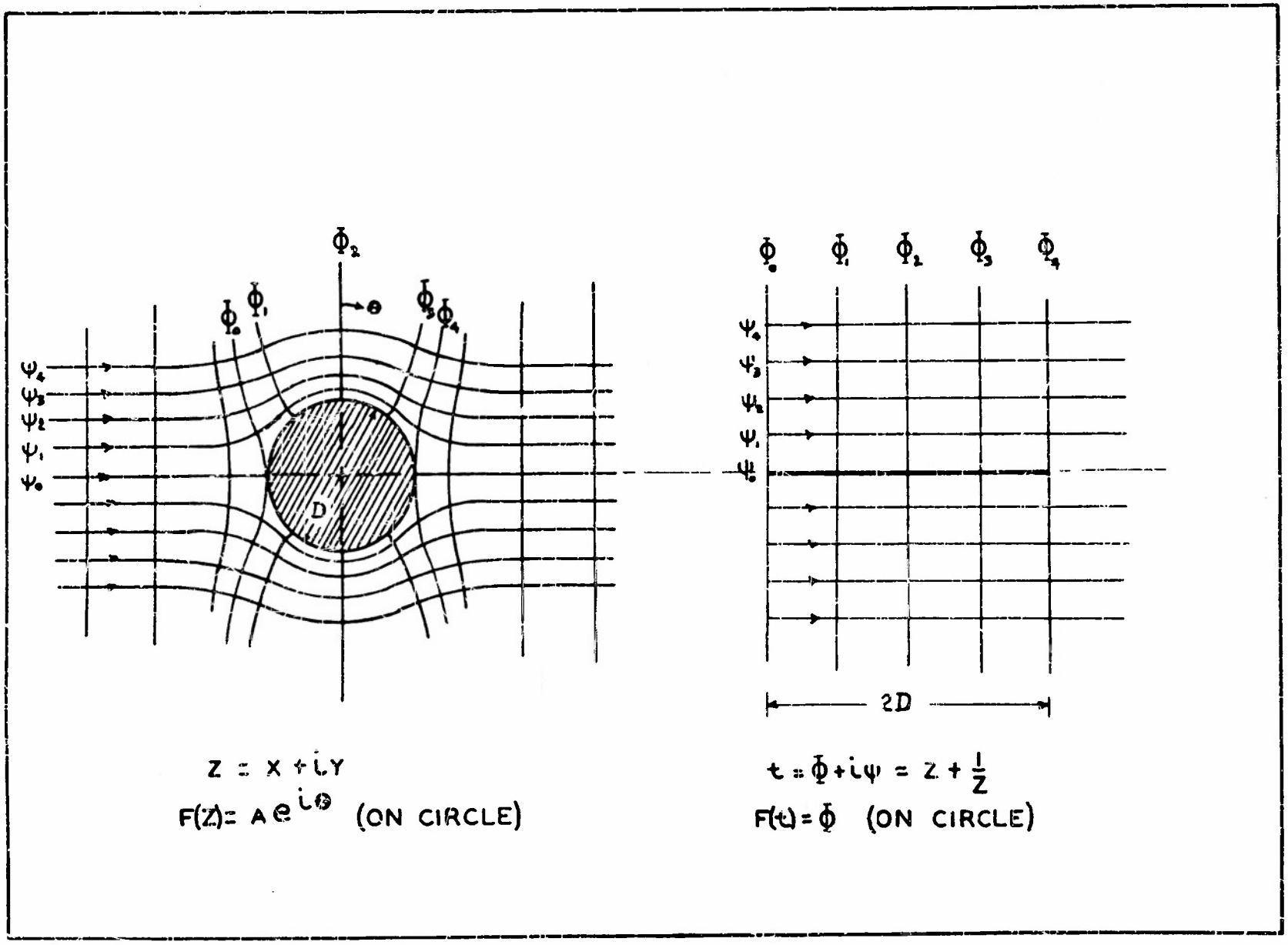


Figure 29. Transformation of flow around a cylinder into flow over a flat plate.

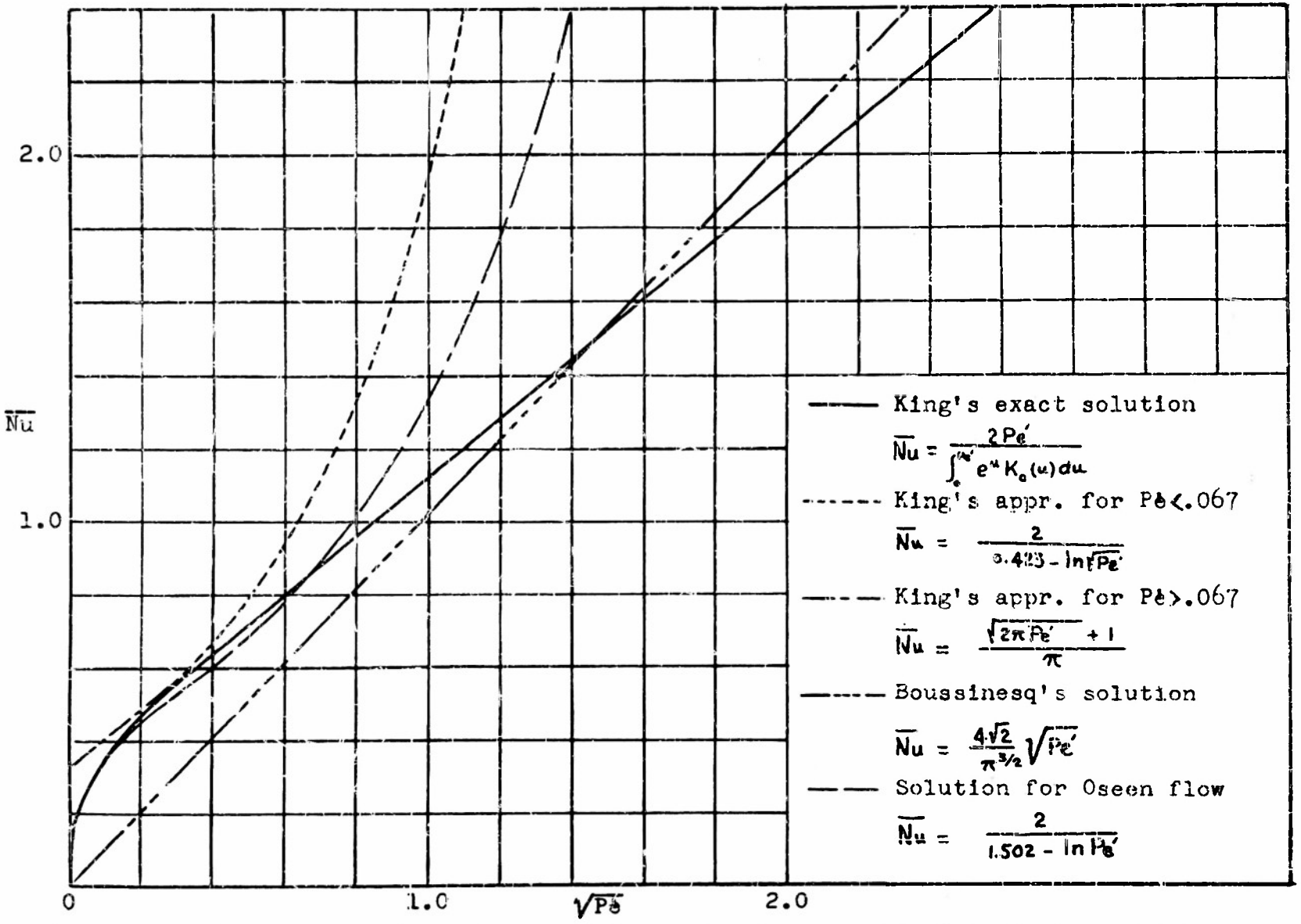


Figure 30. Existing solutions for heat transfer by convection from heated cylinders.

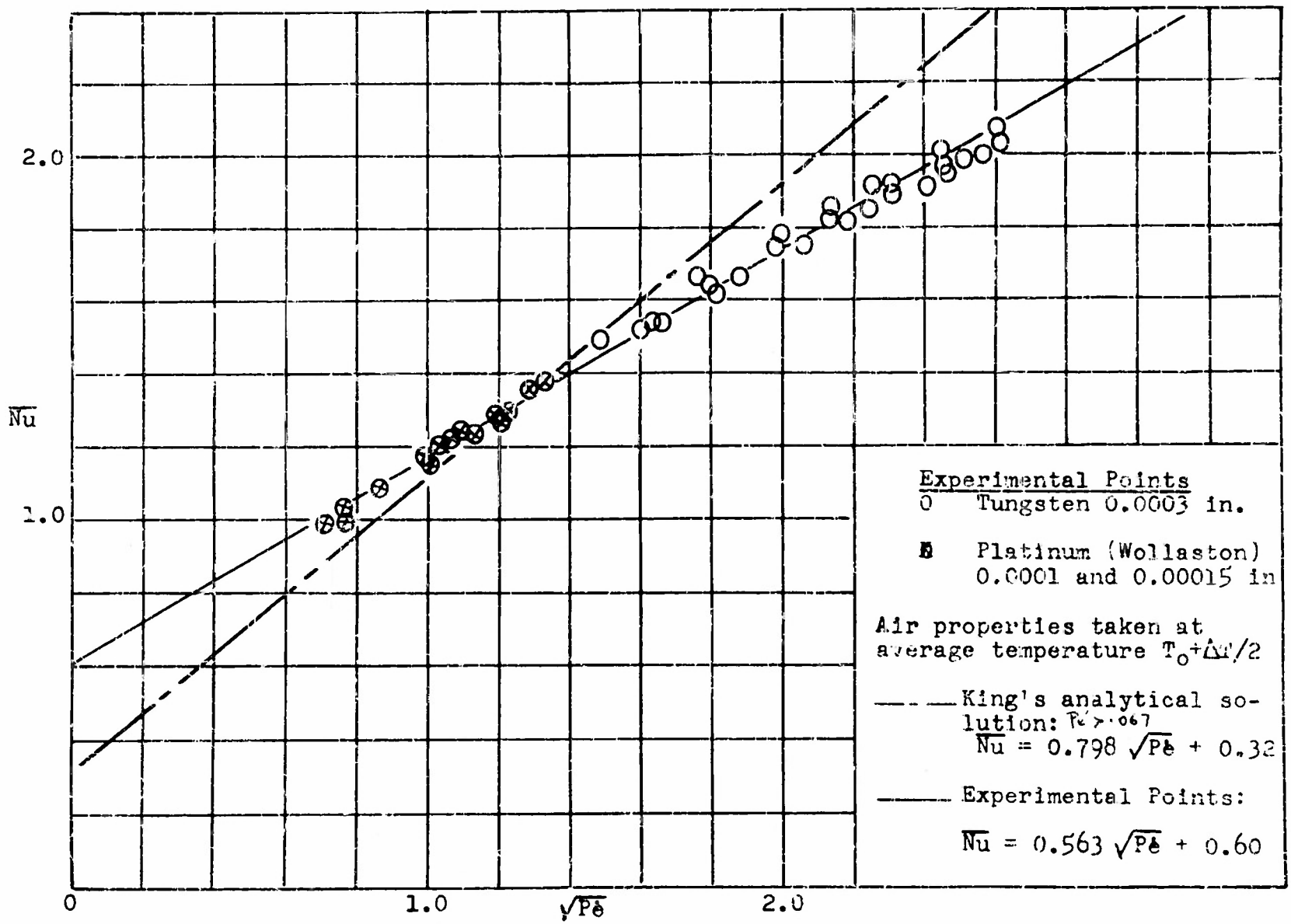


Figure 31. Heat Convection from Small Heated Cylinders.

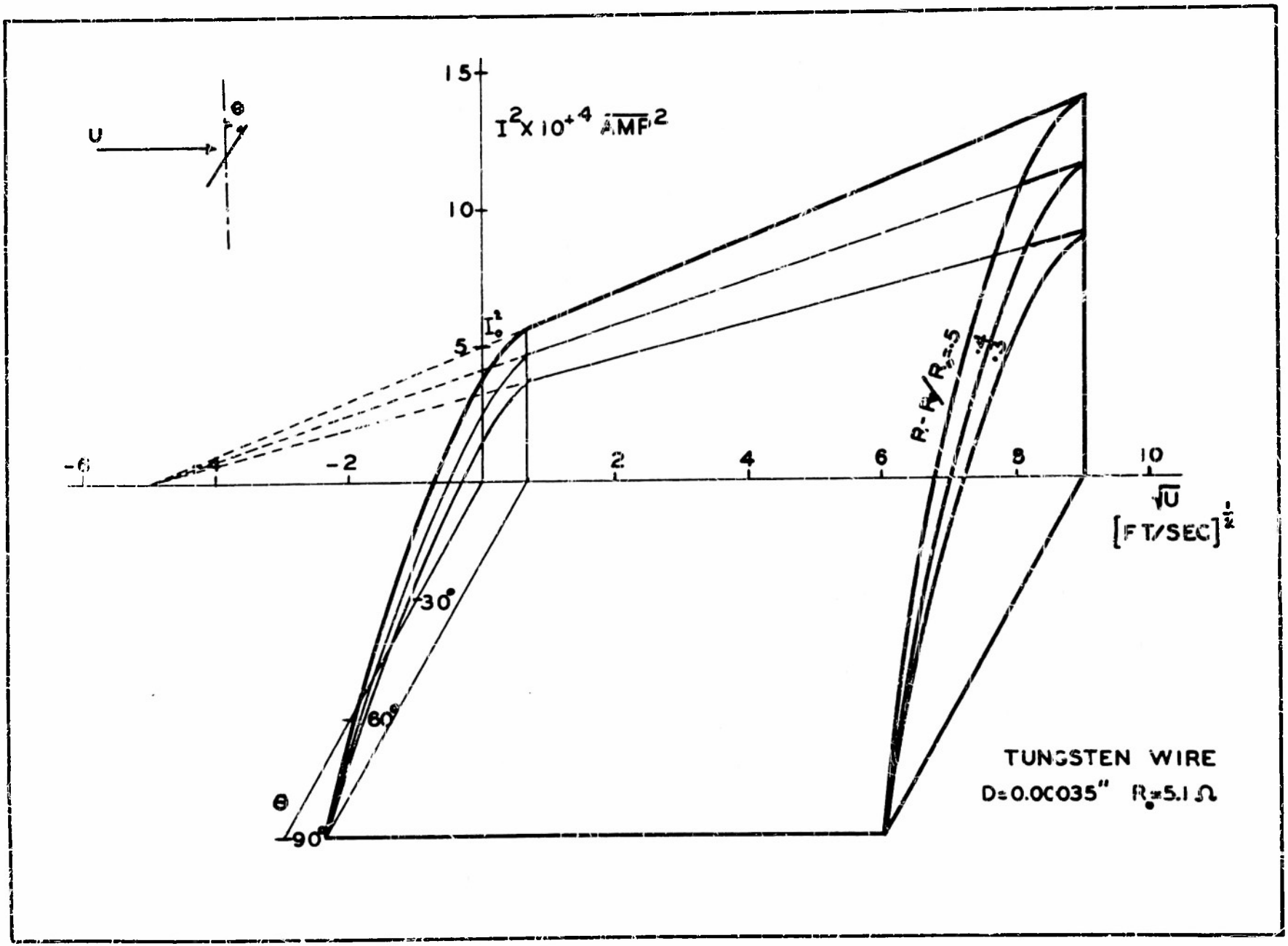


Figure 32. Sensitivity of a heated wire to velocity and incident angle.

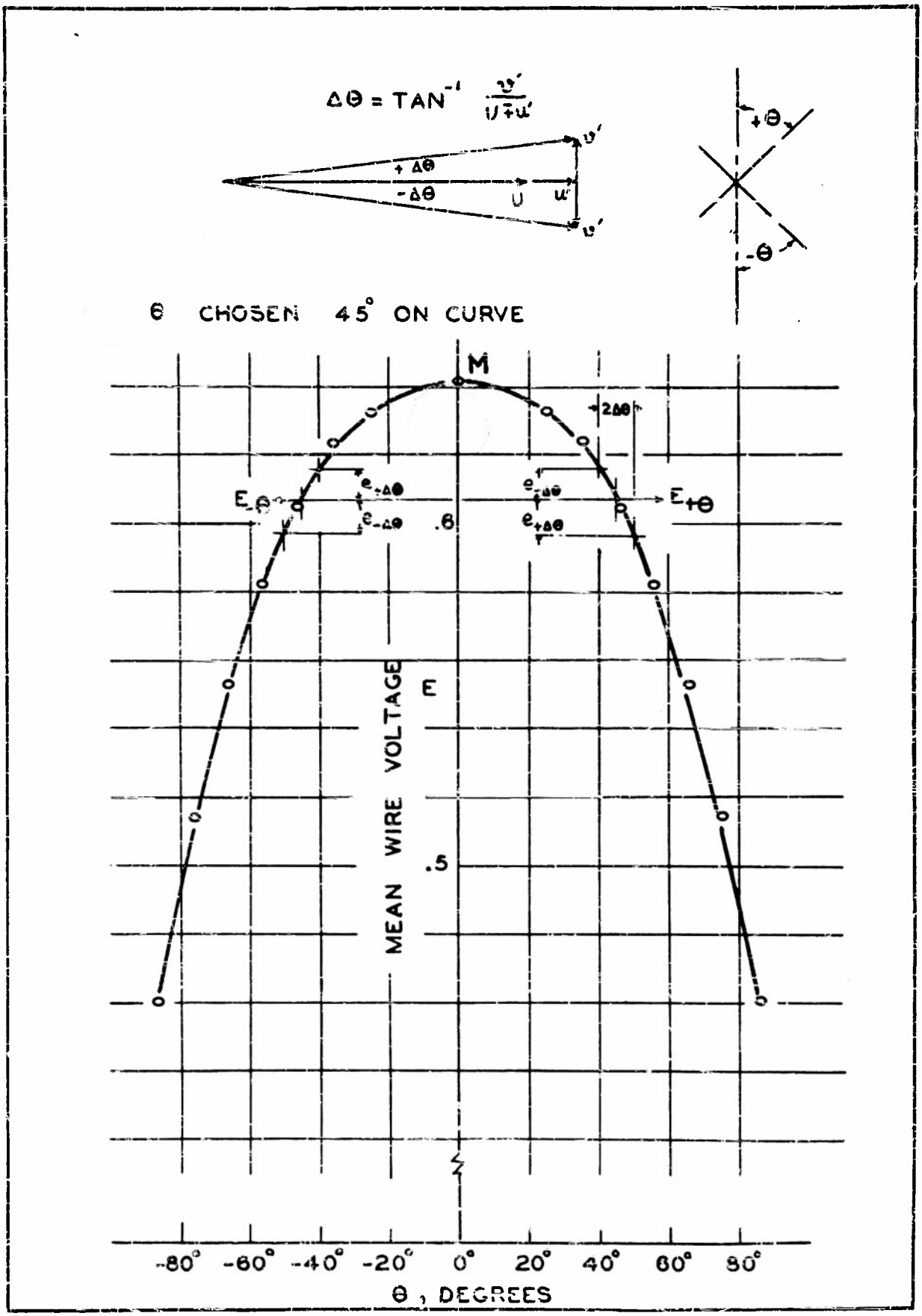


Figure 33. Sensitivity of a heated wire to incident angle.

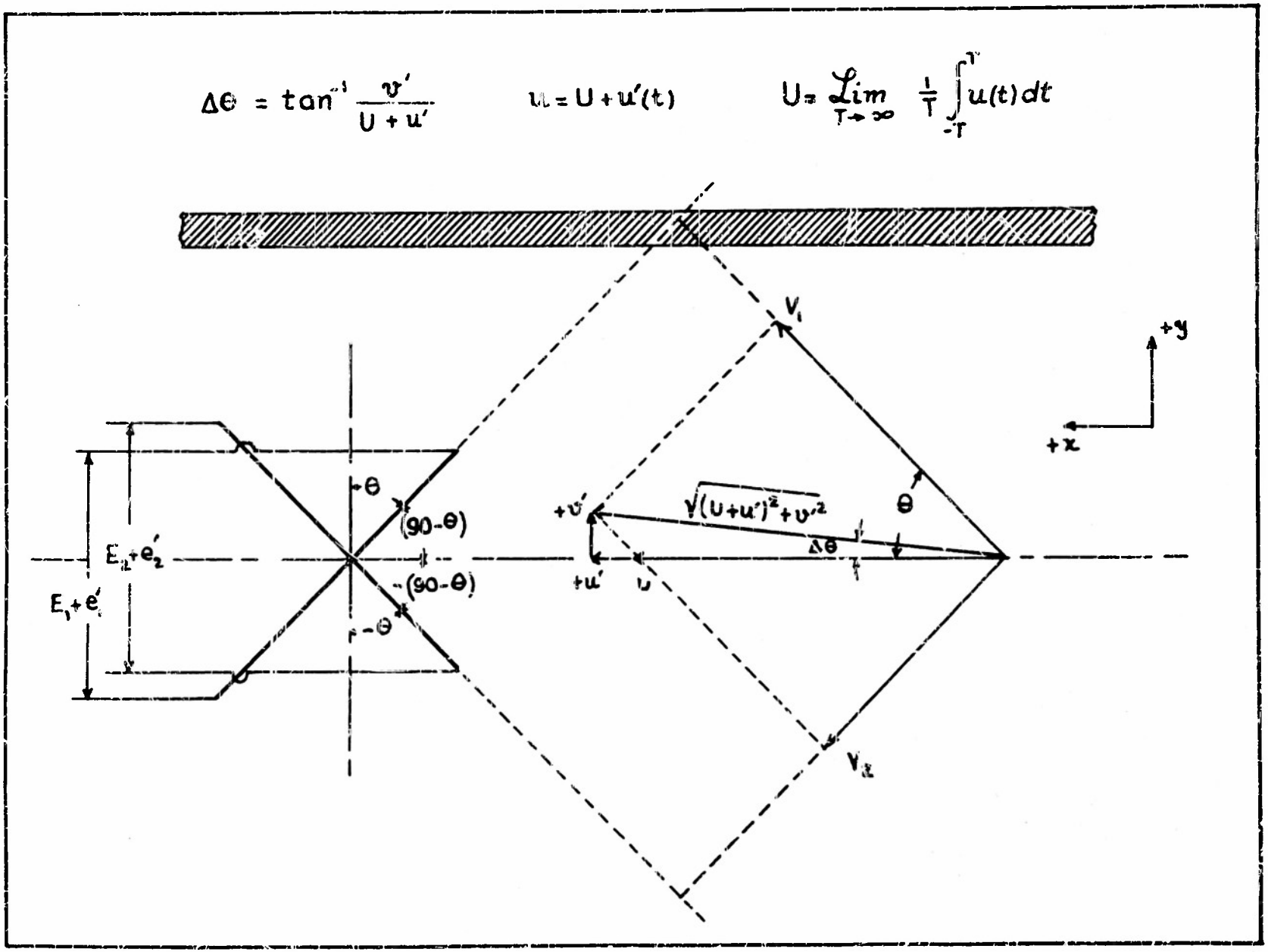


Figure 34. Position of an X-meter in turbulent channel flow.

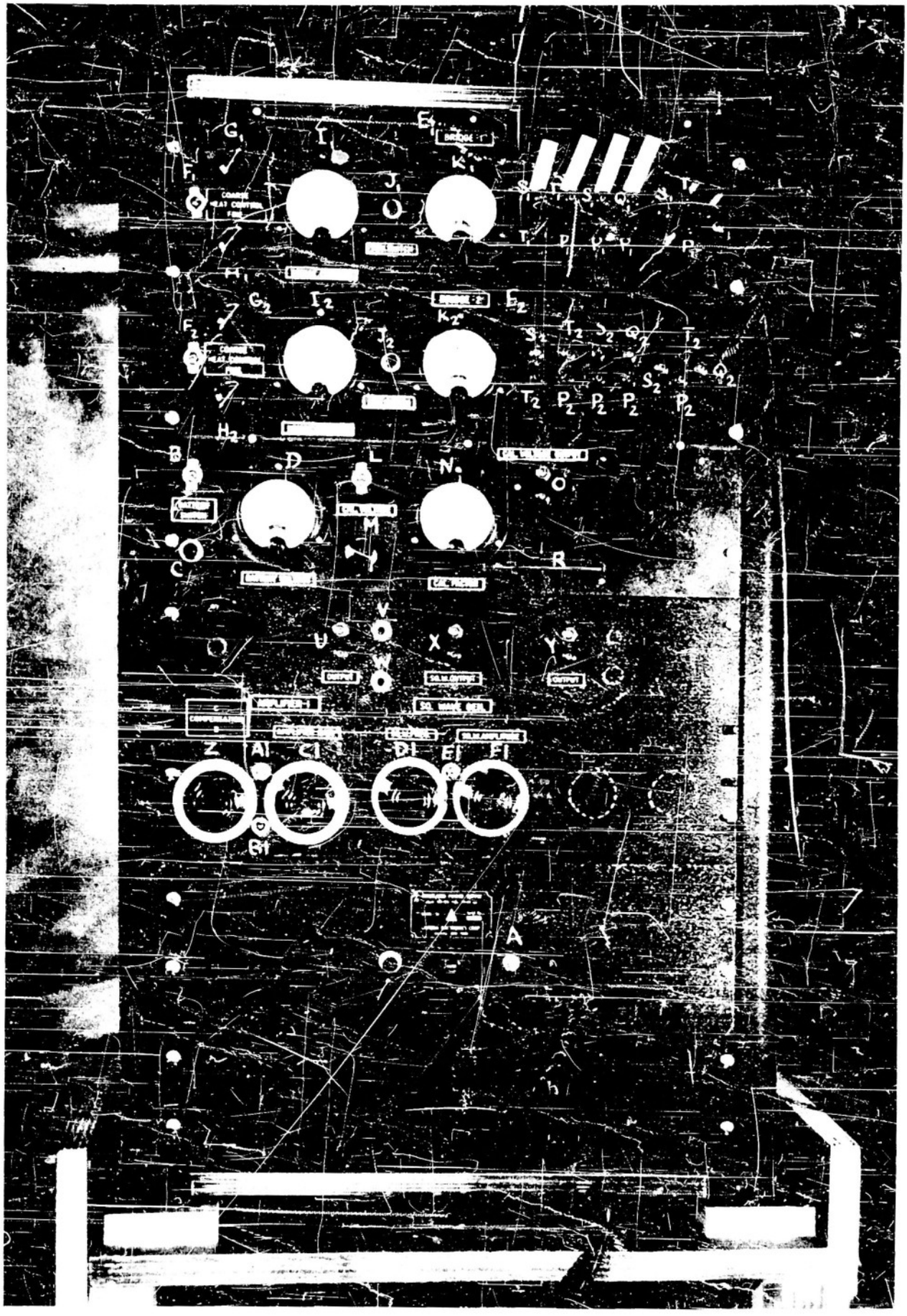


Figure 35. Control panel of hot-wire anemometer.

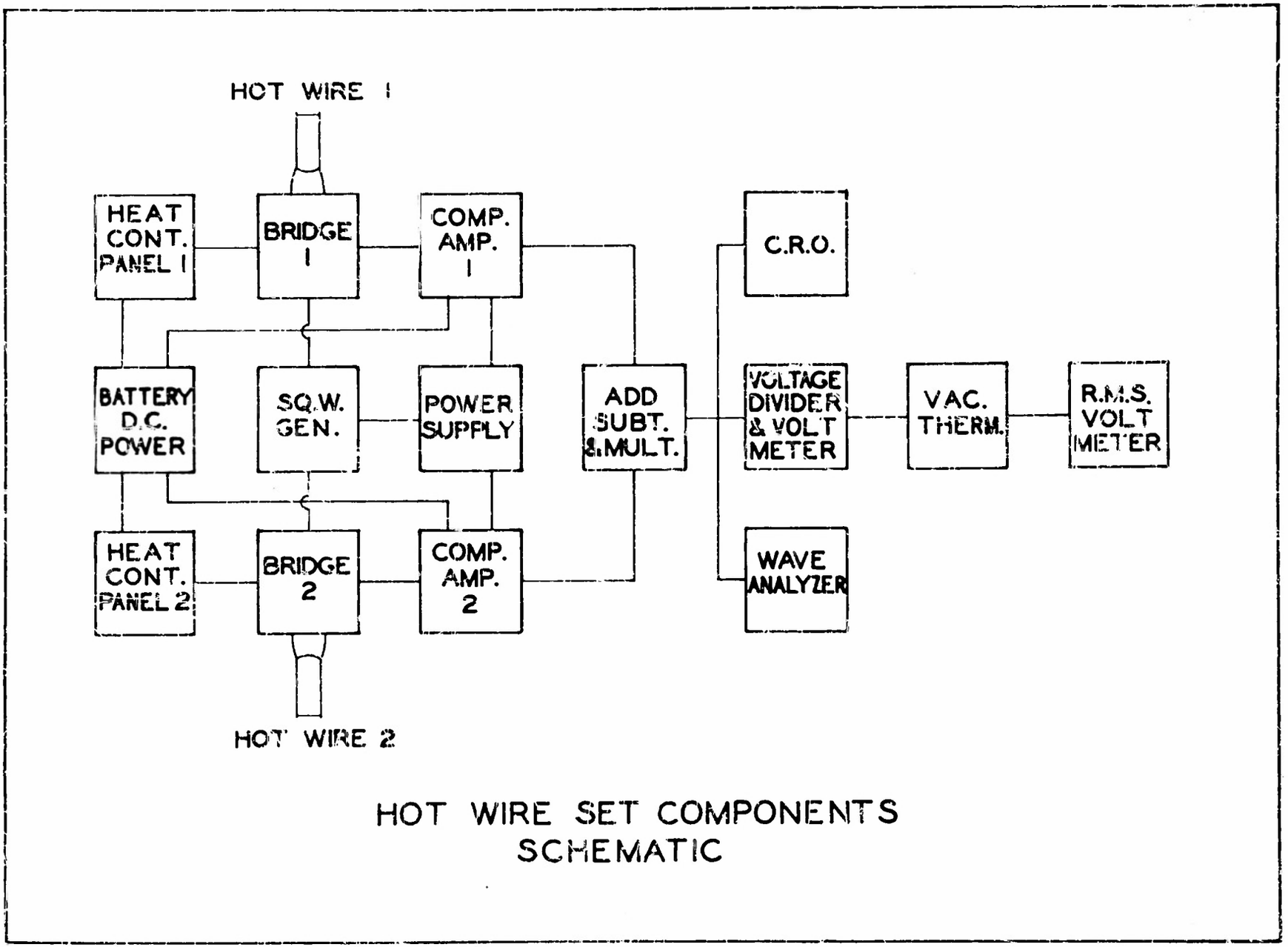


Figure 36. Schematic assembly of turbulence measuring equipment.

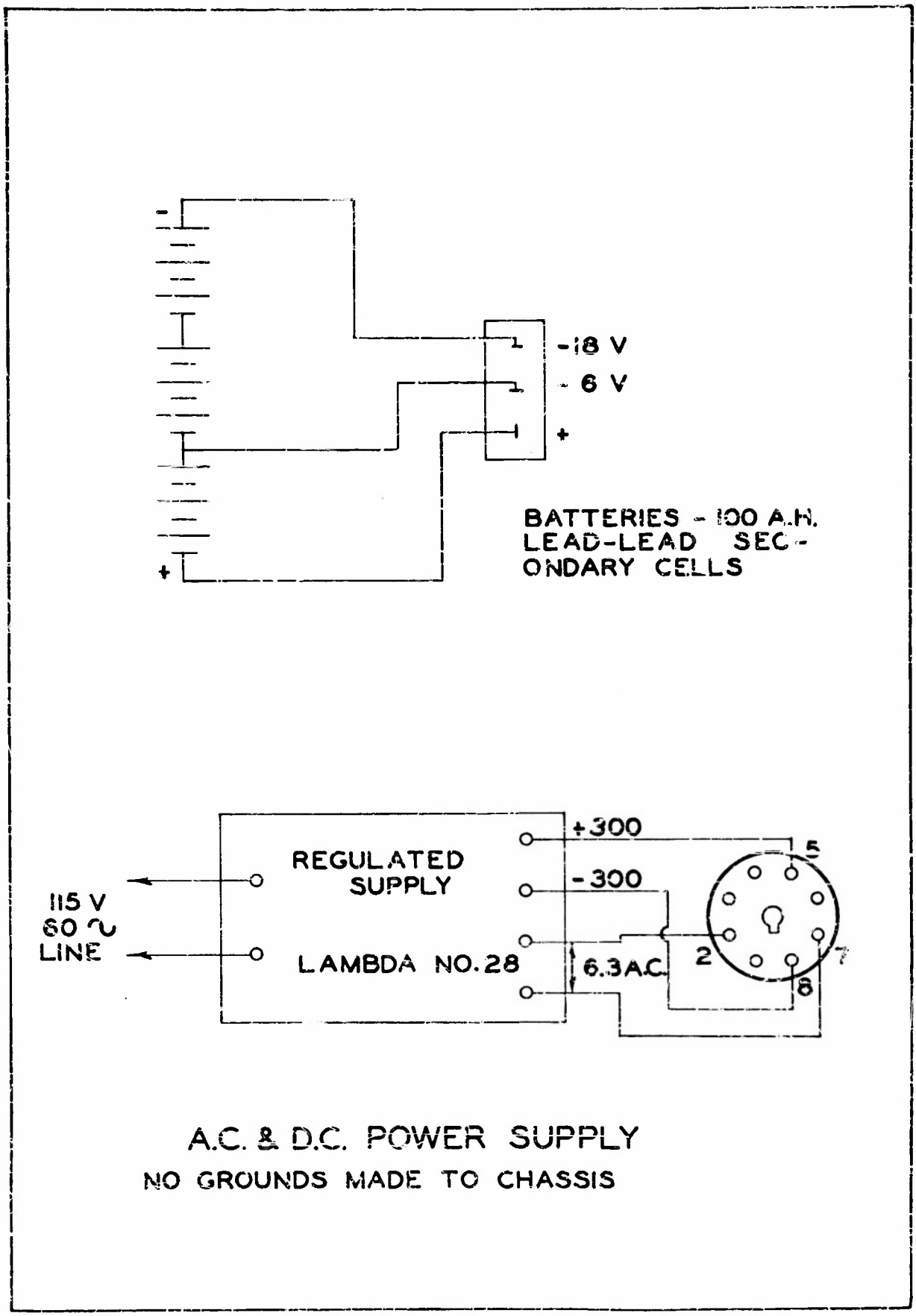


Figure 37. Schematic of AC and DC power supply

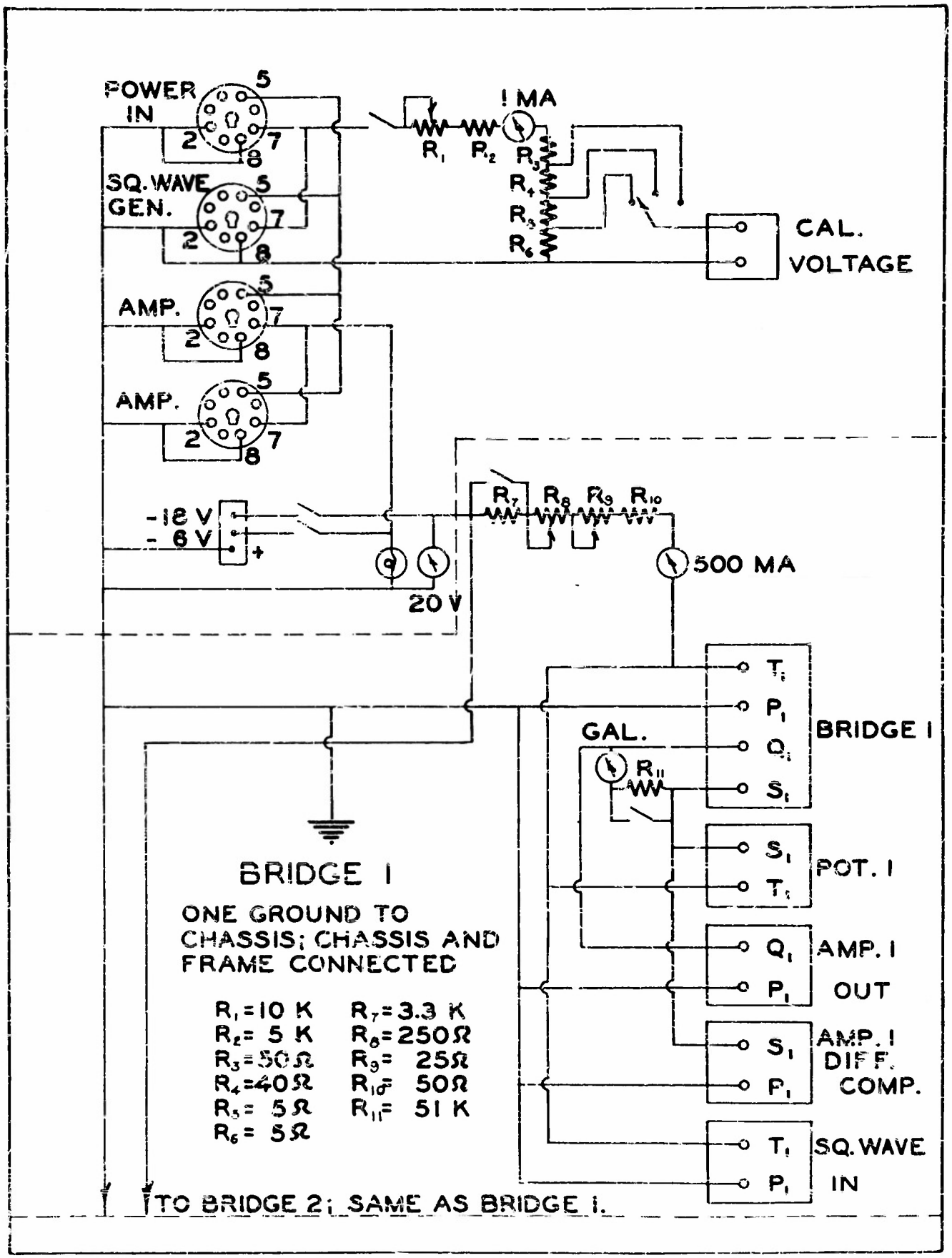


Figure 38. Heat Control and calibration voltage circuit.

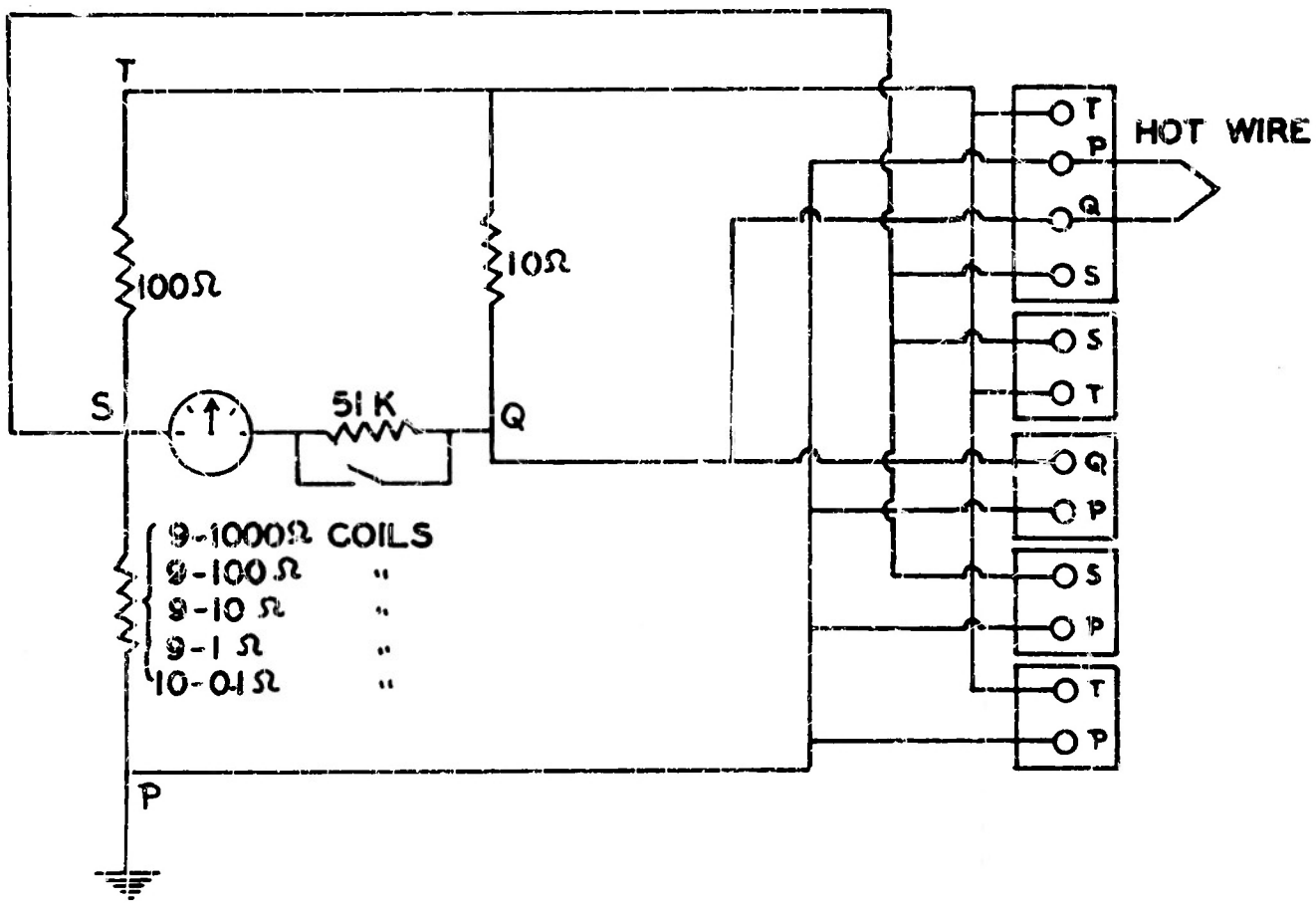


FIG 39. BRIDGE CIRCUIT

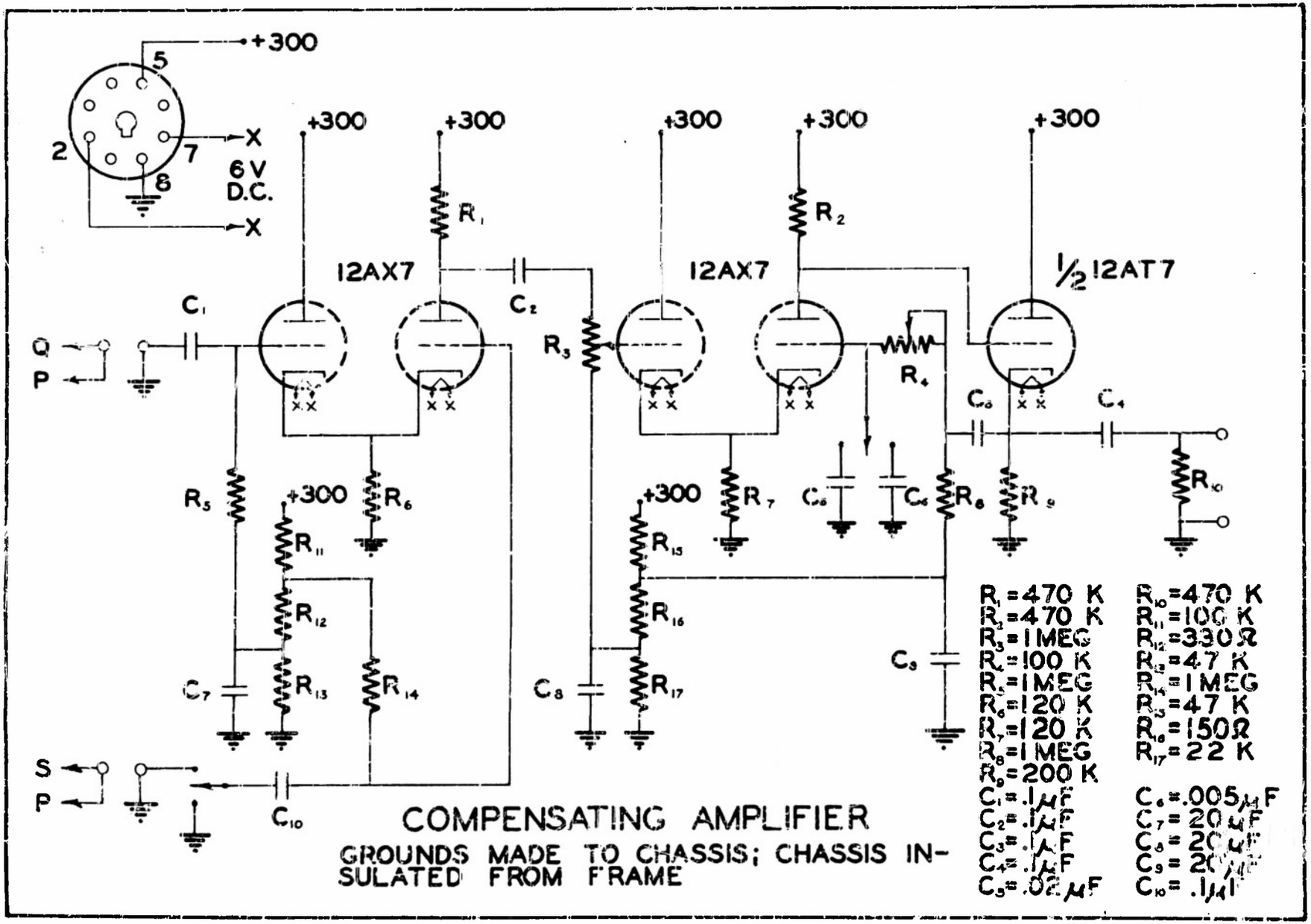


Figure 40. Circuit Diagram of Compensating amplifier.

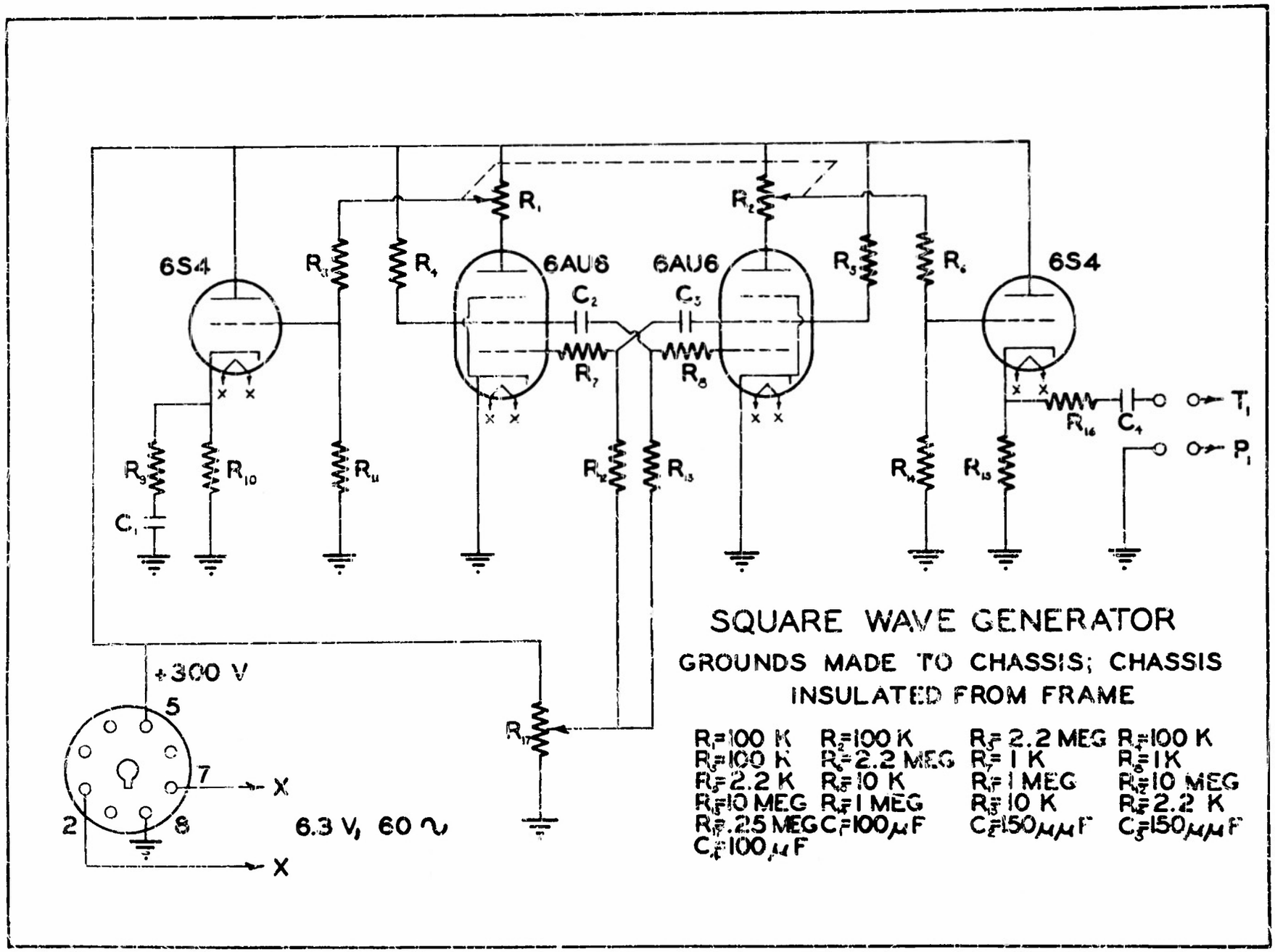


Figure 41. Circuit diagram of square wave generator.

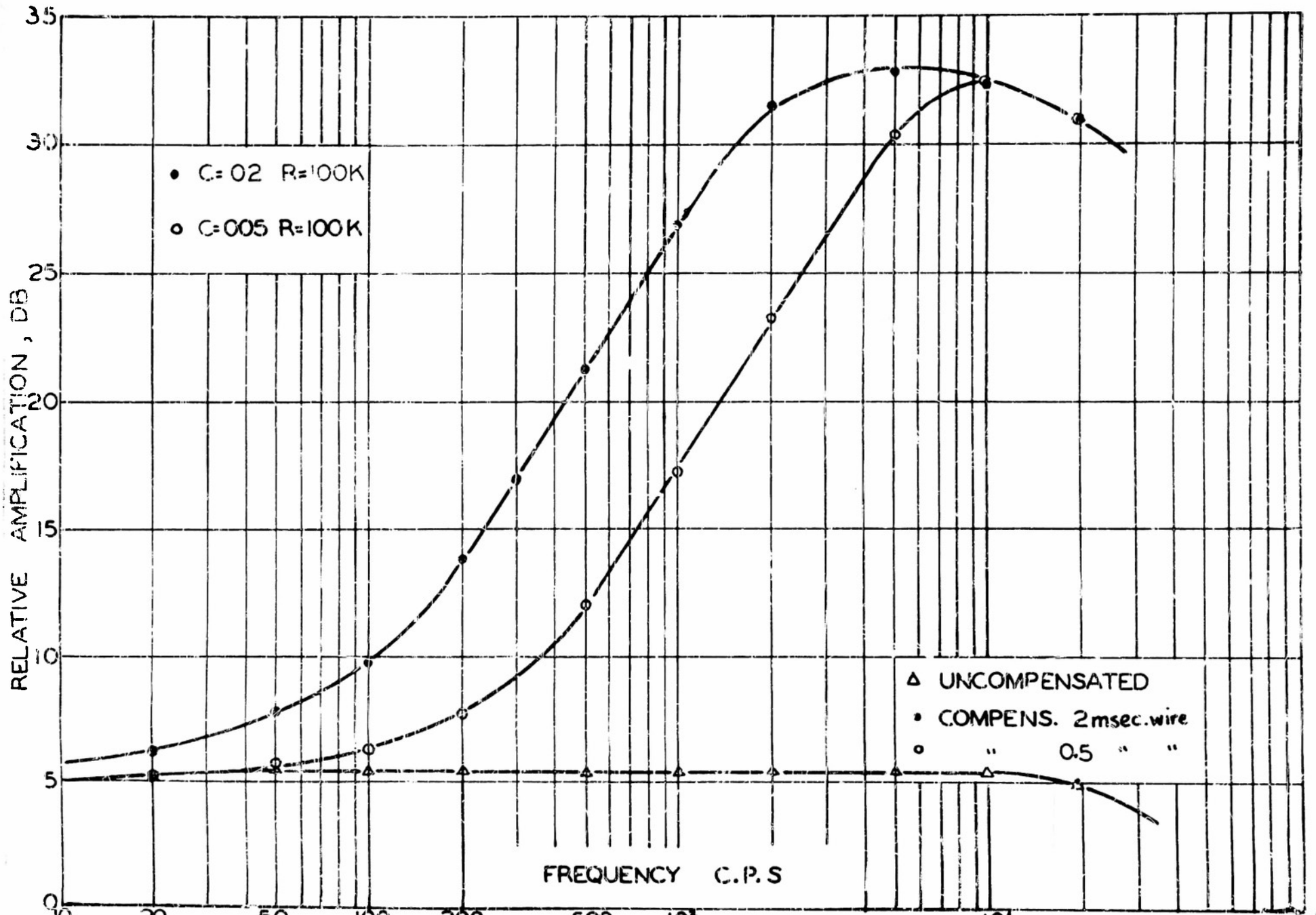


FIG 42. FREQUENCY RESPONSE OF COMPENSATING AMPLIFIER

Armed Services Technical Information Agenc

Because of our limited supply, you are requested to return this copy WHEN IT HAS SERVED YOUR PURPOSE so that it may be made available to other requesters. Your cooperation will be appreciated.

AD 407911

NOTICE: WHEN GOVERNMENT OR OTHER DRAWINGS, SPECIFICATIONS OR OTHER DATA ARE USED FOR ANY PURPOSE OTHER THAN IN CONNECTION WITH A DEFINITELY RELATED GOVERNMENT PROCUREMENT OPERATION, THE U. S. GOVERNMENT THEREBY INCURS NO RESPONSIBILITY, NOR ANY OBLIGATION WHATSOEVER; AND THE FACT THAT THE GOVERNMENT MAY HAVE FORMULATED, FURNISHED, OR IN ANY WAY SUPPLIED THE SAID DRAWINGS, SPECIFICATIONS, OR OTHER DATA IS NOT TO BE REGARDED BY IMPLICATION OR OTHERWISE AS IN ANY MANNER LICENSING THE HOLDER OR ANY OTHER PERSON OR CORPORATION, OR CONVEYING ANY RIGHTS OR PERMISSION TO MANUFACTURE, USE OR SELL ANY PATENTED INVENTION THAT MAY IN ANY WAY BE RELATED THERETO.

Reproduced by

DOCUMENT SERVICE CENTER

KNOTT BUILDING, DAYTON, 2, OHIO

UNCLASSIFIED